

Laboratory Study of Structural Behavior of Alternative Dowel Bars

National Concrete Pavement
Technology Center



Final Report
April 2006

Sponsored by

the Federal Highway Administration (Project 7),
the Iowa Highway Research Board (IHRB Project TR-510), and
the Iowa Department of Transportation (CTRE Project 04-163)

ctre

Center for Transportation
Research and Education

IOWA STATE
UNIVERSITY

About the National Concrete Pavement Technology Center

The mission of the National Concrete Pavement Technology Center is to unite key transportation stakeholders around the central goal of advancing concrete pavement technology through research, tech transfer, and technology implementation.

Disclaimer Notice

The contents of this report reflect the views of the authors, who are responsible for the facts and the accuracy of the information presented herein. The opinions, findings and conclusions expressed in this publication are those of the authors and not necessarily those of the sponsors.

The sponsors assume no liability for the contents or use of the information contained in this document. This report does not constitute a standard, specification, or regulation.

The sponsors do not endorse products or manufacturers. Trademarks or manufacturers' names appear in this report only because they are considered essential to the objective of the document.

Non-discrimination Statement

Iowa State University does not discriminate on the basis of race, color, age, religion, national origin, sexual orientation, gender identity, sex, marital status, disability, or status as a U.S. veteran. Inquiries can be directed to the Director of Equal Opportunity and Diversity, (515) 294-7612.

Technical Report Documentation Page

1. Report No. FHWA DTFH61-01-X-00042 (Project 7) IHRB Project TR-510		2. Government Accession No.		3. Recipient's Catalog No.	
4. Title and Subtitle Laboratory Study of Structural Behavior of Alternative Dowel Bars				5. Report Date April 2006	
				6. Performing Organization Code	
7. Author(s) Max L. Porter, James K. Cable, Fouad S. Fanous, John F. Harrington, and Nathan J. Pierson				8. Performing Organization Report No. CTRE Project 04-163	
9. Performing Organization Name and Address Center for Transportation Research and Education Iowa State University 2901 South Loop Drive, Suite 3100 Ames, IA 50010-8634				10. Work Unit No. (TRAIS)	
				11. Contract or Grant No.	
12. Sponsoring Organization Name and Address Federal Highway Administration Iowa Highway Research Board U.S. Department of Transportation Iowa Department of Transportation 400 7th Street SW, HIPT-20 800 Lincoln Way Washington, DC 20590 Ames, IA 50010				13. Type of Report and Period Covered Final Report	
				14. Sponsoring Agency Code	
15. Supplementary Notes Visit www.ctre.iastate.edu for color PDF files of this and other research reports.					
16. Abstract Load transfer across transverse joints has always been a factor contributing to the useful life of concrete pavements. For many years, round steel dowels have been the conventional load transfer mechanism. Many problems have been associated with the round steel dowels. The most detrimental effect of the steel dowel is corrosion. Repeated loading over time also damages joints. When a dowel is repeatedly loaded over a long period of time, the high bearing stresses found at the top and bottom edge of a bar erode the surrounding concrete. This oblonging creates multiple problems in the joint. Over the past decade, Iowa State University has performed extensive research on new dowel shapes and materials to mitigate the effects of oblonging and corrosion. This report evaluates the bearing stress performance of six different dowel bar types subjected to two different shear load laboratory test methods. The first load test is the AASHTO T253 method. The second procedure is an experimental cantilevered dowel test. The major objective was to investigate and improve the current AASHTO T253 test method for determining the modulus of dowel support, k_D . The modified AASHTO test procedure was examined alongside an experimental cantilever dowel test. The modified AASHTO specimens were also subjected to a small-scale fatigue test in order to simulate long-term dowel behavior with respect to concrete joint damage. Loss on ignition tests were also performed on the GFRP dowel specimens to determine the resin content percentage. The study concluded that all of the tested dowel bar shapes and materials were adequate with respect to performance under shear loading. The modified AASHTO method yielded more desirable results than the ones obtained from the cantilever test. The investigators determined that the experimental cantilever test was not a satisfactory test method to replace or verify the AASHTO T253 method.					
17. Key Words AASHTO T253 test—cantilever test—concrete pavements—dowel bar—oblonging—transverse joint				18. Distribution Statement No restrictions.	
19. Security Classification (of this report) Unclassified.		20. Security Classification (of this page) Unclassified.		21. No. of Pages 99	22. Price NA

LABORATORY STUDY OF STRUCTURAL BEHAVIOR OF ALTERNATIVE DOWEL BARS

**Final Report
April 2006**

Principal Investigator

Max L. Porter
Professor

Department of Civil, Construction and Environmental Engineering, Iowa State University

Co-Principal Investigators

James K. Cable
Associate Professor

Department of Civil, Construction and Environmental Engineering, Iowa State University

Fouad S. Fanous
Professor

Department of Civil, Construction and Environmental Engineering, Iowa State University

Research Assistants

John F. Harrington and Nathan J. Pierson

Sponsored by
the Federal Highway Administration (Project 7)
the Iowa Highway Research Board (IHRB Project TR-510)

Preparation of this report was financed in part
through funds provided by the Iowa Department of Transportation
through its research management agreement with the
Center for Transportation Research and Education.
CTRE Project 04-163.

A report from
Center for Transportation Research and Education

Iowa State University
2901 South Loop Drive, Suite 3100
Ames, IA 50010-8634
Phone: 515-294-8103
Fax: 515-294-0467
www.ctre.iastate.edu

TABLE OF CONTENTS

ACKNOWLEDGEMENTS	XI
1. INTRODUCTION	1
1.1 Background	1
1.2 Research Objective	1
1.3 Research Approach	1
1.4 Scope	2
2. TESTING PROGRAM	3
2.1 Test Descriptions	3
2.1.1 Modified AASHTO T253	3
2.1.2 Cantilever Test	6
2.1.3 Fatigue Test	7
2.2 Construction	8
2.2.1 Modified AASHTO T253	8
2.2.2 Cantilever	9
2.2.3 Strain Gages	10
2.3 Test Matrices	11
3. THEORY	12
3.1 Modulus of Dowel Support	12
3.2 Relative Deflection	14
3.3 Bearing Stress	16
3.4 Strain Gages	16
3.5 Load Distribution and Transfer	17
3.6 Dowel Embedment Length	18
4. ANALYSIS AND RESULTS	19
4.1 Modified AASHTO T253	19
4.1.1 Load Adjustments	19
4.1.2 Modulus of Dowel Support	19
4.1.3 Effects of Joint Width	20
4.1.4 Effects of Dowel Shape	21
4.1.5 Effects of Dowel Material	21
4.1.6 Effects of Dowel Flexural Rigidity	21
4.1.7 Dowel Deflection	22
4.1.8 Bearing Stress	24
4.1.9 Concurrent Dowel Research	25
4.2 Strain Gages	26
4.3 Cantilever Test	31
4.4 Fatigue Tests	32
4.5 Loss on Ignition Results for GFRP Dowels	34
5. SUMMARY OF PERFORMANCE	35
5.1 Modified AASHTO T253	35

5.2 Cantilever Test.....	35
5.3 Fatigue Test.....	35
6. FUTURE NEEDS AND IMPLEMENTATIONS.....	36
6.1 Modified AASHTO T253.....	36
6.2 Cantilever Test.....	37
6.3 Fatigue Test.....	38
6.4 Full Slab Test.....	41
7. SUMMARY AND CONCLUSIONS.....	42
REFERENCES.....	43
APPENDIX A. MODIFIED AASHTO T253 TEST: MODULUS OF DOWEL SUPPORT VS. LOAD DIAGRAMS.....	A-1
APPENDIX B. DOWEL MOMENT DIAGRAMS: THEORETICAL AND STRAIN- GAGE MEASURED.....	B-1
APPENDIX C. DOWEL DISPLACEMENT DIAGRAMS: THEORETICAL AND OBSERVED.....	C-1
APPENDIX D. CANTILEVER TEST MODULUS OF DOWEL SUPPORT VS. LOAD DIAGRAMS.....	D-1

LIST OF FIGURES

Figure 2.1. Iosipescu shear test.....	3
Figure 2.2. AASHTO T253 test (19).....	4
Figure 2.3. Modified AASHTO T253 test (15).....	4
Figure 2.4. Load test frame.....	5
Figure 2.5. Locations of DCDT's.....	6
Figure 2.6. Cantilever test specimen.....	7
Figure 2.7. Troughs for constructing modified AASHTO specimens.....	8
Figure 2.8. Cantilever dowel forms.....	9
Figure 2.9. Strain Gage Placement.....	10
Figure 3.1. Reactions along a deflected beam on an elastic foundation.....	12
Figure 3.2. Semi-infinite beam on an elastic foundation.....	13
Figure 3.3. Relative deflection between slab sections.....	15
Figure 3.4. Tabatabaie's load distribution model.....	18
Figure 4.1. Tabatabaie load distribution for extreme case.....	25
Figure 4.2. Strain gage placement.....	26
Figure 4.3. Two stainless steel dowels with strain gages set in concrete forms.....	27
Figure 4.4. Moment diagram, 1.5-inch diameter steel, 1/2-inch joint, east dowel.....	28
Figure 4.5. Moment diagram, 1.5-inch diameter steel, 1/2-inch joint, west dowel.....	28
Figure 4.6. Dowel displacement diagram, 1.5-inch diameter steel, 1/2-inch joint.....	29
Figure 4.7. Fatigue test minimum and maximum deflections.....	33
Figure 6.1. Proposed revised modified AASHTO specimen.....	36
Figure 6.2. Proposed cantilever dowel specimen.....	38
Figure 6.3. MTS fatigue testing machine.....	39
Figure 6.4. Recommended revised fatigue specimen.....	40
Figure 6.5. Free body diagrams of proposed fatigue specimen.....	40
Figure A.1. k_0 plots, round steel, 0-inch joint, unadjusted loads.....	A-3
Figure A.2. k_0 plots, round steel, 0-inch joint, adjusted loads.....	A-3
Figure A.3. k_0 plots, round steel, 1/8-inch joint, unadjusted loads.....	A-4
Figure A.4. k_0 plots, round steel, 1/8-inch joint, adjusted loads.....	A-4
Figure A.5. k_0 plots, round steel, 1/2-inch joint, unadjusted loads.....	A-5
Figure A.6. k_0 plots, round steel, 1/2-inch joint, adjusted loads.....	A-5
Figure A.7. k_0 plots, large elliptical steel, 0-inch joint, unadjusted loads.....	A-6
Figure A.8. k_0 plots, large elliptical steel, 0-inch joint, adjusted loads.....	A-6
Figure A.9. k_0 plots, large elliptical steel, 1/8-inch joint, unadjusted loads.....	A-7
Figure A.10. k_0 plots, large elliptical steel, 1/8-inch joint, adjusted loads.....	A-7
Figure A.11. k_0 plots, large elliptical steel, 1/2-inch joint, unadjusted loads.....	A-8
Figure A.12. k_0 plots, large elliptical steel, 1/2-inch joint, adjusted loads.....	A-8
Figure A.13. k_0 plots, small elliptical steel, 0-inch joint, unadjusted loads.....	A-9
Figure A.14. k_0 plots, small elliptical steel, 0-inch joint, adjusted loads.....	A-9
Figure A.15. k_0 plots, small elliptical steel, 1/8-inch joint, unadjusted loads.....	A-10
Figure A.16. k_0 plots, small elliptical steel, 1/8-inch joint, adjusted loads.....	A-10
Figure A.17. k_0 plots, small elliptical steel, 1/2-inch joint, unadjusted loads.....	A-11
Figure A.18. k_0 plots, small elliptical steel, 1/2-inch joint, adjusted loads.....	A-11
Figure A.19. k_0 plots, round stainless steel, 0-inch joint, unadjusted loads.....	A-12
Figure A.20. k_0 plots, round stainless steel, 0-inch joint, adjusted loads.....	A-12

Figure A.21. k_0 plots, round stainless steel, 1/8-inch joint, unadjusted loads	A-13
Figure A.22. k_0 plots, round stainless steel, 1/8-inch joint, adjusted loads	A-13
Figure A.23. k_0 plots, round stainless steel, 1/2-inch joint, unadjusted loads	A-14
Figure A.24. k_0 plots, round stainless steel, 1/2-inch joint, adjusted loads	A-14
Figure A.25. k_0 plots, round GFRP, 0-inch joint, unadjusted loads.....	A-15
Figure A.26. k_0 plots, round GFRP, 0-inch joint, adjusted loads.....	A-15
Figure A.27. k_0 plots, round GFRP, 1/8-inch joint, unadjusted loads	A-16
Figure A.28. k_0 plots, round GFRP, 1/8-inch joint, adjusted loads	A-16
Figure A.29. k_0 plots, round GFRP, 1/2-inch joint, unadjusted loads	A-17
Figure A.30. k_0 plots, round GFRP, 1/2-inch joint, adjusted loads	A-17
Figure A.31. k_0 plots, elliptical GFRP, 0-inch joint, unadjusted loads.....	A-18
Figure A.32. k_0 plots, elliptical GFRP, 0-inch joint, adjusted loads.....	A-18
Figure A.33. k_0 plots, elliptical GFRP, 1/8-inch joint, unadjusted loads.....	A-19
Figure A.34. k_0 plots, elliptical GFRP, 1/8-inch joint, adjusted loads.....	A-19
Figure A.35. k_0 plots, elliptical GFRP, 1/2-inch joint, unadjusted loads.....	A-20
Figure A.36. k_0 plots, elliptical GFRP, 1/2-inch joint, adjusted loads.....	A-20
Figure B.1. Theoretical and measured moments, round steel specimen, east dowel, 1/2- inch joint	B-3
Figure B.2. Theoretical and measured moments, round steel specimen, west dowel, 1/2- inch joint	B-3
Figure B.3. Theoretical and measured moments, round steel specimen, east dowel, 0-inch joint	B-4
Figure B.4. Theoretical and measured moments, round steel specimen, west dowel, 0- inch joint	B-4
Figure B.5. Theoretical and measured moments, large elliptical steel specimen, east dowel, 1/2-inch joint	B-5
Figure B.6. Theoretical and measured moments, large elliptical steel specimen, west dowel, 1/2-inch joint	B-5
Figure B.7. Theoretical and measured moments, small elliptical steel specimen, east dowel, 1/2-inch joint	B-6
Figure B.8. Theoretical and measured moments, small elliptical steel specimen, west dowel, 1/2-inch joint	B-6
Figure B.9. Theoretical and measured moments, round stainless steel specimen, east dowel, 1/8-inch joint	B-7
Figure B.10. Theoretical and measured moments, round stainless steel specimen, west dowel, 1/8-inch joint	B-7
Figure B.11. Theoretical and measured moments, round GFRP specimen, east dowel, 0- inch joint	B-8
Figure B.12. Theoretical and measured moments, round GFRP specimen, west dowel, 0- inch joint	B-8
Figure B.13. Theoretical and measured moments, round GFRP specimen, east dowel, 1/8- inch joint	B-9
Figure B.14. Theoretical and measured moments, round GFRP specimen, west dowel, 1/8-inch joint.....	B-9
Figure B.15. Theoretical and measured moments, elliptical GFRP specimen, east dowel, 1/8-inch joint.....	B-10
Figure B.16. Theoretical and measured moments, elliptical GFRP specimen, west dowel, 1/8-inch joint.....	B-10

Figure C.1. Theoretical displacement of round steel dowel, 0-inch joint.....	C-3
Figure C.2. Theoretical displacement of round steel dowel, 1/2-inch joint	C-3
Figure C.3. Theoretical displacement of large elliptical steel dowel, 1/2-inch joint.....	C-4
Figure C.4. Theoretical displacement of small elliptical steel dowel, 1/2-inch joint	C-4
Figure C.5. Theoretical displacement of round stainless steel dowel, 1/8-inch joint.....	C-5
Figure C.6. Theoretical displacement of round GFRP dowel, 0-inch joint	C-5
Figure C.7. Theoretical displacement of round GFRP dowel, 1/8-inch joint.....	C-6
Figure C.8. Theoretical displacement of elliptical GFRP dowel, 1/8-inch joint	C-6
Figure D.1. k_0 vs. load plots for round steel cantilever specimens	D-3
Figure D.2. k_0 vs. load plots for large elliptical steel cantilever specimens	D-3
Figure D.3. k_0 vs. load plots for small elliptical steel cantilever specimens.....	D-4
Figure D.4. k_0 vs. load plots for round stainless steel cantilever specimens	D-4
Figure D.5. k_0 vs. load plots for round GFRP cantilever specimens	D-5
Figure D.6. k_0 vs. load plots for elliptical GFRP cantilever specimens.....	D-5

LIST OF TABLES

Table 2.1. Modified AASHTO T253	11
Table 2.2. Cantilever test	11
Table 2.3. Fatigue test (modified AASHTO specimens)	11
Table 4.1. Average k_0 (pci) values—equal load distribution	19
Table 4.2. Average k_0 (pci) values—adjusted loads	20
Table 4.3. Dowel properties	22
Table 4.4. Dowel flexural rigidity and k_0 comparison	22
Table 4.5. Average deflections—2 kip loading, 1/8-inch joint	23
Table 4.6. Average deflections—2 kip loading, 1/2-inch joint	23
Table 4.7. Average deflections—10 kip loading, 1/8-inch joint	23
Table 4.8. Average deflections—10 kip loading, 1/2-inch joint	23
Table 4.9. Allowable stress and load at which allowable stress is exceeded	24
Table 4.10. Observed and theoretical y_0 values	30

ACKNOWLEDGEMENTS

The research described herein was conducted at Iowa State University in the Department of Civil, Construction, and Environmental Engineering (CCEE) through the National Concrete Pavement Technology Center (CP Tech Center) with contractual administration conducted by the Center for Transportation Research and Education (CTRE). Sponsorship of this research was provided by the U.S. Department of Transportation via the Federal Highway Administration (FHWA) and the Iowa Department of Transportation Highway Research Board.

Additional sponsorship for this project was made possible by the combined efforts of the Hughes Brothers Inc. of Seward, Nebraska, to supply FRP bars for the project. Without the donation of the materials, this project most likely would not have taken place.

The authors would also like to recognize and thank Mr. Mark Swanlund of the FHWA and the staff personnel at FHWA for aiding in processing the sponsorship of this project and providing information related to this work. In addition, the authors wish to thank Doug Gremmel from Hughes Brothers Inc. for arranging the supply of the dowel bars, as well as providing the information about the dowels.

The authors would like to acknowledge the support provided by Douglas L. Wood, Structural Engineering Laboratory Supervisor, for his expertise and assistance in preparing the specimens and collecting the data. Appreciation is also extended to the many hourly laboratory assistants.

1. INTRODUCTION

1.1 Background

Load transfer across transverse joints has always been a factor contributing to the useful life of concrete pavements. For many years, round steel dowels have been the conventional load transfer mechanism. Many problems have been associated with the round steel dowels.

The most detrimental effect of the steel dowel is corrosion. Repeated loading over time also damages joints. When a dowel is repeatedly loaded over a long period of time, the high bearing stresses found at the top and bottom edge of a bar erode the surrounding concrete. This oblonging creates multiple problems in the joint. The void spaces caused by the repetitive loading reduce the ability of the bar to adequately transfer load. If the load is not transferred by the bar, it is carried into the subgrade. Over time, the subgrade is eroded and the pavement eventually cracks. The void spaces also allow greater infiltration of water and alkali solutions, increasing the rate of steel dowel corrosion. The corroded steel increases in volume and loses strength over time. The corroded dowel may also bind the joint and prevent proper lateral movement caused by freeze-thaw pavement expansion.

Over the past decade, Iowa State University (ISU) has performed extensive research (*1-18*) on new dowel shapes and materials to mitigate the effects of oblonging and corrosion. This report evaluates the bearing stress performance (*12-16*) of six different dowel bar types subjected to two different shear load laboratory test methods. The first load test is the AASHTO T253 method. The second procedure is an experimental cantilevered dowel test.

1.2 Research Objective

The objective of this study was to investigate and improve the current AASHTO T253 test method for determining the modulus of dowel support, k_0 . The constant k_0 measures the pressure intensity on the elastic foundation required to cause a unit settlement into the foundation by the dowel bar at the face of the joint. The bearing stress is directly related to k_0 and bar deflection within the concrete. The ability to easily determine k_0 for a dowel aids in the selection of the optimal bar shape and material in the design of new concrete pavements. The investigation also included analysis of a new simplified cantilever dowel test to be used as a verification of the AASHTO procedure.

1.3 Research Approach

A literature review was conducted in order to study the theory regarding the behavior of a beam on an elastic foundation. This theory was applied to the behavior of dowel bars in concrete pavements. Laboratory specimens were built to simulate the application of shear

forces to the dowels and to determine the modulus of dowel support, k_0 , for six different bar types.

1.4 Scope

The scope of this project involved the testing of 78 different dowel specimens, including the following tasks:

- Performing the modified AASHTO test on 54 specimens containing six different dowel shapes and three separate gap widths
- Implementing six fatigue tests on the modified AASHTO specimens in order to observe long-term damage to pavement joints caused by dowel bearing stresses
- Applying cantilever dowel tests on 18 specimens (six shapes with three specimens per shape)
- Determining the resin content of the glass fiber reinforced polymer (GFRP) dowels by using a loss on ignition test
- Evaluating the results obtained by both the AASHTO and cantilever tests
- Comparing laboratory results to field results calculated in past research
- Deciding if the cantilever test is a viable alternative to the AASHTO test
- Recommending changes to the test procedures used in this investigation for future tests

2. TESTING PROGRAM

2.1 Test Descriptions

2.1.1 Modified AASHTO T253

The aim of this study was to test a modified version of the current AASHTO T253 test procedure. The modified AASHTO test was implemented to replace the Iosipescu (2) shear dowel test. The Iosipescu was very effective at creating a pure shear condition at the joint of the test specimen. The problems associated with the Iosipescu test were constructability issues. It was difficult and time-consuming to build the load apparatus to create this pure shear. A diagram of the Iosipescu test is shown below in Figure 2.1.

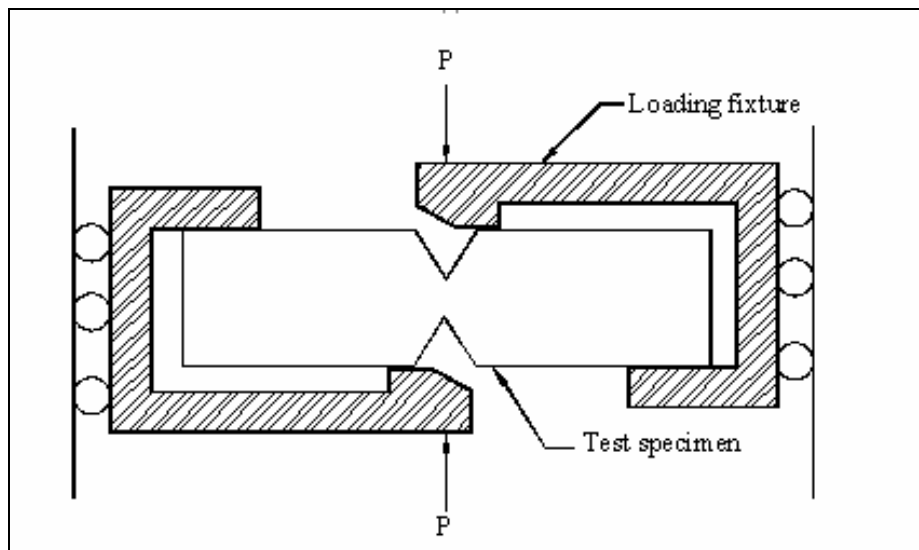


Figure 2.1. Iosipescu shear test

To eliminate the difficulties associated with the execution of the Iosipescu test, the modified AASHTO test was implemented and recommended as the preferred dowel test method. The aim of the modified AASHTO test was to create a shear condition at the concrete joint without the complicated test frame, as shown above in Figure 2.1. The current AASHTO standard is shown below in Figure 2.2. The modified version of the AASHTO test is shown in Figure 2.3.

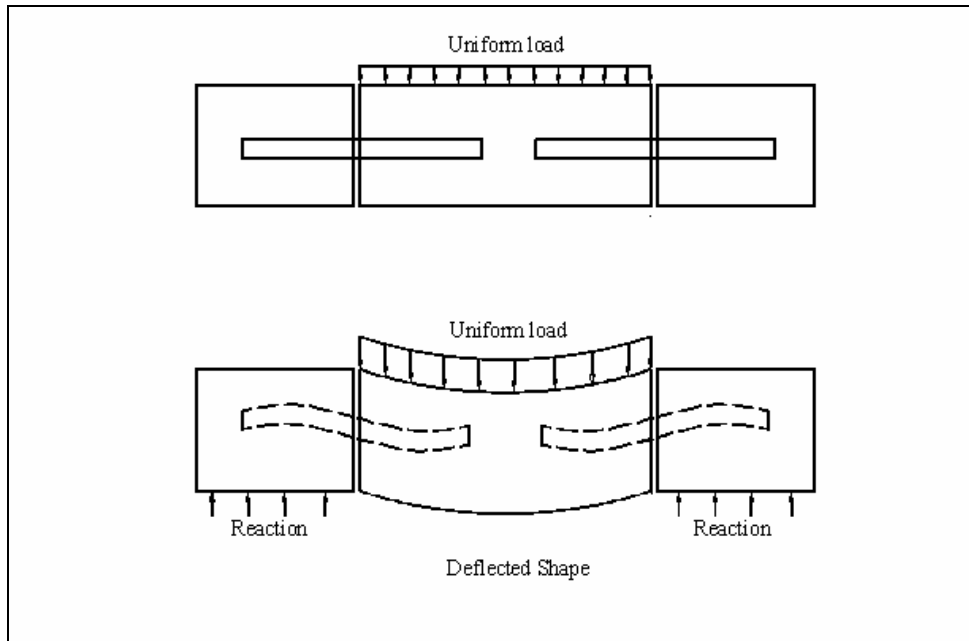


Figure 2.2. AASHTO T253 test (19)

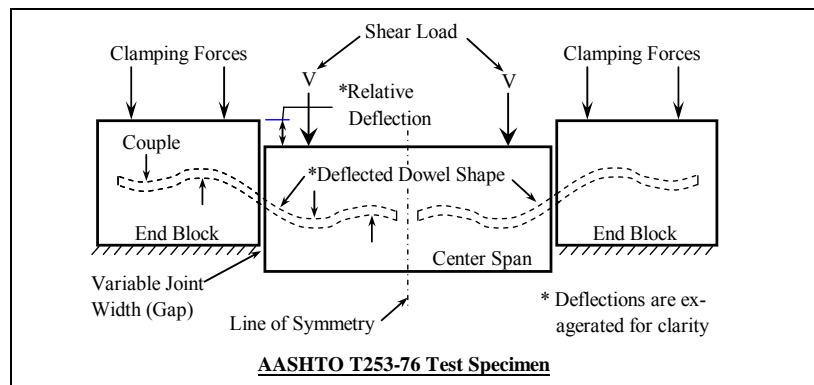


Figure 2.3. Modified AASHTO T253 test (15)

Although the modified version of the AASHTO test was very similar to the current standard, there were key differences between the two tests. The first and most clear difference was the method of load application. The original test applied a uniform load along the center block parallel to the dowel bars. This load application created flexural behavior in the center block. The application of linear loads parallel to the joints, as shown in Figure 2.3, greatly reduced the effects of flexure within the center block. This was implemented even though past ISU research (29) recommended two-point loads instead. The two-point load method increased the risk of load eccentricity in the center block. This eccentricity would have made the center block more vulnerable to rotation about the dowels. Even if rotation was kept to a minimum, the point loads would have also added more uncertainty to the results because it would have been very difficult to place them exactly the same for every specimen. There would have been slight, unaccountable differences in the load location between tests. The investigators believed that the load would be more consistently applied as two linear loads placed at three

inches inside the joints. This distance of three inches allowed the placement of instrumentation to measure block deflection.

The modified dowel tests were performed at ISU in the structures laboratory located in Town Engineering Building. The new tests evaluated round, elliptical, and rectangular bar cross sections. The tests also evaluated dowel bars made of epoxy-coated steel, stainless steel, and glass fiber reinforced polymer (GFRP). The specimens were placed into a load frame shown in Figure 2.4.

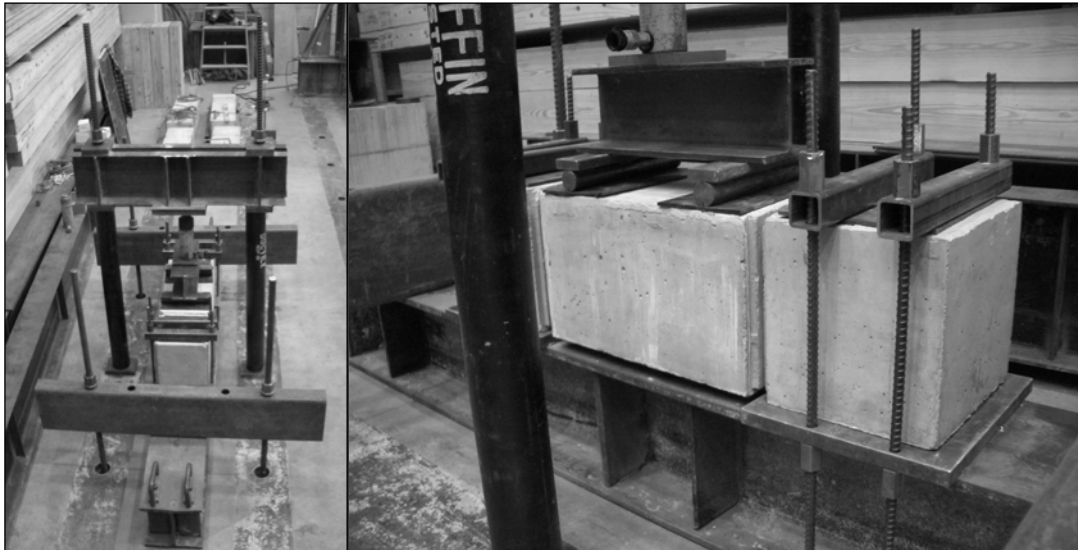


Figure 2.4. Load test frame

The ductile iron structural tubes supporting the top cross beam were post-tensioned to the test floor with a force of 3,000 pounds in each tube. The post-tensioning was done to ensure smooth load transfer from the hydraulic actuator to the concrete test specimen. Downward load was transferred from the hydraulic jack to the concrete by using a stiffened rolled shape steel beam section. Two 1.25-inch diameter solid steel bars were placed 3 inches from each end of the center block in order to transfer the downward load from the beam to the concrete. Thin sheets of neoprene were placed beneath the loaded rollers to allow for an even, transverse load application along each bar.

The end blocks of the specimen were clamped down to the lower steel support plates using high strength Dywidag steel rods. The goal of each end support was to create a fixed-end condition on each side of the specimen. The bars were tightened to prevent end-block rotation and minimize flexural behavior of the dowel bars. The clamping mechanisms were tightened by hand with wrenches. A hydraulic jack was not used to tension the clamping rods because outside stresses acting on the dowels would affect the deflection behavior of the bar under a load. The goal of the fixed-end conditions is to promote shear behavior in the dowel bars.

The specimens were instrumented with direct current deflection transducers (DCDTs). There were a total of eight DCDTs used. Four were used to measure relative deflections

on the right and left ends of the specimen. The placement of the DCDTs on the test specimen is shown below in Figure 2.5.

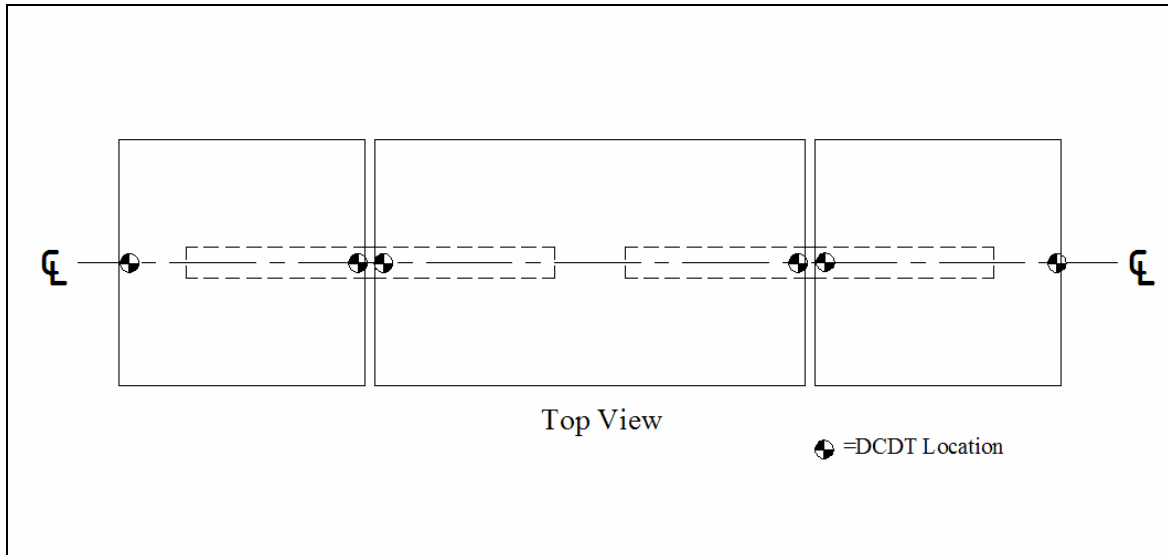


Figure 2.5. Locations of DCDT's

Two DCDTs were placed at the far ends of the end blocks to monitor the movement in the restrained ends. Two more were placed on the base plates that support the specimen in order to monitor movement of the entire testing surface.

The procedure used to calculate k_{θ} with field data from previous ISU dowel research was implemented to analyze the lab data from the modified test procedures. The force acting on each dowel was assumed to be half the total load acting on the apparatus. All deflections not pertaining to the relative deflection of the middle block indicated negligible rotations at the end blocks and test apparatus.

2.1.2 Cantilever Test

The cantilever test was a new experimental dowel test procedure. The aim of the new test was to eliminate some of the unknown parameters involved with the modified AASHTO test. The two main unknowns were the exact deflection of the dowel bar at the face of the joint and the exact shear load carried by the dowel. The cantilever test specimen allowed direct placement of instrumentation in order to directly measure dowel deflection at the joint. It also allowed the investigators to observe the dowel joint and check for concrete abnormalities or debris within the joint. The cantilever test consisted of a 12-inch concrete cube and a single 18-inch dowel. The dowel bar was placed with 9 inches embedded in the concrete. The cantilever test specimen is shown below in Figure 2.6.

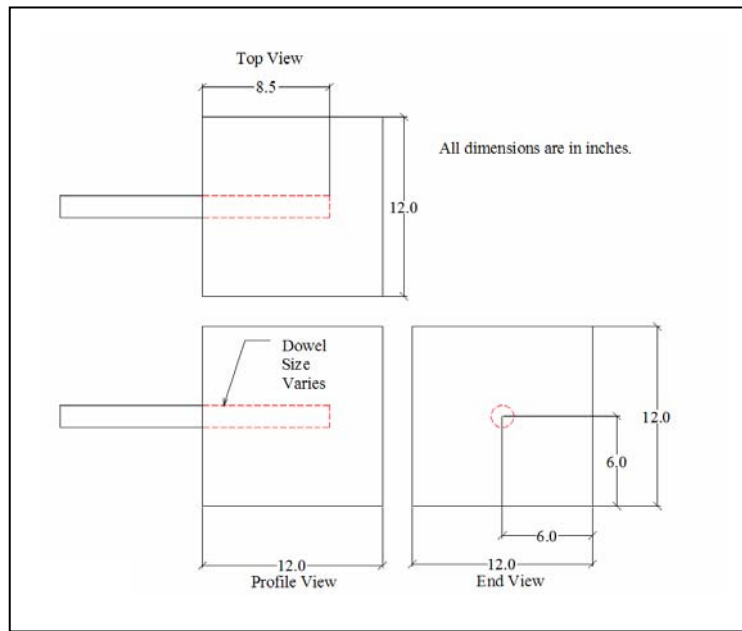


Figure 2.6. Cantilever test specimen

The new test allowed for placement of instrumentation to directly measure dowel deflection at the face of the concrete block.

2.1.3 Fatigue Test

Oblonging of pavement slabs occurs after years of repetitive loading. A small-scale fatigue test was assembled in an attempt to simulate the damage caused by the millions of load cycles applied to a pavement slab. Because a much smaller number of cycles was used, the applied load was much higher than the load applied to a dowel in a real pavement slab. The fatigue test required a load that was large enough to cause visible oblonging after a small number of cycles. The load magnitude also needed to be small enough to avoid breaking the test specimen. Using a trial and error method, the block was loaded with 22,000 pounds at a frequency of 1 Hz for 10,000 cycles.

The dowel specimen was placed on the same base beam used in the previous test methods. The fatigue actuator used was much larger than the 50,000-pound manual actuator. The larger actuator required the use of a much larger loading frame. The frame was post-tensioned to the tie-down floor with a stress of 3000 psi in each Dywidag bar.

All measurements were taken with the internal deflection transducers in the actuator. A true value of k_0 could not be found using the fatigue test. The constant k_0 was calculated under the assumption that the beam is in complete contact with the elastic foundation. The oblonged or damaged dowel hole violates this basic assumption. The main goal of the fatigue test in this study was to determine if a qualitative observation could be made to see which dowels will fatigue less over an extended period of time. While this did not give a value of k_0 , it allowed one to reasonably compare the actual performance of a bar with its predicted performance. If a bar had a lower k_0 value, it would have undergone the least deflection increase over time.

2.2 Construction

2.2.1 Modified AASHTO T253

The modified AASHTO T253 specimen was constructed using prefabricated steel forms by EFCO Manufacturing. The steel forms were fabricated into twelve-inch-wide by twelve-inch-tall troughs. Each trough was twelve-feet-long and fit three specimens per trough.

The joints were formed using 1/8-inch polyvinyl chloride (PVC) sheets. The sheets were held into place with 1/2-inch plywood strips applied to the steel forms with clear silicon adhesive. The dowels were placed across the PVC bulkheads and supported with steel chairs at each end. Each specimen was separated by a plywood bulkhead. Figure 2.7 shows some of the troughs with dowels and bulkheads placed.

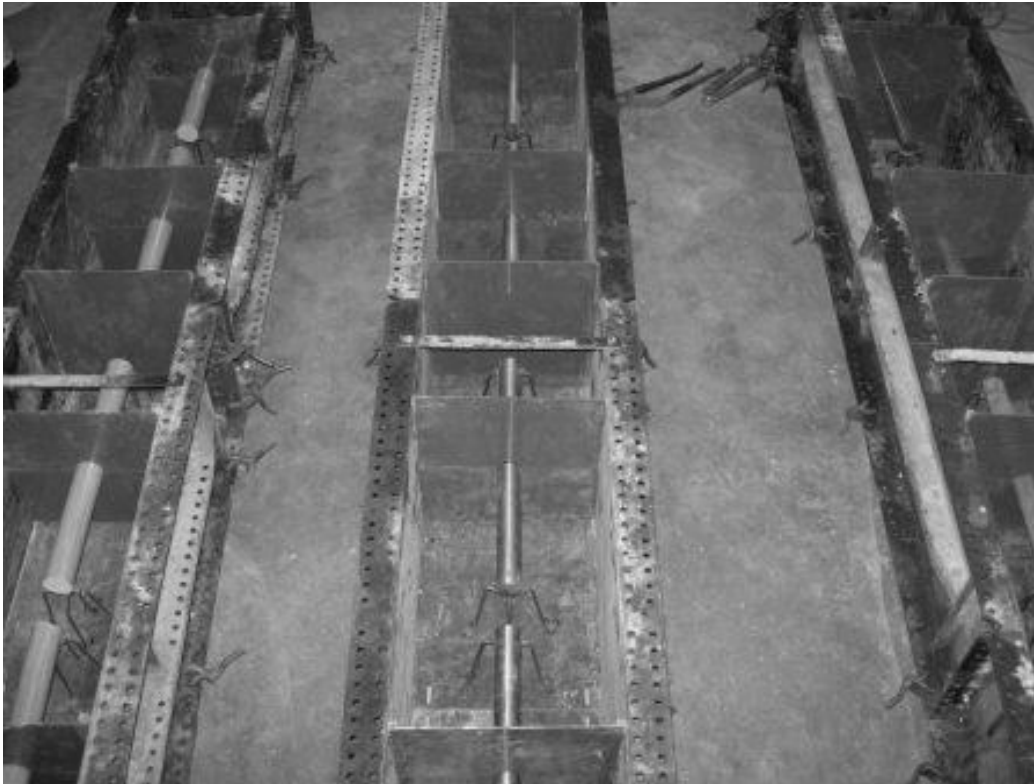


Figure 2.7. Troughs for constructing modified AASHTO specimens

The concrete was a Class-C Portland Cement mix with a target compressive strength of 4000 psi. The concrete was delivered to the laboratory in mixer trucks from Ames Ready Mix.

Concrete was placed by hand using wheelbarrows, shovels, and hand scoops. Special care was taken to not disturb the alignment of the two dowels. A vibrator was used to properly consolidate the concrete.

Previous research (29) recommended the use of high-strength plaster to be placed below the two end blocks to promote a more uniform contact with the beam support structure. The investigators experimented with the application of a high-strength dental plaster to the modified AASHTO specimens. The application of the plaster proved to be costly with respect to both time and money. It also did not improve the end support conditions. Because the steel forms were placed on a level laboratory floor during construction, they were already level and smooth at the base. The addition of plaster did not improve this condition and thus was not implemented for the series of laboratory tests.

2.2.2 Cantilever

The individual cantilevered dowels were built using the same steel troughs used in the construction of the modified AASHTO test specimens. Plywood bulkheads were used to separate the individual twelve-inch blocks. The dowels were placed vertically with one end supported by a 2.5-inch chair at the center of the bottom surface. The dowel was secured with a plywood strip cut to fit the dowel's shape. The cantilever dowel concrete forms are shown below in Figure 2.8.



Figure 2.8. Cantilever dowel forms

The bar was positioned with a hand level and then secured within the strip. The concrete used was the same 4000 psi Class-C mix used in the modified AASHTO test specimens. Concrete was placed entirely by hand with scoops due to the small open spaces in the tops of the forms.

2.2.3 Strain Gages

Strain gages were applied to nine of the 54 modified AASHTO specimens. Specimens chosen to have strain gages covered a variety of dowel types and joint widths. Both dowels in each of the nine specimens were each equipped with twelve strain gages—six on the top and six on the bottom of the dowel located at 1.5, 5.5, and 7 inches from the center of the dowel, as shown in Figure 2.9.

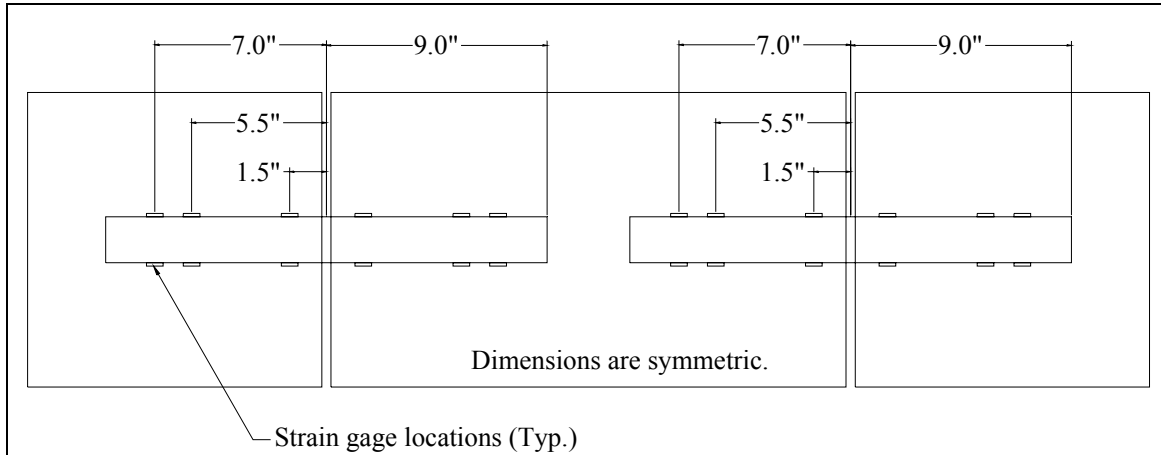


Figure 2.9. Strain Gage Placement

The strain gages measured the strains on the surface of the dowel while the specimens were being loaded. The strains were measured simultaneously with deflection measurements and load. The strains were be used to determine the dowel behavior along the length of the dowel. The measured behavior could have been compared to the theoretical behavior or used to verify observed behavior.

2.3 Test Matrices

The specimens constructed for the previously described laboratory tests are shown in the following tables.

Table 2.1. Modified AASHTO T253

Dowel Material	Dowel Shape	Dowel Size, in.	Gap Width, in.	Quantity
Steel (epoxy coated)	Circular	1.5	0	3*
Steel (epoxy coated)	Circular	1.5	1/8	3
Steel (epoxy coated)	Circular	1.5	1/2	3*
Steel (epoxy coated)	Elliptical	2.00 x 1.375	0	3
Steel (epoxy coated)	Elliptical	2.00 x 1.375	1/8	3
Steel (epoxy coated)	Elliptical	2.00 x 1.375	1/2	3*
Steel (epoxy coated)	Elliptical	1.66 x 1.13	0	3*
Steel (epoxy coated)	Elliptical	1.66 x 1.13	1/8	3
Steel (epoxy coated)	Elliptical	1.66 x 1.13	1/2	3*
Stainless Steel	Circular	1.5	0	3
Stainless Steel	Circular	1.5	1/8	3*
Stainless Steel	Circular	1.5	1/2	3
GFRP	Circular	1.875	0	3
GFRP	Circular	1.875	1/8	3*
GFRP	Circular	1.875	1/2	3
GFRP	Elliptical	2.25 x 1.25	0	3*
GFRP	Elliptical	2.25 x 1.26	1/8	3*
GFRP	Elliptical	2.25 x 1.27	1/2	3

* Indicates one specimen in test series of three specimens has strain gages

Note: The dimension for circular dowels is diameter and the dimensions for elliptical dowels is strong axis diameter (width) x weak axis diameter (height)

Table 2.2. Cantilever test

Dowel Material	Dowel Shape	Dowel Size, in.	Quantity
Steel (epoxy coated)	Circular	1.5	3
Steel (epoxy coated)	Elliptical	2.00 x 1.375	3
Steel (epoxy coated)	Elliptical	1.66 x 1.13	3
Stainless Steel	Circular	1.5	3
GFRP	Circular	1.875	3
GFRP	Elliptical	2.25 x 1.25	3

Table 2.3. Fatigue test (modified AASHTO specimens)

Dowel Material	Dowel Shape	Dowel Size, in.	Gap Width, in.	Quantity
Steel (epoxy coated)	Elliptical	1.66 x 1.13	0	2
Stainless Steel	Circular	1.5	1/8	2
GFRP	Circular	1.875	1/2	2

3. THEORY

3.1 Modulus of Dowel Support

Several researchers have utilized Timoshenko's (20) model of beam on an elastic foundation to investigate the performance of dowel bars in pavement structures. The following briefly describes the analytical model of an infinite beam that is resting on a concrete foundation. This model, which is a Winkler model, assumes a linear force-deflection relationship, so that if the dowel imposes a deflection y on the foundation, the dowel will be resisted with a pressure ky , where k is the foundation modulus (see Figure 3.1). When analyzing the dowel in pavement structures, the modulus k will be replaced by k_0d , where d is the diameter of a circular dowel bar, or by k_0b , where b is the width of other than circular dowel bar, and k_0 is referred to as the modulus of dowel support. The units of k_0 are psi/in.

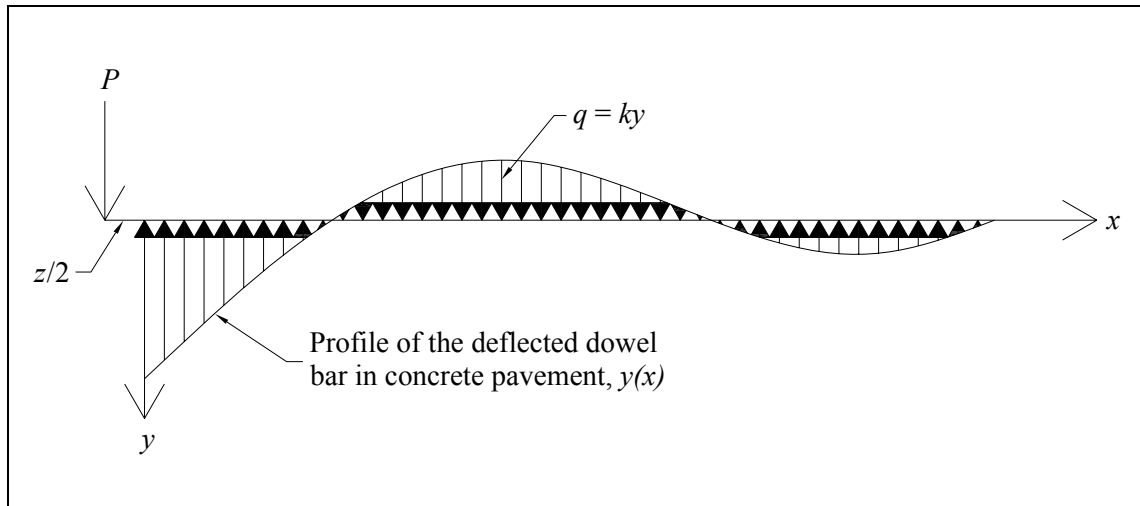


Figure 3.1. Reactions along a deflected beam on an elastic foundation

Following Timoshenko's model, one can write the following relationship:

$$EI \frac{d^4 y}{dx^4} = -(k_0 d) y \quad (3.1)$$

where EI is the rigidity of the dowel and y is the deflection of the dowel.

The general solution of the above differential equation is

$$y = \frac{e^{-\beta x}}{2\beta^3 EI} [P \cos \beta x - \beta M_0 (\cos \beta x - \sin \beta x)] \quad (3.2)$$

where $\beta = \sqrt[4]{\frac{k_0 d}{4EI}}$ and is referred to as the relative stiffness of the dowel on the concrete.

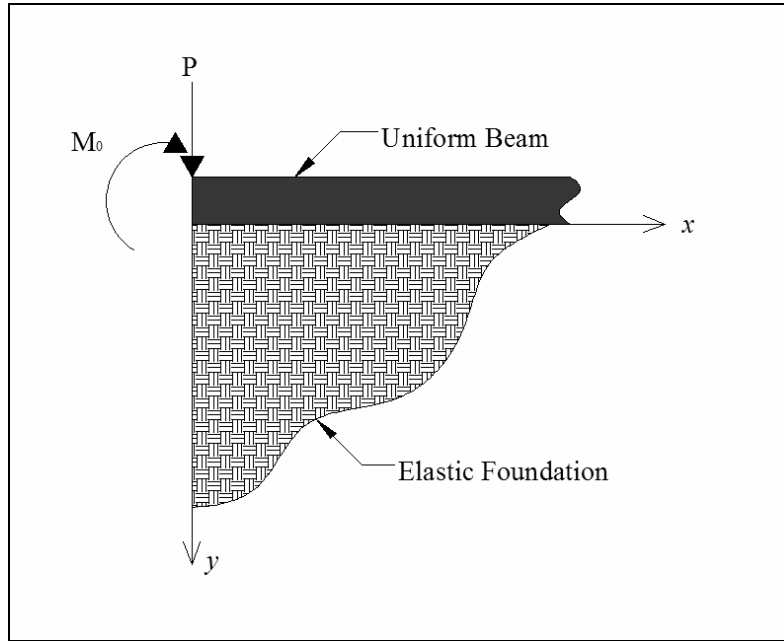


Figure 3.2. Semi-infinite beam on an elastic foundation

Friberg (21) applied the approach outlined above to a dowel with semi-infinite length embedded in concrete. To find the deflection of the dowel at the face of the concrete joint, Friberg set $x = 0$ and $M_0 = \frac{Pz}{2}$ (i.e., the moment from the shear load applied at the center of the joint) in Equation 3.2, which becomes

$$y_0 = \frac{P}{4\beta^3 EI} (2 + \beta z) \quad (3.3)$$

where

$$\beta = \sqrt[4]{\frac{k_0 b}{4EI}} \quad (3.4)$$

k_0 = modulus of dowel support, pounds per cubic inch (pci)

b = dowel bar width, in.

P = load transferred by the dowel, lbs

Z = joint width, in.

E = modulus of elasticity of the dowel, psi

I = moment of inertia of the dowel cross section, in.⁴

3.2 Relative Deflection

The modified AASHTO and cantilever tests were used to obtain y_0 . For a given load, y_0 was used to solve β using Equation 3.3 and β can be used to solve for k_0 using Equation 3.4. For the cantilever tests, y_0 was directly measured. For the modified AASHTO test, y_0 is determined using the equation

$$\Delta = 2y_0 + z \frac{dy_0}{dx} + \frac{Pz^3}{12EI} + \delta \quad (3.5)$$

where Δ is the relative displacement in inches between slabs at the joint and consists of the following components (see Figure 3.3):

- deflection at each joint face, y_0
- deflection due to the slope of the dowel, $\frac{zdy_0}{dx}$
- moment deflection, $\frac{Pz^3}{12EI}$
- shear deflection, δ

where

$$\delta = \frac{\lambda Pz}{AG}$$

λ = shear shape factor = 10/9 for round and elliptical dowels (22)

A = cross-sectional area of the dowel

G = shear modulus of the dowel material

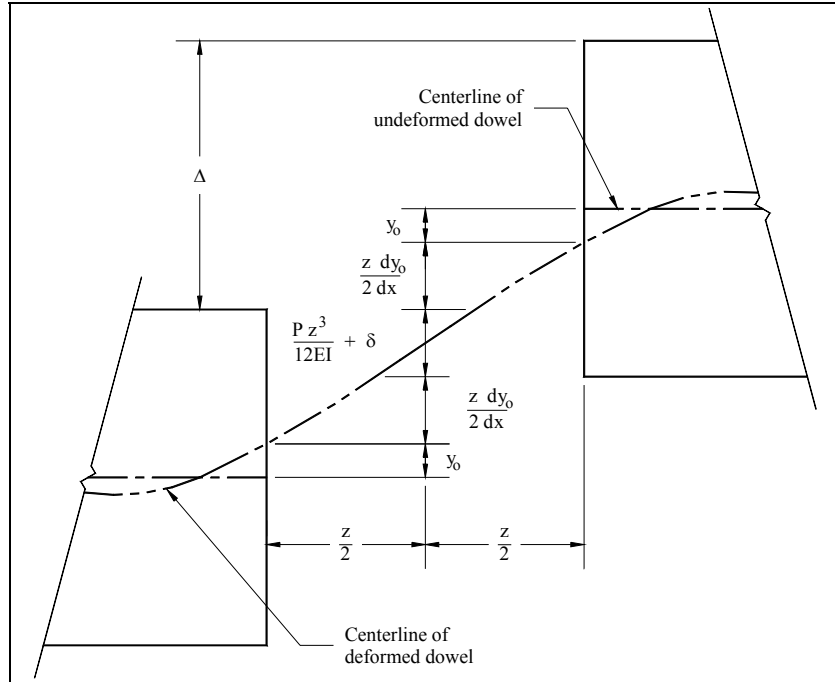


Figure 3.3. Relative deflection between slab sections

In addition to the shear shape factor of 10/9 that was based on geometry, Cowper (23) developed a shear coefficient for Timoshenko's beam theory based on Poisson's ratio so that material properties factor in to shear deflection. Cowper's shear coefficients were slightly greater than 10/9, but 10/9 was used here for convenience and because the resulting changes to k_0 were insignificant. The deflections due to flexural effects in Equation 3.5 were assumed to be negligible due to small joint widths. (For example, even for joint widths of up to 1/2 inch, the moment deflection is on the order of hundred thousandths of an inch). Neglecting the moment deflection and slope deflection leaves

$$\Delta = 2y_0 + \delta$$

Or, solving for y_0 ,

$$y_0 = \frac{(\Delta - \delta)}{2} \quad (3.6)$$

Once the load and deflection data were obtained from testing, a spreadsheet was used to calculate y_0 and k_0 for each data point. To do this, an initial value for k_0 was given so that β could be determined and applied to Equation 3.3. The solver function was used to set Equation 3.3 equal to Equation 3.6 by changing k_0 , thus giving the representative k_0 for a given data point.

3.3 Bearing Stress

Ultimately, the modulus of dowel support, k_0 , is used to determine the bearing stress of the dowel on the concrete at the joint face. Since Timoshenko's model assumed that the intensity of the reaction continuously distributed at every section is proportion to the deflection at a given section, then the bearing stress can be found by multiplying the modulus of dowel support by the deflection at the face of the joint:

$$\sigma_b = k_0 y_0 \quad (3.7)$$

The bearing stress must be kept at a minimum to prevent crushing of concrete above and below the dowel. Equation 3.8 shows an allowable bearing stress given by the American Concrete Institute's Committee 325 (24).

$$\sigma_a = \left(\frac{4-b}{3} \right) f'_c \quad (3.8)$$

where

σ_a = allowable bearing stress, psi

b = dowel bar diameter for circles or major axis for ellipses, in.

f'_c = compressive strength of concrete, psi

Equation 3.8 provides a factor of safety of three. The bearing stress calculated for a given data point load was compared to the allowable stress for a given dowel. The load at which the calculated bearing stress equaled the allowable bearing stress was recorded to compare the six dowel types.

3.4 Strain Gages

Moment along a dowel bar can be found using measured strain values obtained with strain gages. Nine modified AASHTO specimens (18 dowel bars) were installed with 12 strain gages per dowel. Equation 3.9 (based on Equation 3.2) was used to find the deflected shape of the dowel (where $x = 0$ at the face of the slab joint).

$$y(x) = \frac{e^{-\beta x}}{2\beta^3 EI} [P \cos \beta x - \beta M_0 (\cos \beta x - \sin \beta x)] \quad (3.9)$$

$$M(x) = -EI \frac{d^2 y}{dx^2} = -\frac{e^{-\beta x}}{2\beta} [2(P - M_0 \beta) \sin \beta x - 2M_0 \beta \cos \beta x] \quad (3.10)$$

$$V(x) = -EI \frac{d^3 y}{dx^3} = -\frac{e^{-\beta x}}{2} [2(P - M_0 \beta)(\cos \beta x - \sin \beta x) + 2M_0 \beta(2 \sin \beta x + \cos \beta x)] \quad (3.11)$$

where

$$M_0 = \frac{Pz}{2}$$

The strain reading from the strain gages can be used to find moment by $\sigma = \frac{Mc}{I}$,

where $\sigma = \varepsilon E$, therefore,

$$M(x) = \frac{\varepsilon EI}{c} \quad (3.12)$$

where,

ε = strain reading from strain gage at x

σ = stress at x determined from strain gage reading at x , psi

c = half the vertical diameter of the dowel, in.

E = modulus of elasticity of the dowel bar material, psi

I = flexural moment of inertia for the dowel bar, in.⁴

3.5 Load Distribution and Transfer

Although this study did not include the analysis of actual pavement slabs, the methodology for determining wheel load distribution across a doweled joint was still relevant to this investigation. The determination of wheel load distribution was used to calculate the maximum shear force transferred by a dowel bar in a given transverse joint. These maximum shear forces in actual pavements were compared to the loads applied to laboratory specimens. The comparison of theoretical versus laboratory dowel shear forces was used to determine the load transfer adequacy of the six dowel types included in this study.

In highway applications, wheel loads are transferred through multiple dowels in such a way that no dowel sees a full wheel load. The number of dowels actively transferring a wheel load can be found by determining the radius of relative stiffness, l_r , defined by Westergaard (25) as,

$$l_r = \sqrt[4]{\frac{E_c h^3}{12(1-\mu)^2 K}} \quad (3.13)$$

where

E_c = modulus of elasticity of the pavement concrete, psi

h = pavement thickness, in.

μ = Poisson's ratio for pavement concrete

K = modulus of subgrade reaction, pci

Tabatabaie's (26) finite element modeling shows that $1.0l_r$ is a better approximation for dowels currently in use. Figure 3.4 shows Tabatabaie's load distribution model.

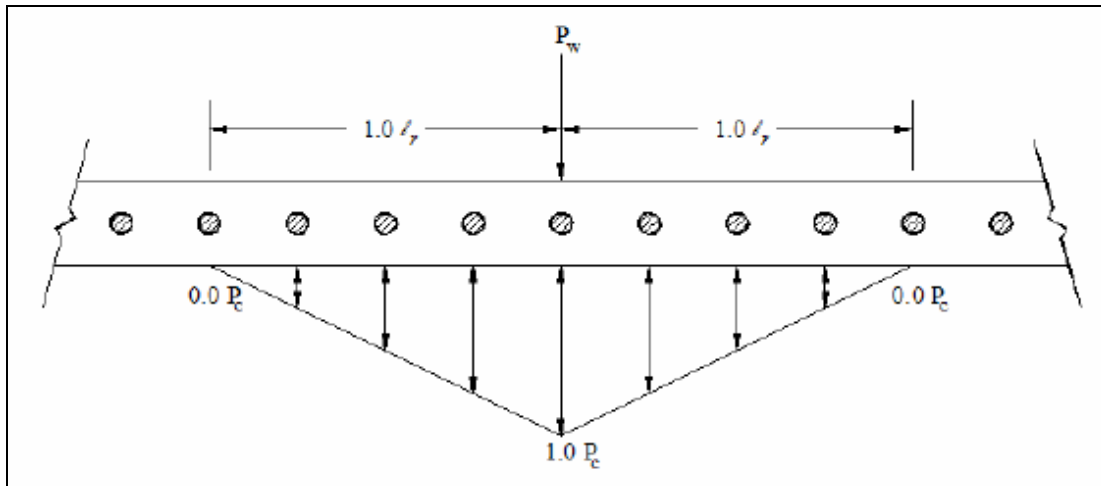


Figure 3.4. Tabatabaie's load distribution model

The variable P_c is determined by dividing P_w by the number of effective dowels, where

P_w = wheel load, lbs

P_c = load applied to dowel directly beneath wheel load, lbs

The number of effective dowels is found by summing the height of the load distribution model (in terms of P_c) at each dowel within $1.0l_r$ of the wheel load.

Assuming dowels have 100 percent load transfer efficiency, half of a wheel load should be transferred to the soil subgrade and half should be transferred to the adjacent slab by the dowels (2). The 100 percent load transfer efficiency can no longer be achieved once repetitive loading of the joint creates voids in the slab directly above and below a dowel at the face of the joint. To account for the voids, Yoder and Witzak (27) suggest a 5 to 10 percent reduction in load transfer. Therefore, the design transfer load should be about 45 percent of the design wheel load.

$$P_t = 0.45P_w \quad (3.14)$$

where

P_t = load transferred across the joint

P_w = applied wheel load

3.6 Dowel Embedment Length

Timoshenko's (Equation 3.2) and Friberg's (Equation 3.3) theories apply to a beam (dowel) of semi-infinite length. However, dowels are of measurable finite length. Albertson and others (28, 29) have shown that the theory can be applied to dowel bars given that βL_e is greater than or equal to 2 (where L_e is the embedment length of the dowel within the slab).

4. ANALYSIS AND RESULTS

4.1 Modified AASHTO T253

4.1.1 Load Adjustments

The load applied to the center block of the modified AASHTO T253 specimens was assumed to be distributed evenly between the two dowels. Analysis of load-deflection data for the test showed inconsistencies between the relative deflections measured on either joint. Many factors could have caused the inconsistencies. One inconsistency was that the load was not necessarily distributed equally between dowels. Because of this, the data were analyzed two ways:

1. Load was distributed evenly between the two dowels
2. Load was distributed proportionally between the two dowels based on the relative deflection measurements

The difference in k_0 values determined using the unadjusted loads and the adjusted loads was usually within ten percent.

4.1.2 Modulus of Dowel Support

Tables 4.1 and 4.2 show the average k_0 value (see Section 2.1) for the tested dowels broken down by dowel type, joint width, and load adjustment. Appendix A shows k_0 versus load graphs for all specimens tested.

Table 4.1. Average k_0 (pci) values—equal load distribution

Dowel Type	Dowel Size	Joint Width		
		0"*	1/8"	1/2"
Round Steel	1.5	2,770,000	1,280,000	610,000
Large Elliptical Steel	2.00 x 1.375	1,280,000	510,000	540,000
Small Elliptical Steel	1.66 x 1.13	3,410,000	520,000	510,000
Round Stainless Steel	1.5	3,590,000	710,000	790,000
Round GFRP	1.875	1,100,000	340,000	400,000
Elliptical GFRP	2.25 x 1.25	1,240,000	640,000	500,000

*Cold joint

Table 4.2. Average k_0 (pci) values—adjusted loads

Dowel Type	Dowel Size	Joint Width		
		0"*	1/8"	1/2"
Round Steel	1.5	2,980,000	1,220,000	620,000
Large Elliptical Steel	2.00 x 1.375	1,280,000	640,000	560,000
Small Elliptical Steel	1.66 x 1.13	3,690,000	530,000	560,000
Round Stainless Steel	1.5	3,840,000	790,000	810,000
Round GFRP	1.875	1,190,000	360,000	410,000
Elliptical GFRP	2.25 x 1.25	1,260,000	690,000	520,000

*Cold joint

4.1.3 Effects of Joint Width

Neglecting the cold joint specimens, Tables 4.1 and 4.2 show that joint width had some effect on the value of k_0 . The values for the 0-inch joint (i.e. cold joint) are significantly greater than for the 1/8-inch and 1/2-inch joints. This difference in k_0 can be attributed to the absence of a gap. The cold joint specimens were affected by arching action taking place within the center block. The center block did not undergo an ideal vertical translation. Each end of the center block experienced a different downward deflection, causing a slight rotation within the block. The 1/2-inch and 1/8-inch gap specimens allowed enough clear space to avoid contact between the center block and the end blocks. The cold-jointed specimens resisted this rotation and contributed to large normal forces between the middle and end blocks. These normal forces caused significant frictional forces between the blocks. The addition of these unknown frictional forces reduced the amount of shear force being transferred through the dowel bars. The significantly higher values of k_0 supported the assertion that large normal forces were present in the specimens. The high normal forces would greatly reduce the deflection of the center block at a given load. When comparing two dowel specimens at equal loading, the dowel experiencing a smaller deflection has a higher k_0 value. Thus, the dowel loads measured for a given relative deflection are exaggerated and significantly increase the k_0 value. Because of this, all comparisons herein are based on 1/8-inch and 1/2-inch joints only.

The k_0 values calculated for the 1/8-inch and 1/2-inch joints were similar except for the 1.5-inch round epoxy-coated steel dowels, which exhibited much greater k_0 values for the 1/8-inch specimens than for the 1/2-inch specimens. The “ k_0 vs. load” plots (in Appendix A) for the round steel specimens also had the largest data spreads. The data did not provide hard evidence for significant differences in k_0 for 1/8-inch and 1/2-inch joint widths in terms of dowel material or shape.

There was a greater tendency for specimens with larger gaps to rotate about the dowel (i.e., for the unrestrained center block to twist while the end blocks remained restrained) during testing at higher loads and during handling of specimens after testing.

4.1.4 Effects of Dowel Shape

Of the six dowel types tested, three had circular cross sections and three had elliptical cross sections. The theory behind using elliptically shaped dowel bars is to provide a greater bearing area for the dowel on the concrete to reduce bearing stresses and more effectively transfer loads without crushing the concrete above and below the dowel. However, providing the greater bearing width of the dowel places the dowel in weak axis flexural bending.

The elliptically shaped dowel bars exhibited lower k_0 values than the circular dowels. The exception to this is the 1.875-inch diameter GFRP dowel, which exhibited lower k_0 values than any other dowel tested. The reason for this is more a matter of material properties rather than dowel shape, as will be discussed shortly.

The data show that both sizes of elliptical steel (2.00 x 1.375 and 1.66 x 1.13 inches) performed similarly in terms of k_0 .

Although the elliptically shaped dowel bars provided smaller k_0 values, they also had smaller allowable bearing stresses since they are oriented in such a way that load is transferred by weak axis bending. That is, increasing the theoretical bearing area of the dowel on the concrete by using an elliptical shape comes with the cost of using a larger dowel to provide the same flexural strength as an equivalent round dowel.

4.1.5 Effects of Dowel Material

The GFRP dowels produced lower k_0 values than the epoxy-coated steel dowels and the stainless steel dowels. This is expected since GFRP is a softer material than steel and because the GFRP dowels tested were of larger sizes than the steel dowels, providing a greater dowel–concrete bearing area to distribute the reaction. Steel has greater k_0 values for 1/8-inch joints than stainless steel, and stainless steel has greater k_0 values for 1/2-inch joints than steel because of the inconsistencies between 1/8-inch and 1/2-inch joints for the steel dowels. However, others (2) have demonstrated that steel exhibits a higher k_0 value than stainless steel.

The three steel dowel types were all epoxy coated, while the stainless steel dowel naturally was not. This soft (relative to the steel) coating around the perimeter of the dowels provides for more initial displacement at lower loads than the non-coated stainless steel dowel. The softness of the epoxy coating explains why lower relative deflections were observed for stainless steel than for a similar-sized epoxy-coated steel, even though steel has a slightly greater flexural rigidity than stainless steel. The dowel stiffness and relative deflections will be discussed in the next two sections.

4.1.6 Effects of Dowel Flexural Rigidity

Table 4.3 breaks down modulus of elasticity, the moment of inertia about the horizontal axis, and the dowel flexural rigidity, EI , for the six dowel types.

Table 4.3. Dowel properties

Dowel Type	Dowel Size, (in.)	Modulus of Elasticity, E (psi)	Moment of Inertia, I (in. ⁴)	Flexural Rigidity EI (lb-in. ² x10 ⁶)
Round Steel	1.5	29 x 10 ⁶	0.2485	7.21
Large Elliptical Steel	2.00 x 1.375	29 x 10 ⁶	0.2552	7.40
Small Elliptical Steel	1.66 x 1.13	29 x 10 ⁶	0.1176	3.41
Stainless Steel	1.5	28 x 10 ⁶	0.2485	6.96
Round GFRP	1.875	6.51 x 10 ⁶	0.6067	3.95
Elliptical GFRP	2.25 x 1.25	8.66 x 10 ⁶	0.2157	1.87

Table 4.4. Dowel flexural rigidity and k_0 comparison

Dowel Type	k_0 * (pci)	EI (lb-in. ² x10 ⁶)
Round GFRP	400,000	3.95
Elliptical GFRP	500,000	1.87
Small Elliptical Steel	510,000	3.41
Large Elliptical Steel	540,000	7.4
Round Steel	610,000	7.21
Stainless Steel	790,000	6.96

*For 1/2" joint unadjusted loading

Table 4.4 suggests that as EI of the dowel bar increases, k_0 increases. The discrepancies in Table 4.4 were assumed to be caused by external factors. The first issue is the softness of the GFRP material compared to steel. The GFRP was more likely to experience small localized deformation at the location of the joint due to the high stresses caused by the concrete edge of the joint. The epoxy coating on the round steel bars is another example of softer materials undergoing localized deflections. This table is for 1/2-inch joint width so that flexural activity across the joint is maximized for the comparison of stiffness.

4.1.7 Dowel Deflection

Tables 4.5 through 4.8 show the average relative deflections (measured), shear deflections (Equation 3.5), and displacements (Equation 3.6) at the joint face for the six dowel types. Tables are shown for both 1/8-inch and 1/2-inch joints and for a small (2 kip) and large (10 kip) loads.

Tables 4.5 through 4.8 show that the stainless steel and large elliptical steel dowels were better at limiting overall displacement. However, the additional flexural rigidity leads to greater bearing stresses between the dowel and concrete, especially for round dowels like the stainless steel dowels. Round FRP and small elliptical steel dowels did not perform as

well as the others in limiting displacement because they have lower dowel flexural rigidity and narrower bearing areas.

Table 4.5. Average deflections—2 kip loading, 1/8-inch joint

Dowel Bar	Average Δ , in.	Average δ , in.	Average y_0 , in.
Round GFRP	0.005794	0.000039	0.002877
Elliptical GFRP	0.005118	0.000037	0.002541
Large Elliptical Steel	0.006573	0.000012	0.003281
Small Elliptical Steel	0.006441	0.000017	0.003212
Round Steel	0.003534	0.000015	0.001760
Stainless Steel	0.004502	0.000015	0.002243

Table 4.6. Average deflections—2 kip loading, 1/2-inch joint

Dowel Bar	Average Δ , in.	Average δ , in.	Average y_0 , in.
Round GFRP	0.006965	0.000162	0.003401
Elliptical GFRP	0.006340	0.000146	0.003097
Large Elliptical Steel	0.005274	0.000045	0.002615
Small Elliptical Steel	0.008616	0.000065	0.004276
Round Steel	0.004368	0.000055	0.002157
Stainless Steel	0.003314	0.000058	0.001628

Table 4.7. Average deflections—10 kip loading, 1/8-inch joint

Dowel Bar	Average Δ , in.	Average δ , in.	Average y_0 , in.
Round GFRP	0.032065	0.000195	0.015935
Elliptical GFRP	0.019268	0.000182	0.009543
Large Elliptical Steel	0.016194	0.000057	0.008068
Small Elliptical Steel	0.022264	0.000084	0.011090
Round Steel	0.022447	0.000070	0.011188
Stainless Steel	0.018396	0.000073	0.009162

Table 4.8. Average deflections—10 kip loading, 1/2-inch joint

Dowel Bar	Average Δ , in.	Average δ , in.	Average y_0 , in.
Round GFRP	0.028660	0.000773	0.013944
Elliptical GFRP	0.026095	0.000733	0.012681
Large Elliptical Steel	0.016064	0.000229	0.007918
Small Elliptical Steel	0.032607	0.000337	0.016135
Round Steel	0.022575	0.000267	0.011154
Stainless Steel	0.018402	0.000297	0.009052

4.1.8 Bearing Stress

The bearing stress at the face of a joint is the product of k_0 and y_0 . The allowable stresses (see Section 3.3) for each dowel bar type are presented in Table 4.9.

Table 4.9. Allowable stress and load at which allowable stress is exceeded

Dowel Type	Allowable Stress, psi*	Load (lbs)
Round Steel	4583	6000-8500
Large Elliptical Steel	3666	7000-8000
Small Elliptical Steel	4290	6500-8500
Stainless Steel	4583	6000-8000
Round GFRP	3895	6500-8000
Elliptical GFRP	3208	5000-6000

*Per ACI Committee 325 [24]

Note: $f_c' = 5500$ psi

The last column in Table 4.9 shows the range of loads for each dowel type when the allowable bearing stress was reached during testing, that is, when σ_b (Equation 3.7) equals σ_a (Table 4.9).

Tabatabaie's load distribution model (see Section 2.5) for a 18 kip axle load (9 kip wheel load) can be used to determine the maximum load a dowel will see in a slab joint by assuming the following extreme conditions:

- Wheel load is applied directly over dowel at edge of slab (reducing the number of effective dowels)
- Relatively large spacing (18 inches)
- Concrete strength $f_c' = 4000$ psi and slab thickness of 8 inches
- Load transfer efficiency of 100% (i.e., no load distributed to subgrade)

In this case (see Figure 4.1), the maximum dowel load $F_{c1,2}$ is about 7000 pounds. Therefore, all six dowel types should perform adequately in terms of bearing stress in normal conditions. Moreover, even for this extreme case, the assumption that no load is distributed to the subgrade more than doubles the maximum dowel load.

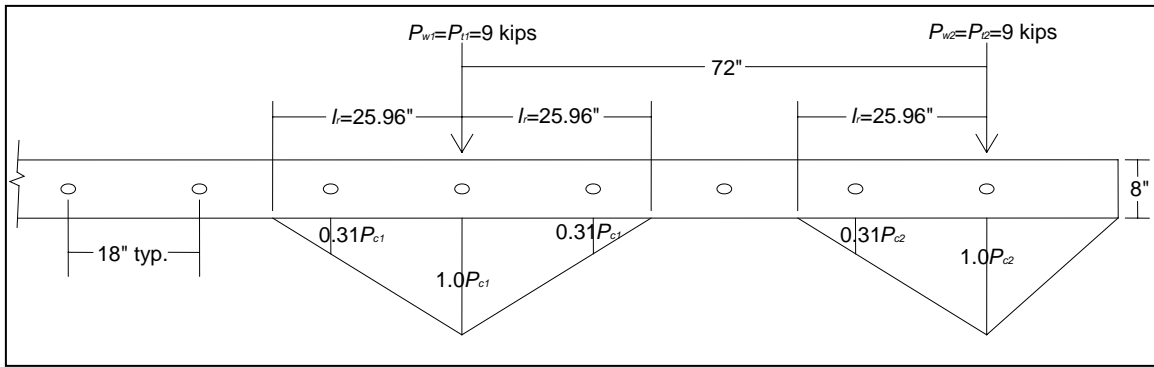


Figure 4.1. Tabatabaie load distribution for extreme case

4.1.9 Concurrent Dowel Research

In addition to the round and elliptical dowels of steel, stainless steel, and GFRP studied in this project, there was research being conducted concurrently (30) on dowels with building floor-slab application. These dowels were of much smaller sizes and of no application to highway joint-load transfer. They do, however, provide information on rectangular-shaped dowels. Three different rectangular cross sections (4.50 x 0.25, 6.36 x 0.25, and 2.00 x 0.375 inches) and one round cross section (0.75-inch diameter)—all made of steel—were analyzed. Although all four dowels exhibited similar load-deflection data, the rectangular dowels had lower bearing stresses than the round dowel.

Achieving good concrete consolidation beneath the flat surface of the rectangular dowels is more difficult than beneath the round dowels. Rectangular dowels require much more cross-sectional area than round dowels (although not as much embedment length is required to meet the $L_e = \beta L > 2$ requirement). Just as stress concentrations occur at the bottom and top of round dowels, stress concentrations also occur at the corners of rectangular dowels (2).

Using rectangular dowels as an alternative to round dowels does provide similar displacement resistance and reduces bearing stresses. However, stress concentration (2) and concrete consolidation issues exist. Even when concrete consolidation under dowels was addressed during test specimen construction, there were still instances of voids under rectangular dowels accounting for up to 40% of the dowel footprint. Even more voids should be expected in actual construction where the problem is not addressed like it is in the lab.

4.2 Strain Gages

Nine of the modified AASHTO T253 test specimens were equipped with strain gages. Both dowels in each specimen were installed with twelve strain gages each. Figure 4.2 shows the placement of the strain gages. Figure 4.3 shows two dowels with strain gages prior to concrete placement.

The following is a list of specimens with strain gages:

- 1.5-inch diameter steel with 0-inch joint
- 1.5-inch diameter steel with 1/2-inch joint
- Large elliptical steel with 1/2-inch joint
- Small elliptical steel with 1/2-inch joint
- 1.5-inch diameter stainless steel with 1/8-inch joint
- 1.875-inch diameter FRP with 0-inch joint
- 1.875-inch diameter FRP with 1/8-inch joint
- Elliptical FRP with 1/8-inch joint

(Note: there was also one small elliptical steel with 0-inch joint specimen that had strain gages installed but provided unusable data.)

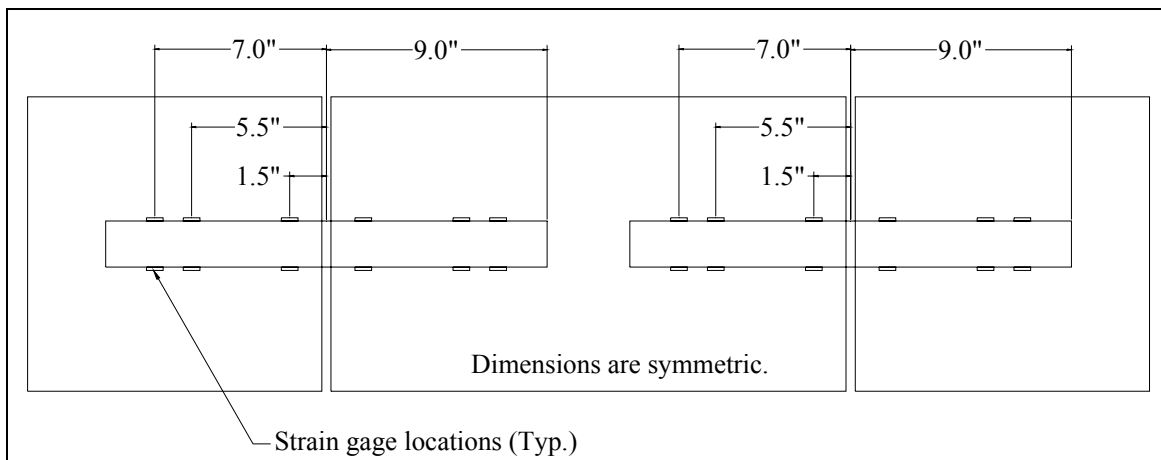


Figure 4.2. Strain gage placement

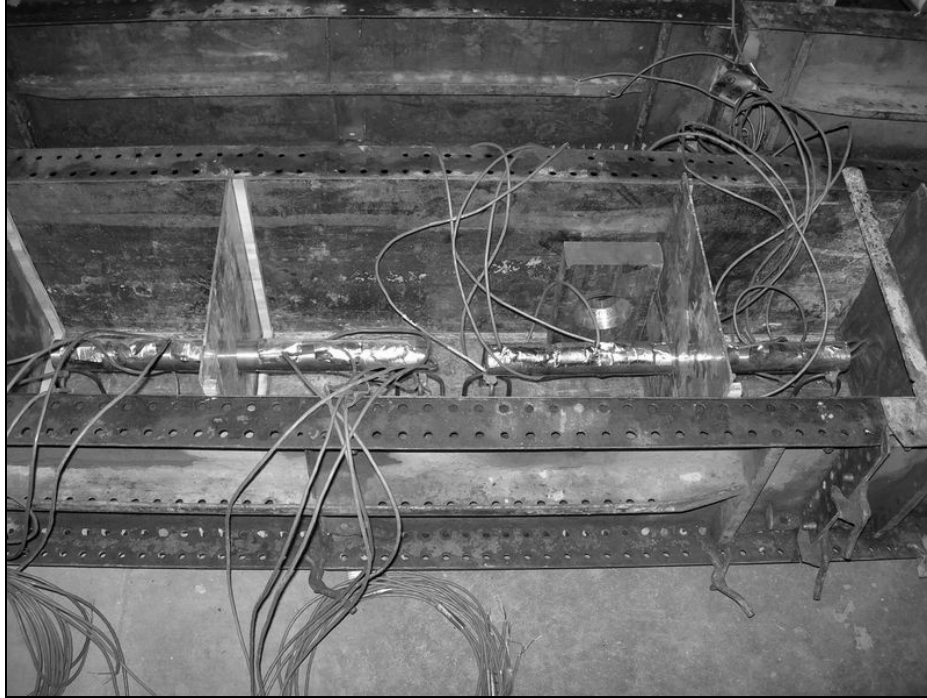


Figure 4.3. Two stainless steel dowels with strain gages set in concrete forms

The strain gages are wired into the same data acquisition system as the DCDTs so that load, deflections, and strains are read simultaneously. The strain readings are used to determine the moment using Equation 3.12. These moments can be plotted and compared to the theoretical moments based on Equation 3.10.

The strain gage moment plots are created assuming zero moments at the ends of the dowels and a moment, M_0 , at the face of the joint. Figures 4.4 and 4.5 show plots of strain-gage-measured moment versus theoretical moment along a 1.5-inch diameter epoxy-coated steel dowel specimen with 1/2-inch joints. Both the measured and the theoretical plots are determined using the measured k_0 value for each specimen.

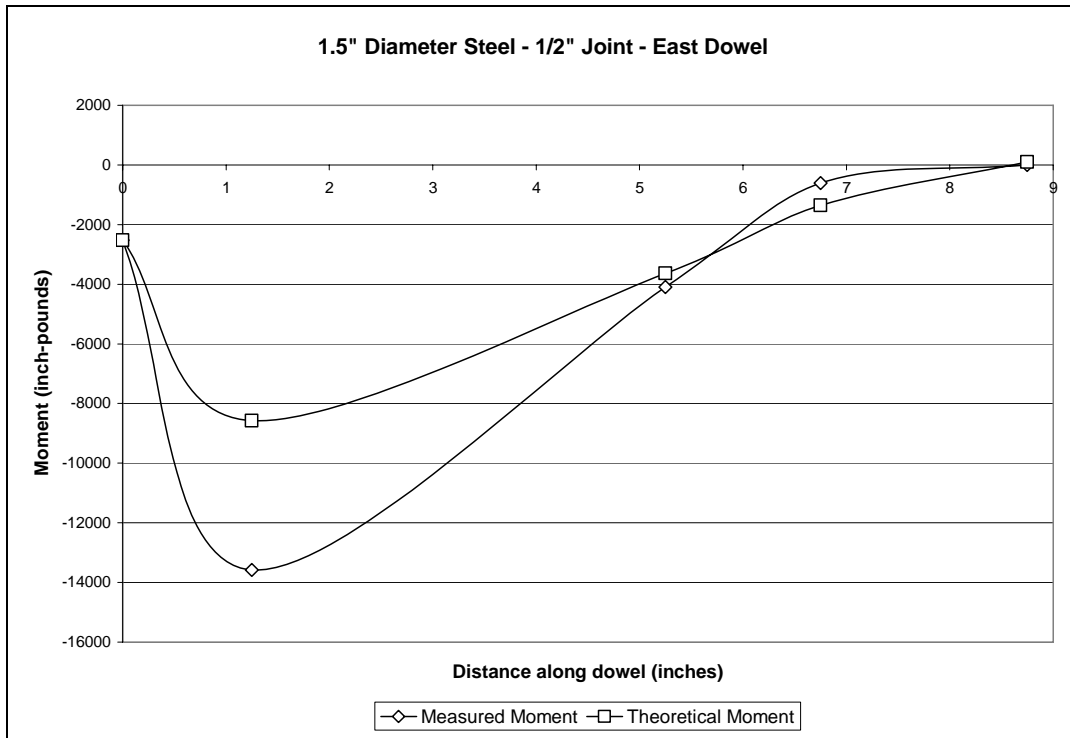


Figure 4.4. Moment diagram, 1.5-inch diameter steel, 1/2-inch joint, east dowel

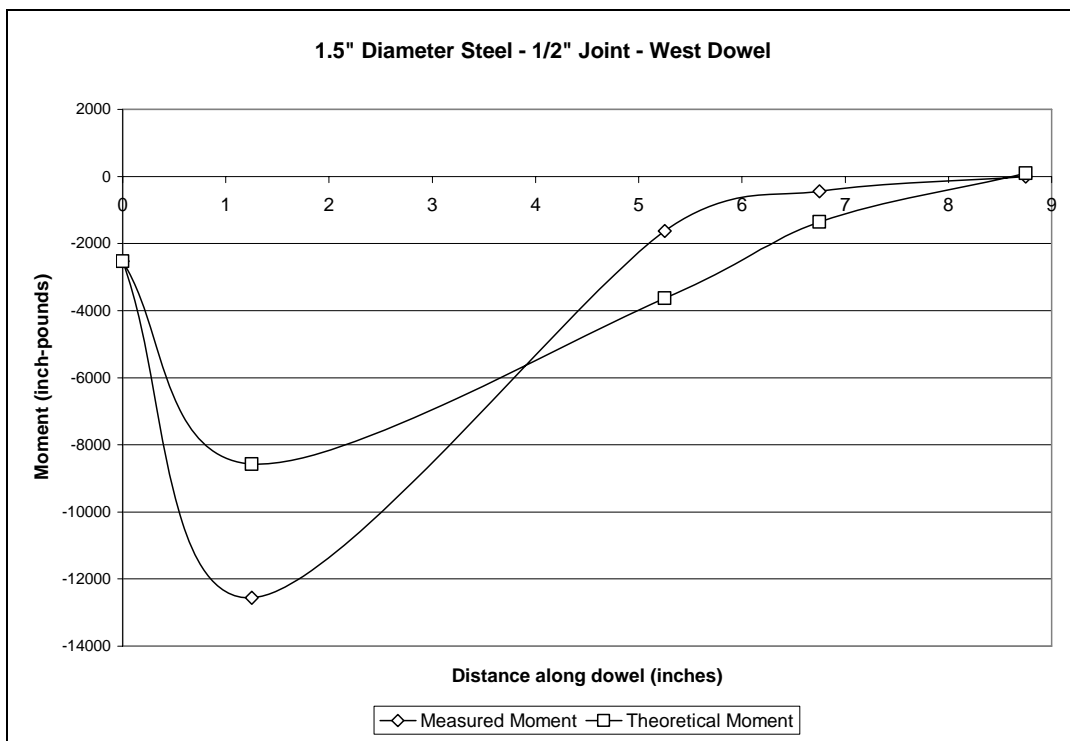


Figure 4.5. Moment diagram, 1.5-inch diameter steel, 1/2-inch joint, west dowel

Figure 4.6 shows a dowel displacement diagram based on Equation 3.9 for the 1.5-inch diameter steel specimen with 1/2-inch joint.

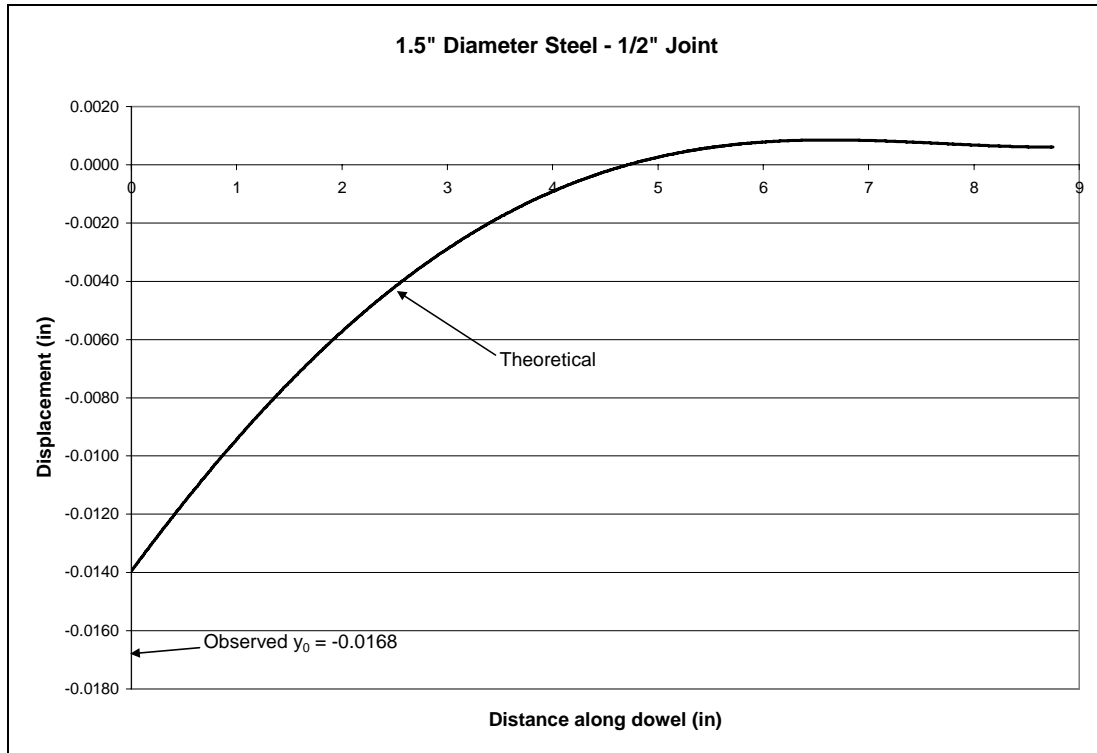


Figure 4.6. Dowel displacement diagram, 1.5-inch diameter steel, 1/2-inch joint

Appendix B contains representative moment diagrams for all the strain-gage-equipped specimens. The moment diagrams are for various arbitrary loads that occur within the linear region of the load-deflection plot. Typically, 10 kip loads are used to maximize moment action in the dowel for the strain gage readings.

The strain gage readings for the different dowels show that the actual moment diagram follows a similar shape as the theoretical moment diagram. The following observations were also made:

- The moments observed from the gages 1.5 inches from the center of the dowel were less than the theoretical moments for 13 of the 16 dowels.
- The gages furthest from the center of the dowel (7 inches) usually read values close to zero and were closer to zero than the theoretical for 11 of 16 dowels.
- Reviewing the moment diagrams for each specimen does not show any pattern for or against the theoretical moments (i.e., the actual moment diagrams are not collectively similar to each other while being different from theoretical).

There are many factors that could influence the slight discrepancies between the observed and theoretical moments. The moments in the dowel at the face of the joint and the end of the dowel are assumed to be M_0 and zero, respectively, when developing the moment diagram using the strain gages. These moment value assumptions are based on the

assumption that an inflection point occurs at the center of the dowel (and center of the joint). The strain gage data from gages closest to either side of the joint show that the moments are not symmetrical about the center of the dowel. Thus, the value M_0 at the face of the joint is incorrect. Finite element analysis has also shown that the assumption that the inflection point is located at the center of the joint is incorrect (18).

Since the moments at opposite faces of a joint are not equal, then it is likely that y_0 at either face is not equal either. But as far as the modified AASHTO test goes, this is not a major concern because y_0 is determined from the relative deflection, which takes into account two y_0 terms that are essentially averaged to find a representative y_0 value to use to determine k_0 .

The theoretical y_0 for the 1.5-inch diameter steel dowel with 1/2-inch joints shown in Figures 4.4 and 4.5 is 0.014 inch. The observed y_0 determined from the relative deflection and averaged for the two dowels was 0.017 inch. Table 4.10 shows the observed and theoretical y_0 values for each of the strain gage specimens (typically for a 10 kip load).

Table 4.10. Observed and theoretical y_0 values

Dowel Type	Joint Width, in.	Observed y_0 , in.	Theoretical* y_0 , in.
Round Steel	0	0.004	0.004
Round Steel	1/2	0.014	0.017
Large Elliptical Steel	1/2	0.006	0.008
Small Elliptical Steel	1/2	0.020	0.027
Round Steel	1/8	0.005	0.006
Round GFRP	0	0.006	0.006
Round GFRP	1/8	0.022	0.023
Elliptical GFRP	1/8	0.015	0.010

*Equation 3.9

The observed y_0 values were similar to the theoretical y_0 values. The largest differences occurred for the small elliptical steel and elliptical GFRP specimens, which both exhibited significantly unsymmetrical loading.

Appendix C shows the theoretical displacement diagrams for the eight strain gage specimens with the observed joint face displacement.

4.3 Cantilever Test

The results of the cantilever test were expected to be more consistent than those obtained during the modified AASHTO test. The reasons for the positive prediction were as follows:

1. Instrumentation was used to directly measure y_0 at the face of the block. This was supposed to eliminate the potential errors caused by calculating it relative to measured block displacements.
2. Only one bar was used. The presence of only one bar allowed the investigators to know the exact load being carried by the dowel bar. The single bar also took out the possibility of a rotating load caused by an unstable middle block like in the modified AASHTO test. The two-bar construction of the modified AASHTO specimens required the bars to be perfectly collinear to avoid load eccentricity.
3. Fewer instruments were needed to measure block displacement.
4. The bar was placed more consistently during construction. Leveling the dowel bar was made easier because half of it was exposed.
5. The bar was positioned vertically during concrete placement. This placement ensured uniform concrete consolidation around all surfaces of the bar. Consolidation was initially a concern with the elliptical bars but later proven not to be a problem.
6. The specimens were smaller, lighter, and contained fewer components. The specimens were less vulnerable to damage during storage and transport. The lighter blocks also eliminated the need for a crane to move and set the blocks.

The cantilever test was not an effective alternative to the modified AASHTO test. The k_0 results obtained from the cantilever test were inconsistent and not accurate with respect to the current accepted ranges of k_0 values. There are many reasons why the cantilever test was not as effective as the modified AASHTO test.

The first variable was the length of the block. A short clamping distance from the block's point of rotation allowed the block to be vulnerable to unwanted movement during the test. The large moment produced by the increased distance from the joint face to the applied load required larger clamping forces to restrain the block. Lack of uniform tensile forces among the four Dywidag rods caused greater vulnerability to eccentric rotation. The increased clamping forces required to restrain the block created indeterminate normal forces on the dowel within the concrete, thus changing the expected behavior of the dowel.

The next issue was the precision of the instrumentation. A string transducer was used and wrapped around the base of the dowel. This was done in order to gauge the deflection of the bottom surface because the top of the dowel would theoretically deflect more due to shear deformation. The bottom deflection was measured rather than the top deflection because the aim of this experiment was to directly measure y_0 instead of calculating it relative to other deflections. The initial test was run with the string transducer and gave optimistic results. The load-deflection curve was linear and the deflections appeared to be

consistent with other specimens of the same dowel type. The remaining tests were run under the assumption that results would be consistent.

Displacement of the bottom beam supporting the steel base plates was also an unknown factor. There were movements within the beam, although small, that could have had a confounding effect on the results obtained. The beam did not appear to have an effect on the results of the modified AASHTO test, so it was assumed that the beam would be adequate for the cantilever test since the load used in the modified AASHTO test was reduced by more than half for the cantilever test. Both steel base plates were checked with a level before the cantilever test was conducted. The plates were both level in the parallel and perpendicular direction of the test dowel.

The placement of the load on the dowels did not appear to be a negative factor in the cantilever test. The load was applied to each dowel through a steel bracket machined to its specific shape.

Because of the highly erratic nature of the data obtained, the precision of the instrumentation and the increased clamping force demand appear to have been the main reasons why the results are not satisfactory.

A slightly modified version of the theory used in the modified AASHTO test was used in the cantilever test. The main modification was that the load was applied directly to the dowel 2.5 inches from the concrete face. This load distance replaced the gap width parameter in Equation 3.3. It also included the vertical displacement due to flexural effects because of the significant moment applied to the dowel bar. This width was the distance from the face of the concrete to the inside face of the loading bracket. The k_0 results from the cantilever procedure were significantly different than those obtained from the modified AASHTO test. Plots showing k_0 versus load are displayed in Appendix D.

4.4 Fatigue Tests

The fatigue test yielded largely inconclusive results. The goal of the fatigue test was to qualitatively observe the long-term deterioration of the concrete surrounding the dowel bar. Because time and budget were constraining factors with regard to this test, the loads were much higher than those normally seen in concrete pavements. The number of cycles was also greatly reduced from the millions applied to a pavement over an extended period of time.

Initially, the block was set and loaded with 5000 cycles at 20,000 pounds with a frequency of 1Hz. The data output file was plotted and observed. There did not appear to be any increased deterioration of the dowel hole. The number of cycles was doubled to 10,000. This showed only slightly larger deformations. The load was then increased to 22,000 pounds. This increased the deflections, but the block experienced shear failure at the dowel long before the 10,000 cycles were reached. The load was then dropped back down to 20,000 pounds. The specimens were tested and their minimum and maximum deflections were plotted. These plots are shown below in Figure 4.10.

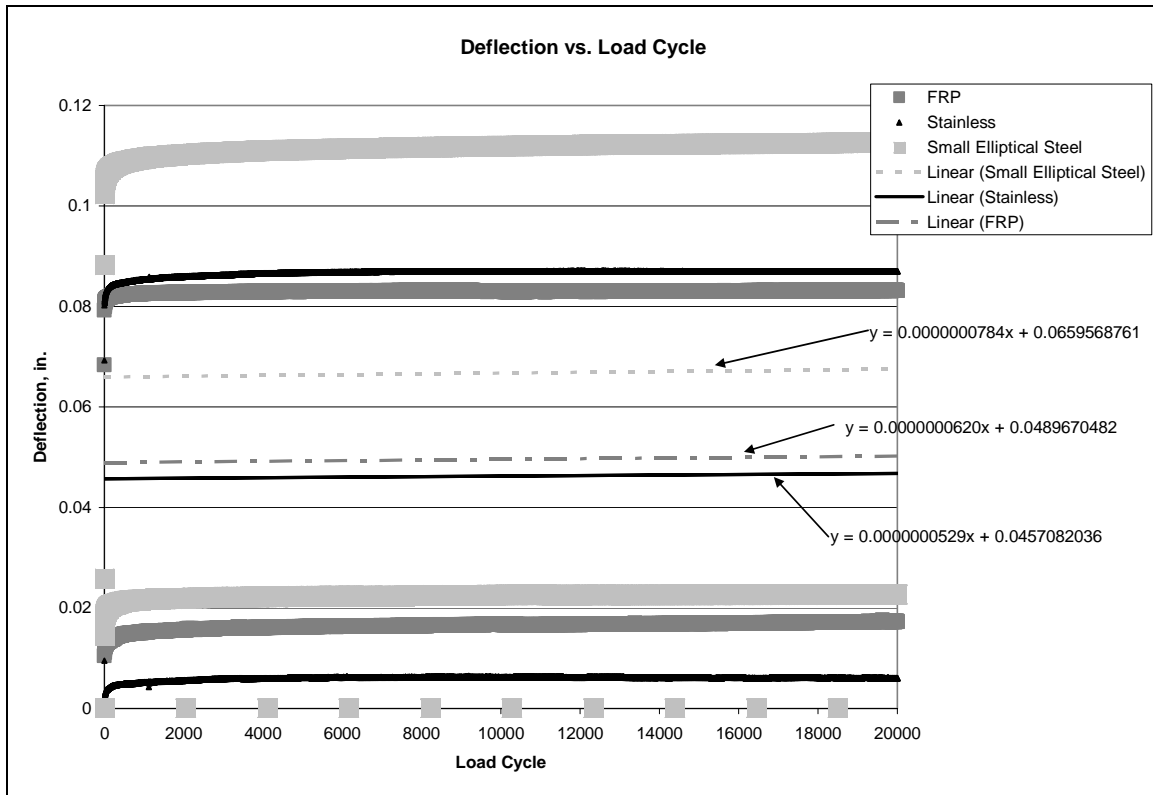


Figure 4.7. Fatigue test minimum and maximum deflections

The slope of each linear-fit equation in Figure 4.7 shows the increase in deflection over time. The results show different outcomes than the ones expected. The stainless steel bar was expected to apply the most damage on the concrete after the cyclical loading. Stainless steel has the highest value of k_0 and should inflict the greatest amount of bearing stress on the surrounding concrete. The slope values of round GFRP and small elliptical steel are very close to one another. This result appears reasonable because there is not a large difference in the k_0 values between the two bar shapes.

Because of the limited number of cycles and exaggerated load values, this fatigue test does not allow an accurate comparison to the millions of wheel loads seen by an actual concrete slab. The blocks were dismantled following the fatigue tests to observe the surrounding concrete after the repeated loading. While a fine white powder was found in the dowel holes, there were no visible elongations in the dowel holes.

A specimen containing old strain gauges was also tested to observe fatigue behavior. The strain gauges were covered in foil tape and a thin layer of butyl rubber, so their results are not comparable to the ones obtained from the other tests. The gauged specimen was loaded at the higher value of 22,000 pounds because the butyl rubber around the gauges acted as a cushion between the bar and concrete. The reason for using the gauged specimen was to elongate a dowel hole without causing a shear concrete failure. The presence of the gauges and surrounding material allowed greater dowel deflections and yielded localized spalling and elongation of concrete holes around the dowel.

The results of this test were limited to a small-scale qualitative assessment. A future dowel project should focus on the fatigue behavior of the dowel bars on concrete. The test should involve a more compact dowel specimen to allow the use of a more sophisticated fatigue test machine. It should also apply a load more comparable to a wheel load. The load should be applied in millions of cycles in order to more accurately model the performance of a dowel over the useful life of a pavement.

4.5 Loss on Ignition Results for GFRP Dowels

The ignition loss of cured reinforced resins (ASTM D 2584-02 (31)) results for the two GFRP dowel specimens were

- Elliptical–24.83% weight loss
- Round–31.75% weight loss

This test determines the ratio of resin to fiber by weight of the GFRP dowels.

5. SUMMARY OF PERFORMANCE

The laboratory tests yielded mixed results. General bearing stress behavior was demonstrated with the modified AASHTO test and the trends obtained were similar to those expected.

5.1 Modified AASHTO T253

The modified AASHTO test specimens yielded scattered results but were more consistent than those numbers obtained during the cantilever test. On some specimens, the middle block experienced rotation about the dowels at higher loads.

The modified AASHTO specimens also contained strain gages on some of the specimens. The gages were placed inches away from the joint, but had an effect on the bearing behavior of the bar within the concrete. The presence of the gage wires, butyl rubber, and foil tape within the specimen presented confounding variables that were not quantifiable. Each strain-gaged dowel had a different amount of butyl rubber and foil tape. The gage wires were also varied among the specimens.

5.2 Cantilever Test

The cantilever test was less reliable than the modified AASHTO test and less reliable than predicted. Although y_0 was measured directly, other factors had an effect on the test results. The base support beam experienced small deflections. The large moments increased the demand for a more sophisticated clamping mechanism. The clamping method applied to this test allowed undesirable effects such as large normal forces on the dowel and small, unpredictable rotations.

5.3 Fatigue Test

The fatigue test was inconclusive in demonstrating which dowel bar will cause the least deterioration after a long period of time. The scope and budget of this project did not allow for an adequate number of cycles to be applied to the specimens. The use of the modified AASHTO specimens presented difficulties regarding a proper test apparatus. Both the modified AASHTO and cantilever specimens were too large or eccentric for the optimal fatigue test machine. The procedure used for this test allowed only for a qualitative observation of fatigue over time. The test recorded deflections from the test specimen and the load frame as well. The base beam which supported the blocks also experienced some movement.

6. FUTURE NEEDS AND IMPLEMENTATIONS

Whereas tests conducted during this experiment provided good information resulting from the modified AASHTO test, improvements are still desired in order to obtain more precise results for calculation of k_0 . After performing the modified AASHTO, cantilever, and fatigue tests, certain observations were made in order to improve future dowel test procedures.

6.1 Modified AASHTO T253

A revised version of the modified AASHTO T253 specimen is recommended for future testing of dowel bar bearing stresses. The proposed modified specimen is shown below in Figure 6.1. All units shown below are in inches.

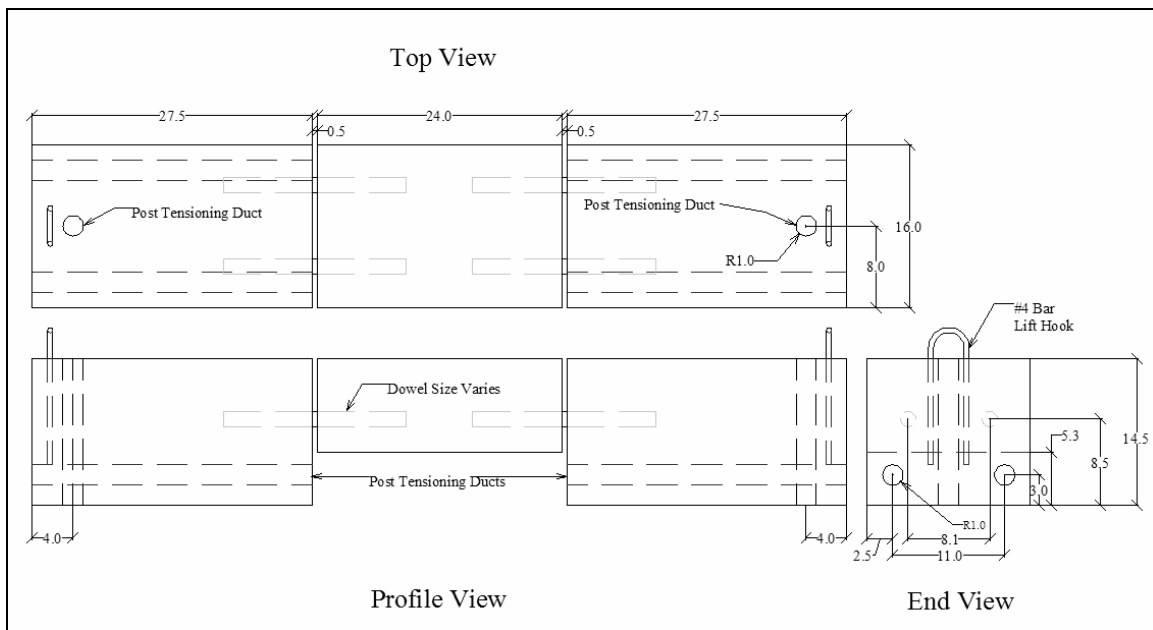


Figure 6.1. Proposed revised modified AASHTO specimen

The possibility of block rotation would be reduced with the addition of at least one more line of dowels. For greater ease of load calculation per dowel, a four-bar specimen is recommended for future tests. This configuration would be much more economical and simple than a full-scale slab test. Although the three-block model still poses the possibility of uneven deflections at each joint, the researchers found that simply dividing the load in half did not significantly affect k_0 results, provided that the possibility of uneven deflection was controlled.

The joint width should be kept at 1/8 inch for a modified test. The 1/2-inch joint yielded the most consistent results, but as Table 4.1 and Appendix A show, they were not significantly different from the 1/8-inch gap. The 1/8-inch gap specimen provides for a

closer proximity to actual pavement joint widths. The cold joint did not allow the dowels to carry all of the applied load in shear. As mentioned earlier, the cold joints experienced significant “arching action” and carried high compressive stresses while the center block was loaded. The cold joint specimen is not recommended for future study. In addition to the 1/8-inch gap, a wider gap of one inch or greater should be investigated to observe dowel behavior within a control joint.

The load shall be applied as two linear loads spanning perpendicular to the dowel bars at the joint locations. This application method produced limited rotation effects and allowed for adequate load distribution estimation.

A staggered block design (Figure 6.1) would eliminate the need for steel baseplates to be used on the testing surface. The staggered block would allow direct placement and post-tensioning on the reaction floor or test frame. The new proposed block design will be larger than the current blocks used in this report. At each joint, the two dowel bars shall be placed 12 inches apart on center. The bars will have additional 6 inches of concrete on their outside edges in order to simulate an incremental piece of a full highway slab.

The new test will also need to include tension ties between the two end blocks. The tension ties will serve two purposes. The first use is to protect the specimen from damage while moving with an overhead crane. The second purpose of the tension ties is to restrain end block rotation during the load test. The block shown previously in Figure 6.1 is designed to be post-tensioned to a floor with 3-foot spaces between tie-down holes.

The tension tie must only be tightened to a nominal force of roughly 200 pounds. The bars need only act as regular reinforcement and not as a prestressed tendon. Any reverse moment effect of the tension ties due to excessive tensioning will distort results.

The end blocks shall be post-tensioned to the load floor or test frame with a force of 4000 pounds in each end block. A rough analysis performed on the proposed block found that the force of 4000 pounds per side would be more than adequate to support the middle block loading.

6.2 Cantilever Test

The cantilever test was much more vulnerable to block rotation due to the large couple produced when the dowel bar was loaded directly. Verification of this test is required before it can be accepted as an adequate tool to test for k_{θ} . A possible solution to this is to cast a longer cantilever specimen with a hole at the end of the block in order to allow the block to be post-tensioned down to the loading floor. Post tensioning would greatly reduce the chances of block rotation during the test. The location of the tie-down hole allows the post-tensioning without adding excess compressive stresses on the embedded dowel. An example of this proposed test specimen is shown below in Figure 6.2.

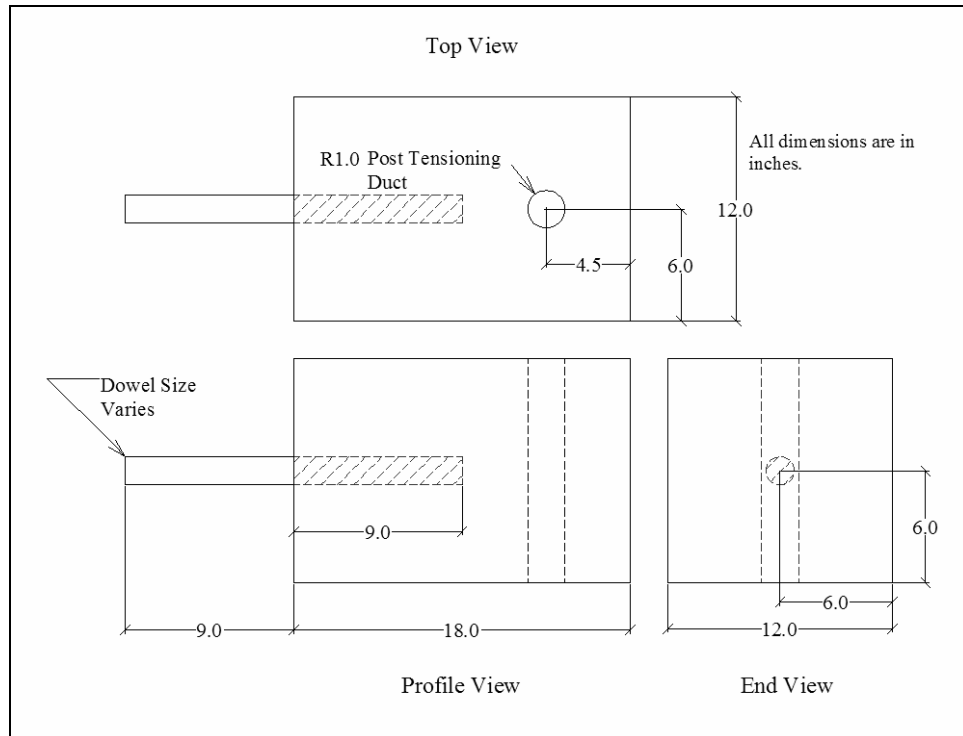


Figure 6.2. Proposed cantilever dowel specimen

The specimens would be better suited to be cast horizontally instead of vertically because of the addition of the tie-down hole. The vertical casting ensured more optimal concrete consolidation, but consolidation is not a concern with the round and elliptical dowel shapes used in the modified AASHTO specimens.

6.3 Fatigue Test

The fatigue test requires significant modification to yield more conclusive results. The first problem with using the modified AASHTO specimens was the size. The test specimens were too long to place in the MTS machine shown below in Figure 6.3.

The length of the specimens would have caused too much eccentricity during the fatigue test. The eccentricity causes a risk of damaging the testing machine.

The frame used during the fatigue test described in this report allowed many deflections during the test. The transducer used to measure deflection during the test was located within the load actuator. Because of its location, the transducer measured the deflection of the test specimen and the upward deflection of its suspension beam.

The test would be more suited for the MTS machine. The apparatus allows the specimen to be bolted down securely. The MTS machine output would record only the deflection of the center block of the specimen. In order to use the MTS machine, a different elemental fatigue specimen needs to be designed.

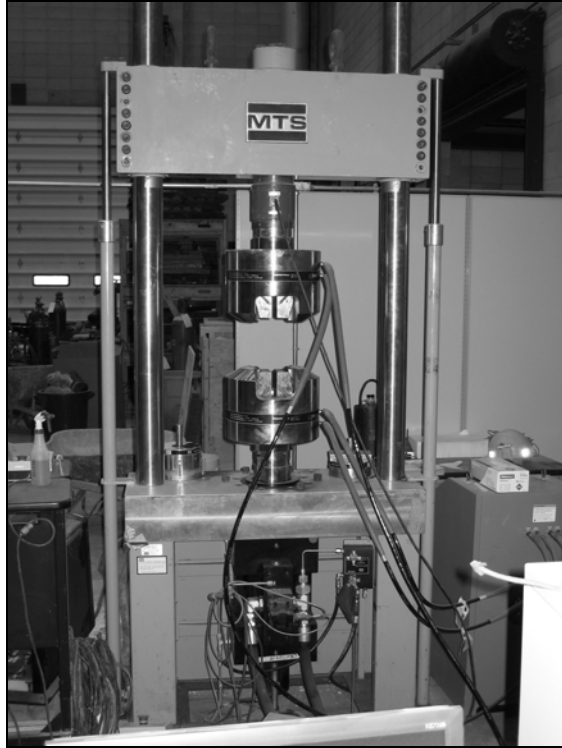


Figure 6.3. MTS fatigue testing machine

The fatigue specimen shall consist of three concrete panels connected with two dowel bars. The dowel bars are located parallel to one another. The recommended fatigue specimen is shown below in Figure 6.4.

Figure 6.4 shows a specimen that will be used for a qualitative analysis of joint fatigue and not a quantitative analysis of k_0 . A fatigued, damaged joint violates the necessary initial conditions in the determination of k_0 . The equations used to calculate k_0 are based on the fact that the beam is resting perfectly on an elastic foundation. When the surrounding concrete is eroded away, the bar is no longer supported uniformly by the concrete. Although specific values of k_0 cannot be correctly determined from this procedure, it offers valuable information. The reason to calculate k_0 is to determine the bearing stress a bar will produce when deflected. The initial k_0 values shall be calculated and the fatigue test will serve as a verification of each value. Specimens undergoing greater deflection and oblonging over time will theoretically have a higher k_0 value.

This specimen eliminates the excessive eccentricity associated with the modified AASHTO test. With the use of the MTS machine, the specimen can be bolted down securely to a fabricated steel plate apparatus. The steel plate is secured to the MTS machine and a quantitative fatigue analysis can be executed in order to see how much a dowel hole is elongating. The fatigue test will involve cyclical shear deformations controlled by the amount of shear force placed on the dowel. This will cause increased deflections as the number of load cycles increases given a fixed load. The clamping and shear forces applied by the MTS machine are illustrated below in Figure 6.5.

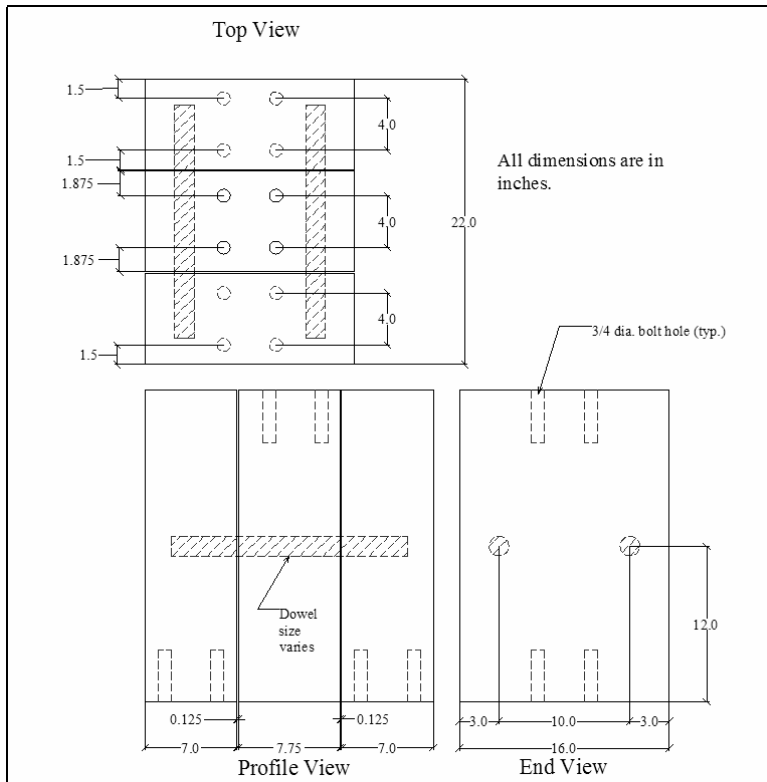


Figure 6.4. Recommended revised fatigue specimen

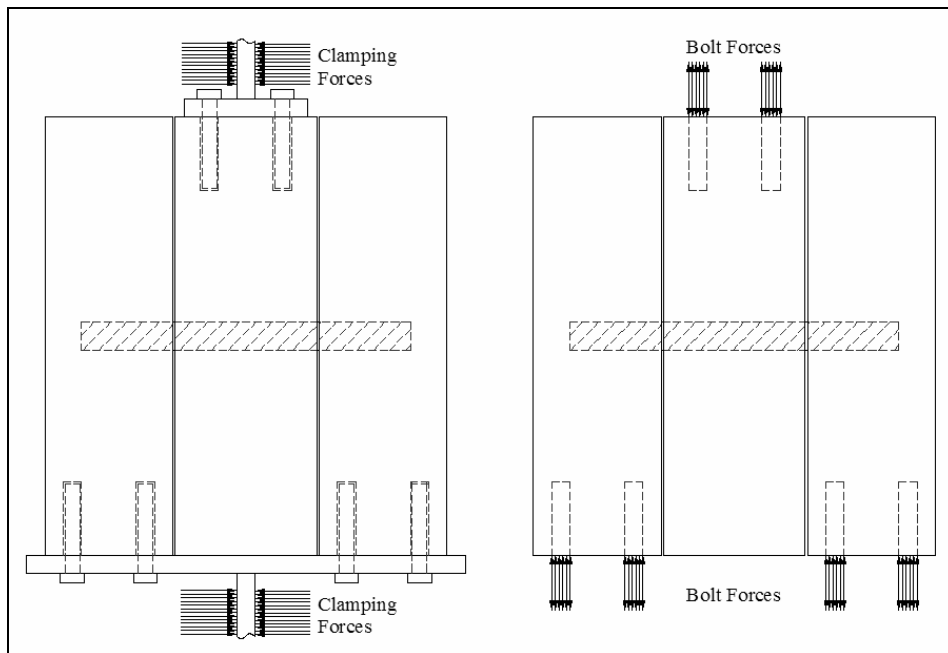


Figure 6.5. Free body diagrams of proposed fatigue specimen

This machine would provide more reliable results than simply observing incremental changes in deflection during a consistent load cycle. The deflections will be accurately quantified with their corresponding shear loads.

6.4 Full Slab Test

The modified AASHTO test is a relatively economical method for determining a value of k_0 , but does not accurately replicate actual roadway conditions. Another future recommendation is to build a replica of an actual pavement over a soil subbase in a controlled environment in order to observe and closely monitor dowel behavior in a more realistic setting.

7. SUMMARY AND CONCLUSIONS

Altogether, 78 full-sized dowels were tested in this study. The major objective was to investigate and improve the current AASHTO T253 test method for determining the modulus of dowel support, k_0 . The modified AASHTO test procedure was examined alongside an experimental cantilever dowel test. The modified AASHTO specimens were also subjected to a small-scale fatigue test in order to simulate long-term dowel behavior with respect to concrete joint damage. Loss on ignition tests were also performed on the GFRP dowel specimens to determine the resin content percentage.

The modified version of the AASHTO test used in this study was an improvement over the current standard. The replacement of one linear load parallel to the dowels with two linear loads parallel to the joint allowed for greater direct shear behavior. The modified loading condition also allowed for a simpler, more reliable application of shear forces to the dowels. The end block support used in the modified test was more reliable than in the standard test which was implemented in the previous ISU laboratory study (2). The previous test method allowed too much end block rotation due to the orientation of the support beams. The new test transferred the end block couples about the major axis of the support beam. The AASHTO standard needs to be modified in order to specify the support conditions at the end blocks of the test specimen to mitigate unwanted end block rotation.

Though it needs further improvement, the modified AASHTO test procedure yielded the best results for determining the modulus of dowel support, k_0 , using Timoshenko's model of a beam on an elastic foundation (20). The k_0 values obtained from the modified AASHTO procedure were consistent with the predicted behavior of each dowel bar. Although some differences are apparent in the calculated k_0 values, the bars are not significantly different from one another in terms of performance. This conclusion is consistent with the field study conducted recently at ISU (16). All bars performed adequately under the loading conditions.

Even though the data obtained from the modified AASHTO test were scattered, the overall performance of the modified test is an improvement over the older methods used in previous research.

The cantilever specimen test did not adequately produce results that would make it a viable alternative to the modified AASHTO test. The cantilever test requires extensive revisions in order to be used as a verification tool to determine k_0 .

Future studies need to be conducted to determine the long-term performance of GFRP while exposed to salt solutions. Static tests have shown that, although there are some differences among steel, stainless steel, and GFRP and between circular and elliptical dowels, the dowels tested all perform adequately. Hygroscopic testing of GFRP dowels should be used to determine the effects of swelling on joint behavior. In addition, the long-term performance of GFRP should be compared to epoxy-coated steel with respect to repeated exposure to alkali deicing solutions and stormwater.

REFERENCES

1. Davis, D.D. "Fatigue Behavior of Glass Fiber Reinforced Polymer Dowels." Master Thesis. Iowa State University, 1999.
2. Porter, M.L., R.J. Guinn, Jr., A.L. Lundy, Dustin D. Davis, and John G. Rohner. *Investigation of Glass Fiber Composite Dowel Bars for Highway Pavement Slabs: Final Report*. Iowa Highway Research Board Project TR-408. Ames, Iowa: Engineering Research Institute, Iowa State University, June 2001.
3. Porter, M.L., B.W. Hughes, K.P. Viswanath, and B.A. Barnes. *Non-Corrosive Tie Reinforcing and Dowel Bars for Highway Pavement Slabs: Progress Report*. Iowa Highway Research Board Project HR-343. Ames, Iowa: Department of Civil and Construction Engineering, Iowa State University, January 1993.
4. Porter, M.L., E.A. Lorenz, K.P. Viswanath, B.A. Barnes, and M. Albertson. *Thermoset Composite Concrete Reinforcement: Final Report—Part II*, Project HR-325. Ames, Iowa: Engineering Research Institute, Iowa State University, October 1992.
5. Hughes, B.W., and M.L. Porter. *Experimental Evaluation of Non-Metallic Dowel Bars in Highway Pavements*. Proceedings of Fiber Composites in Infrastructure, edited by H. Saadatmanesh and M.R. Ehsani. First International Conference on Composites in the Infrastructure (ICCI96), January 1996.
6. Porter, M. L., Bradley W. Hughes, and Bruce A. Barnes, *Fiber Composite Dowels in Highway Pavements*. Proceedings of Semisesquicentennial Transportation Conference. Ames, Iowa: Iowa Department of Transportation and Iowa State University, May 13-14, 1996.
7. Porter, Max L. *FRP Dowel Bars*. Proceedings of the 1999 International Composites Expo. Harrison, NY: Composite Institute, May 1999.
8. Porter, M.L., and R.L. Braun. *Preliminary Assessment of the Potential Use of Alternative Materials for Concrete Highway Pavement Joints: Final Report*. Highway Innovative Technology Evaluation Center (HITEC) Report. Ames, Iowa: Department of Civil and Construction Engineering, Iowa State University, January 1997.
9. Porter, M.L., and D.D. Davis. *Glass Fiber Reinforced Polymer Dowel Bars for Transverse Pavement Joints*. Proceedings of the FRP Symposium, ACI Fall Convention. Baltimore, MD, November 2, 1999.
10. McConnel, Vicki. "FRP Reinforcement Durability and FRP Dowel Bars." *Transportation Composites Newsletter*, 1999.

11. Porter, M.L., and R.J. Guinn. *Assessment of Highway Pavement Slab Dowel Bar Research: Final Report*. Iowa Highway Research Board Project HR-1080. Ames, Iowa: Center for Transportation Research and Education, Iowa State University, August 2002.
12. Cable, James K., L. Edgar, and J. Williams. *Field Evaluation of Elliptical Steel Dowel Performance*. Construction Report. Ames, Iowa: Center for Portland Cement Concrete Pavement Technology, Iowa State University, July 2003.
13. Porter, M.L., E.A. Lorenz, R.J. Guinn, and A.L. Lundy. *Solutions for Structural Dowel Bar Alternatives*. Ames, Iowa: Center for Transportation Research and Education, Center for Portland Cement Concrete Pavement Technology, Iowa State University, Draft created 2004.
14. Cable, J.K., M.L. Porter, J. Hoffman, L.L. Rold, L.E. Edgar. *Demonstration and Field Evaluation of Alternative Portland Cement Concrete Pavement Reinforcement Material*, HR-1069. The Highway Division of the Iowa Department of Transportation, the Iowa Highway Research Board, and the Federal Highway Administration Demonstration Projects Program. Ames, Iowa: Iowa State University, June 2003.
15. Porter, M.L., R.J. Guinn, Jr., and A.L. Lundy. *Dowel Bar Optimization—Phases I and II: Final Report*. American Highway Technology Report. Ames, Iowa: Center for Portland Cement Concrete Pavement Technology, Iowa State University, October 2001.
16. Porter, M.L., J.K. Cable, J.F. Harrington, N.J. Pierson, and A.W. Post. *Field Evaluation of Elliptical Fiber Reinforced Polymer Dowel Performance*. Ames, Iowa: Center for Transportation Research and Education, Center for Portland Cement Concrete Pavement Technology, Iowa State University, June 2005.
17. Applied Pavement Technology, Inc. *Evaluation of Alternative Dowel Bar Materials*. Highway Innovative Technology Evaluation Center (HITEC) Draft Interim Report. Champaign, Illinois, March 2005.
18. Ingram, Dominique. “The effect of the dowel bar shape and spacing in Portland cement concrete pavements on the load transfer efficiency of the transverse joint.” Master Thesis. Iowa State University, 1999.
19. American Association of State Highway and Transportation Officials (AASHTO). *AASHTO Guide for Design of Pavement Structures*. Washington, DC: AASHTO, 1993.
20. Timoshenko, S., and J.M. Lessels. 1925. *Applied Elasticity*. Pennsylvania: Westinghouse Technical Night School Press.
21. Friberg, B.F. “Design of Dowels in Transverse Joints of Concrete Pavements.” *Transactions, American Society of Civil Engineers*, Vol. 105, No. 2081, 1940.

22. Young, W.C., and Budynas, R.G. *Roark's Formulas for Stress and Strain*, 7th ed. New York: McGraw-Hill, Inc, 2002.
23. Cowper, G.R. "The shear coefficient in Timoshenko's beam theory." *Journal of Applied Mechanics*, 1966, 335-340.
24. American Concrete Institute (ACI) Committee 325. "Structural Design Considerations for Pavement Joints." *Journal of the American Concrete Institute*, Vol. 28, No. 1, July 1956, pp. 1-28.
25. Westergaard, H.M. 1925. *Computation of Stresses in Concrete Roads*. Proceedings, 5th Annual Meeting of the Highway Research Board. Washington, DC.
26. Tabatabaie, A.M., E.J. Barenburg, and R.E. Smith. 1979. *Longitudinal Joint Systems in Slipformed Rigid Pavements: Vol. II-Analysis of Load Transfer Systems for Concrete Pavements*. Report No. DOT/FAA.RD-79/4. Washington DC: U.S. Department of Transportation, Federal Aviation Administration.
27. Yoder, E.J., and M.W. Witzak. *Principles of Pavement Design*. 2nd ed. New York: John Wiley & Sons, Inc., 1975.
28. Albertson, M.D. "Fibercomposite and Steel Pavement Dowels." Master Thesis. Iowa State University, 1992.
29. Porter, M.L., B. Barnes, B. Hughes, and K. Viswanath. *Non-Corrosive Tie Reinforcing and Dowel Bars for Highway Pavement Slabs*. Final Report HR-343 Submitted to Highway Division of the Iowa Department of Transportation and Iowa Highway Research Board. Ames, IA, November 1993.
30. Porter, Max L., J.F. Harrington, and N.J. Pierson. *Greenstreak Dowel*. Final Report. Ames, IA: Iowa State University, June 2006.
31. ASTM. *Annual Book of ASTM Standards 2002*. West Conshohocken, PA: ASTM International, 2002.

**APPENDIX A. MODIFIED AASHTO T253 TEST: MODULUS OF DOWEL
SUPPORT VS. LOAD DIAGRAMS**

Figures A.1 through A.36 show k_0 vs. load plots for all 18 modified AASHTO T253 series of specimens where k_0 is determined as described in Chapter 3. There are three specimens for each series (54 specimens total) and two dowels per specimen for a total of six plots per figure. Each series has two plots: one with unadjusted loading and one with adjusted loading (see Section 4.1.1). The dowels are broken down by specimen number and specimen orientation (east or west).

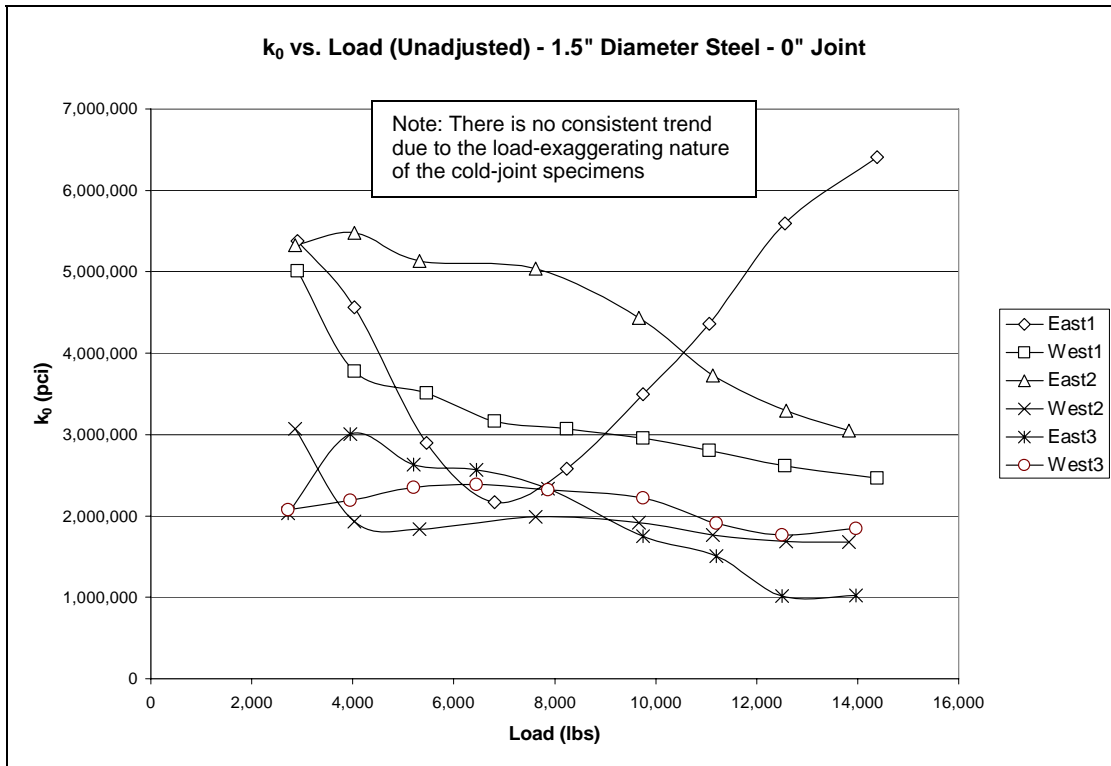


Figure A.1. k_0 plots, round steel, 0-inch joint, unadjusted loads

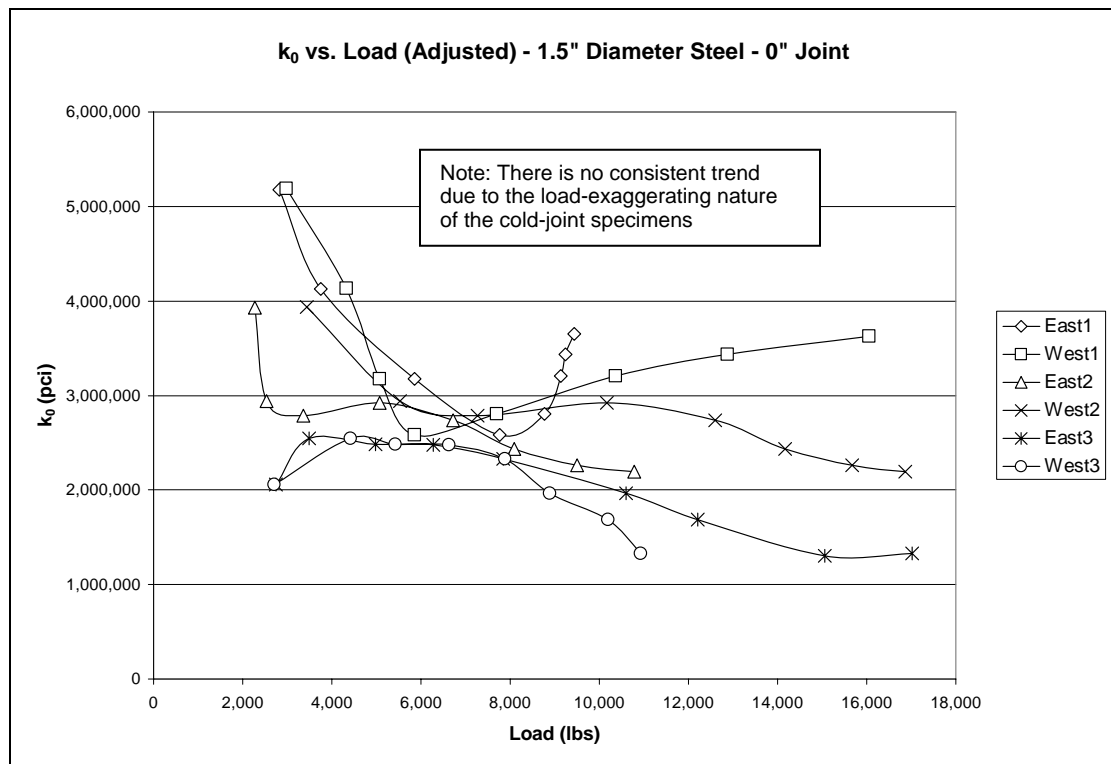


Figure A.2. k_0 plots, round steel, 0-inch joint, adjusted loads

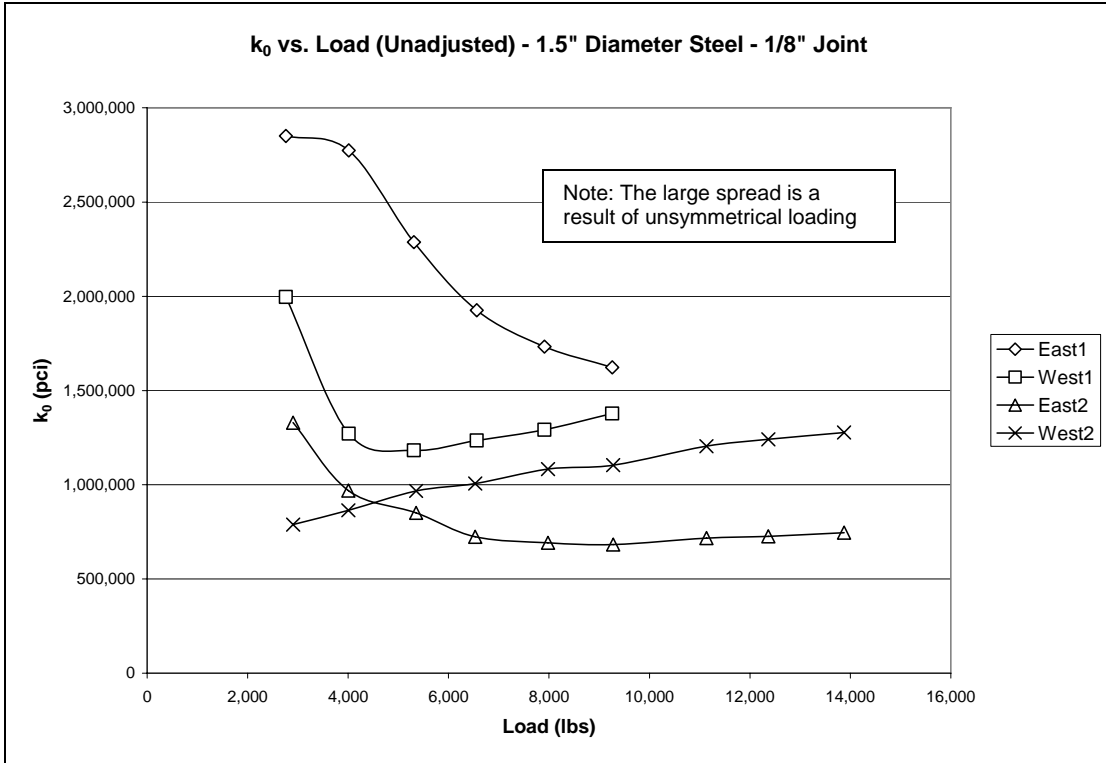


Figure A.3. k_0 plots, round steel, 1/8-inch joint, unadjusted loads

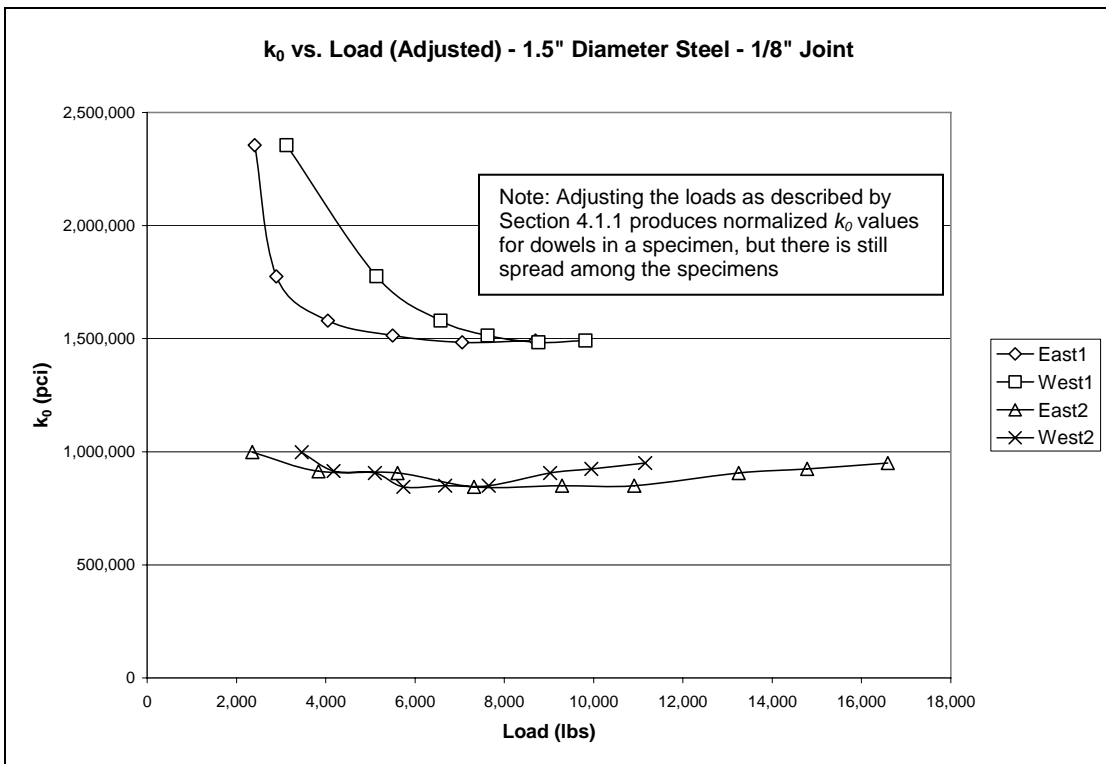


Figure A.4. k_0 plots, round steel, 1/8-inch joint, adjusted loads

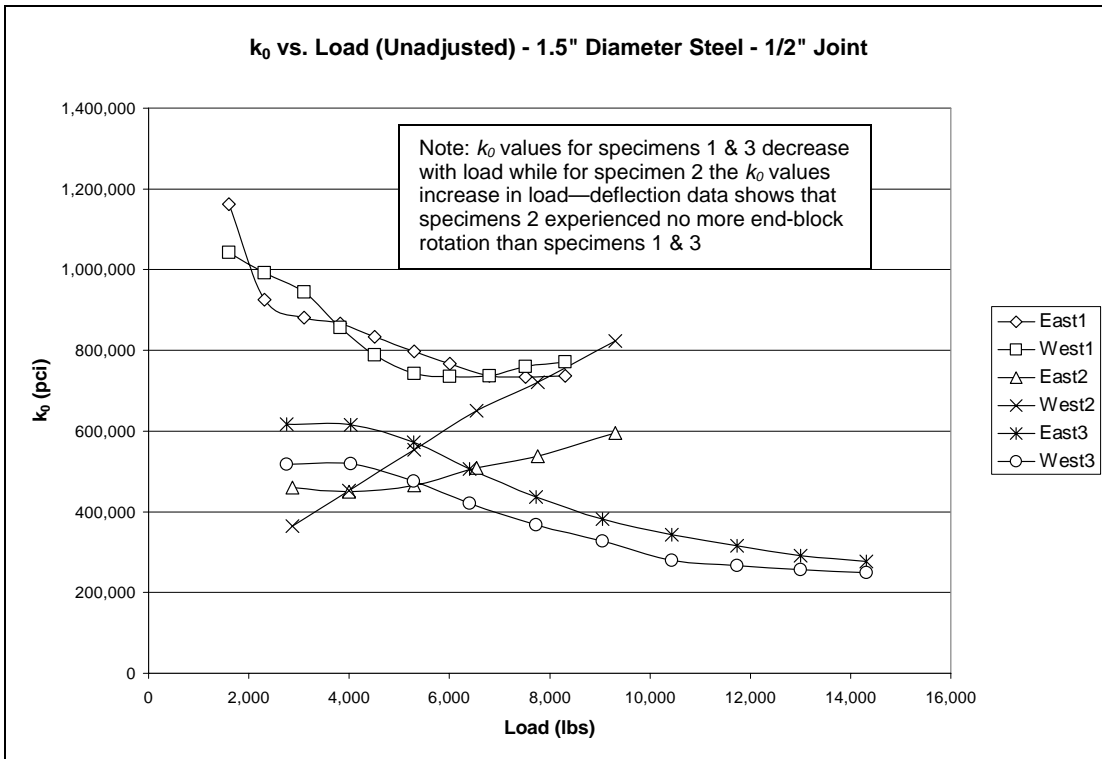


Figure A.5. k_0 plots, round steel, 1/2-inch joint, unadjusted loads

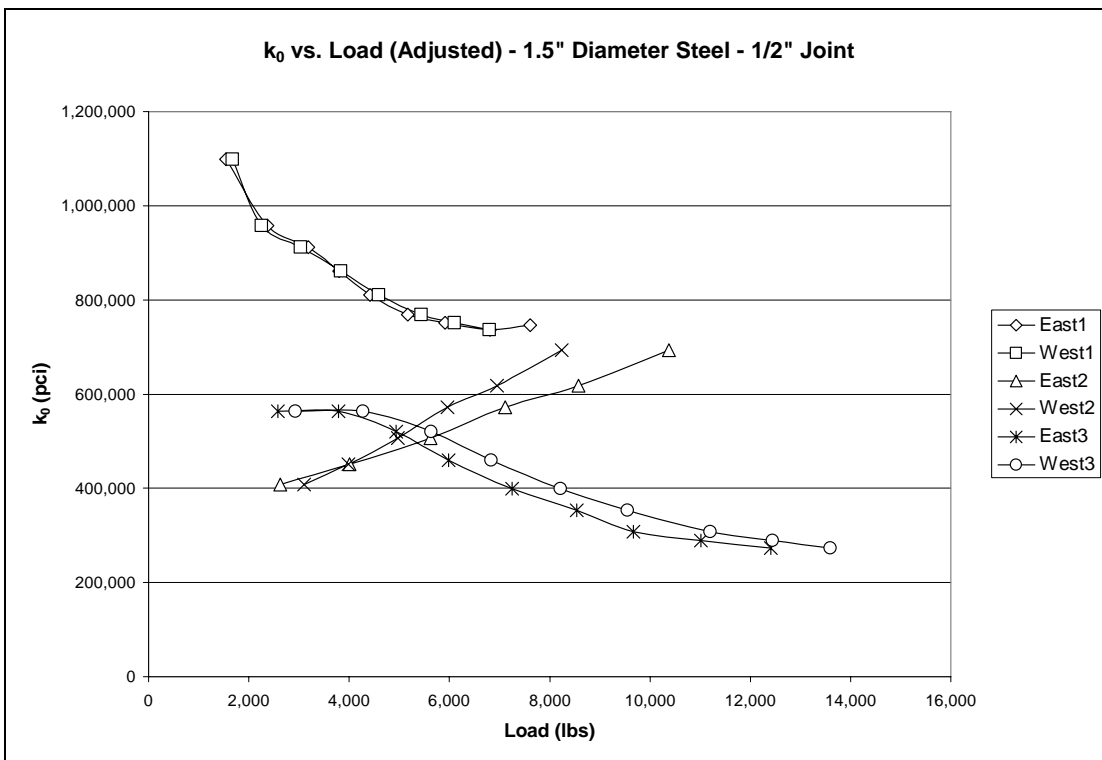


Figure A.6. k_0 plots, round steel, 1/2-inch joint, adjusted loads

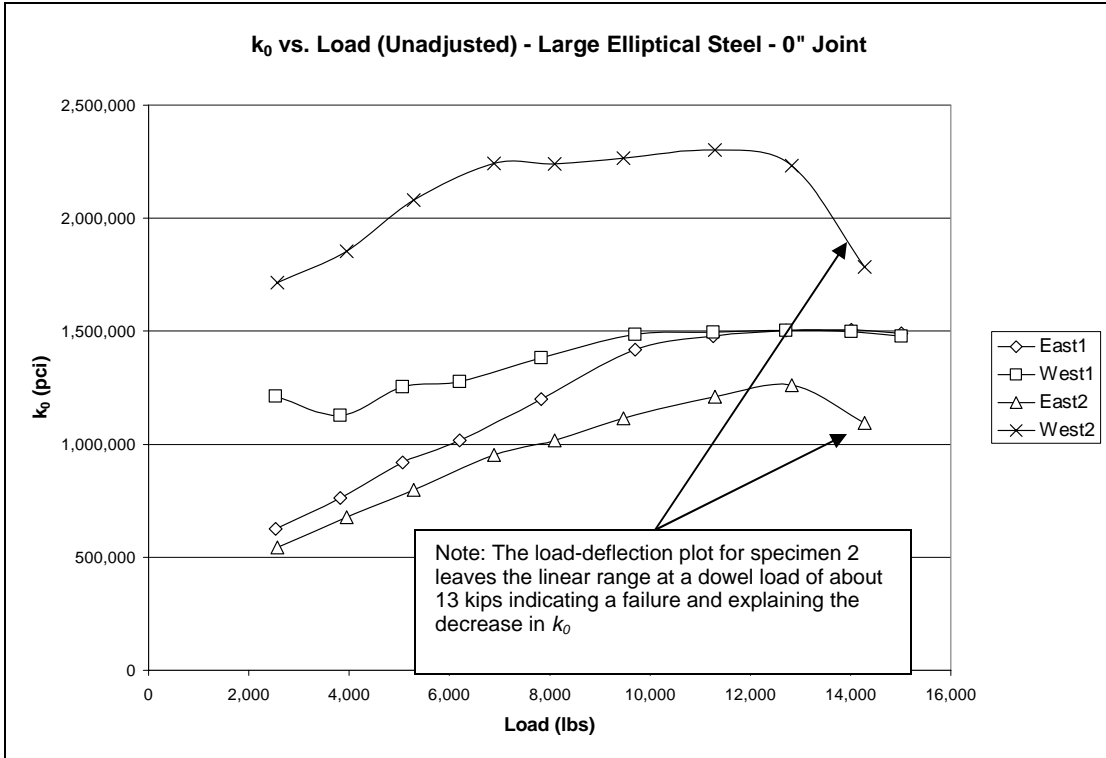


Figure A.7. k_0 plots, large elliptical steel, 0-inch joint, unadjusted loads

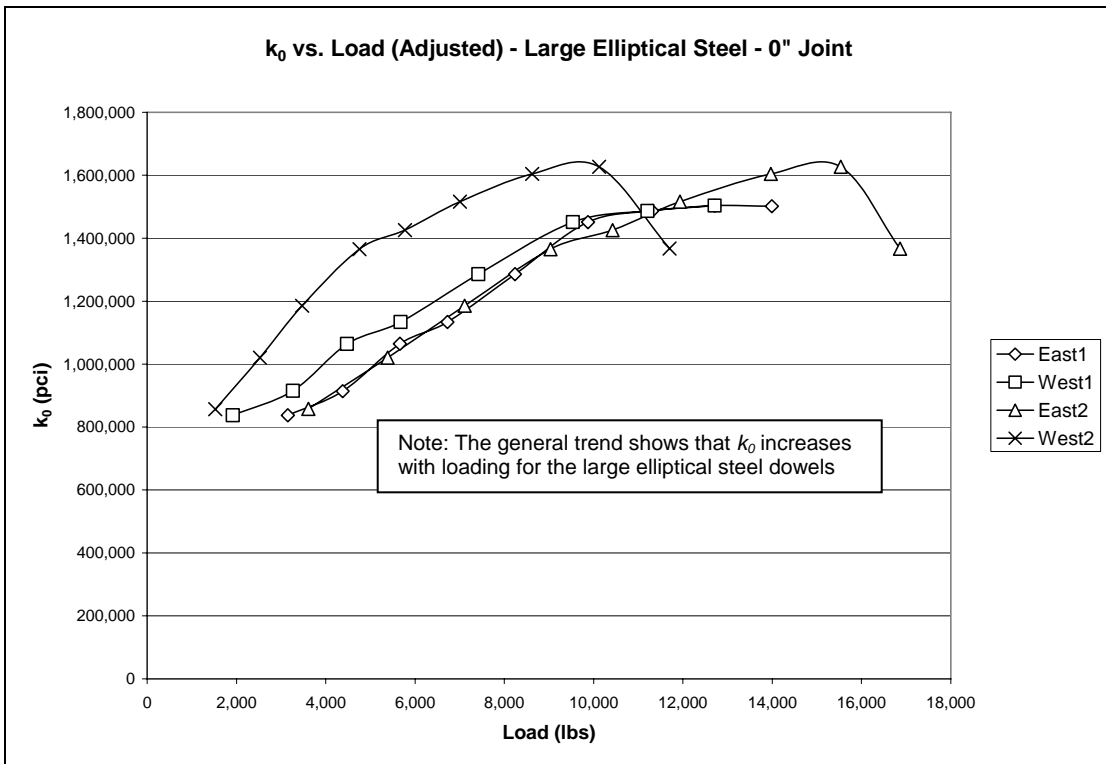


Figure A.8. k_0 plots, large elliptical steel, 0-inch joint, adjusted loads

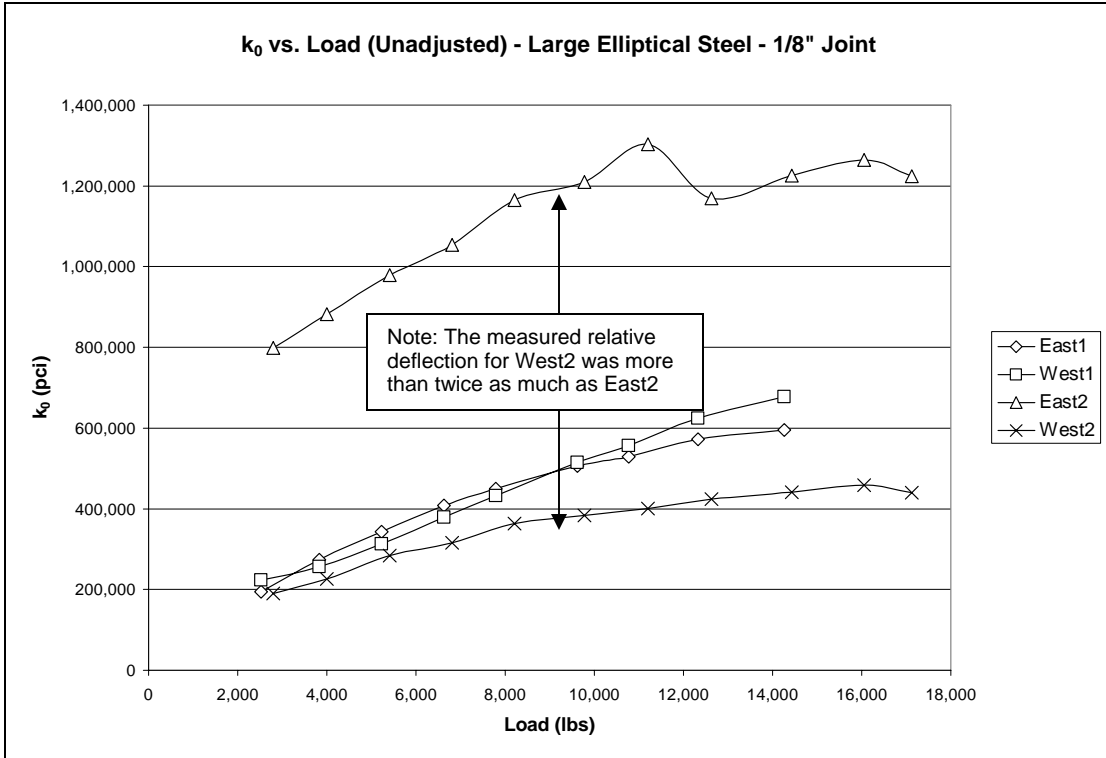


Figure A.9. k_0 plots, large elliptical steel, 1/8-inch joint, unadjusted loads

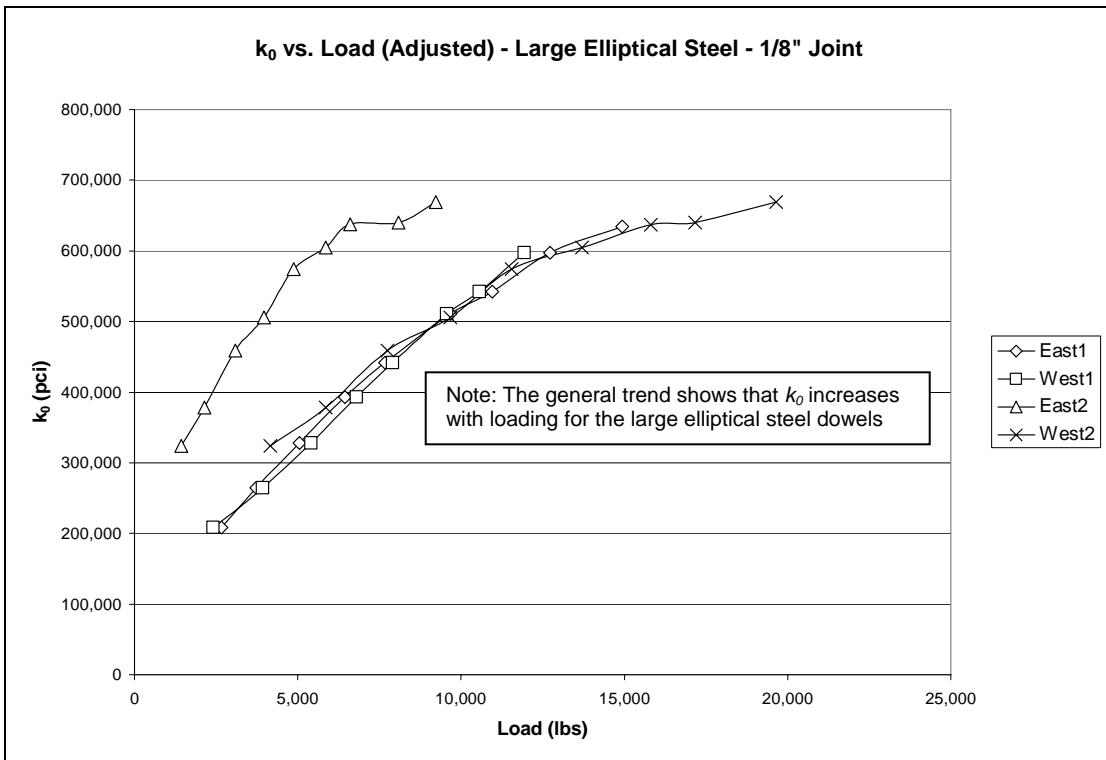


Figure A.10. k_0 plots, large elliptical steel, 1/8-inch joint, adjusted loads

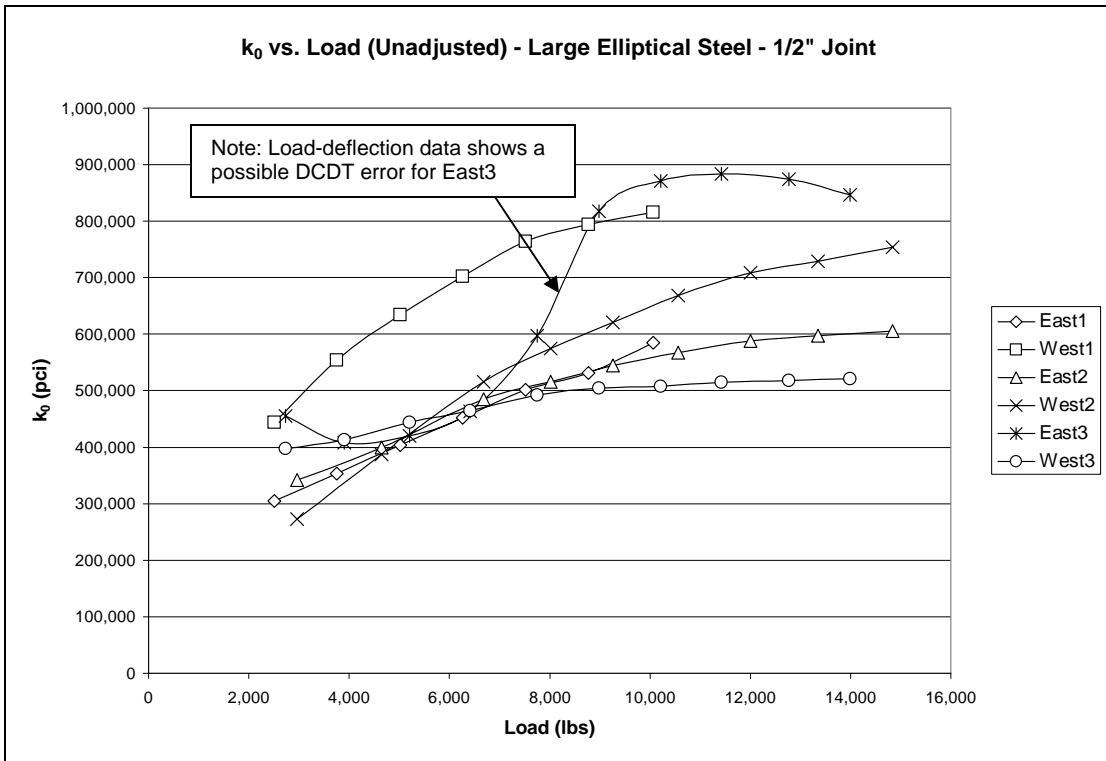


Figure A.11. k_0 plots, large elliptical steel, 1/2-inch joint, unadjusted loads

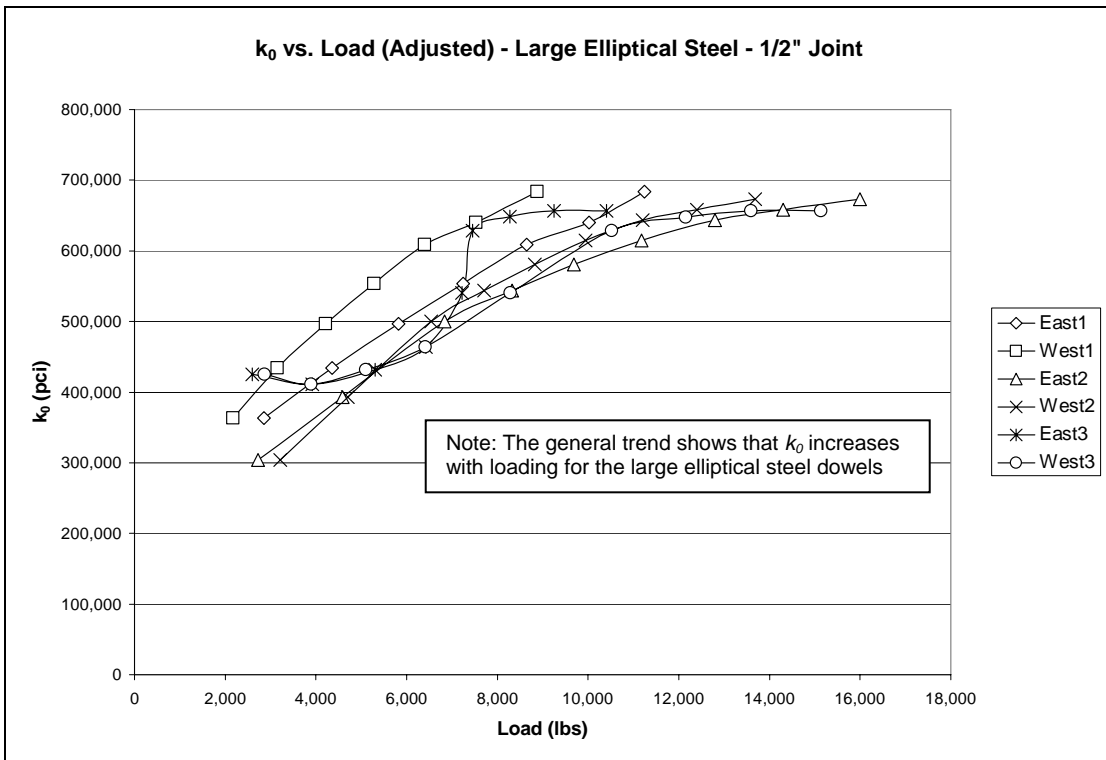


Figure A.12. k_0 plots, large elliptical steel, 1/2-inch joint, adjusted loads

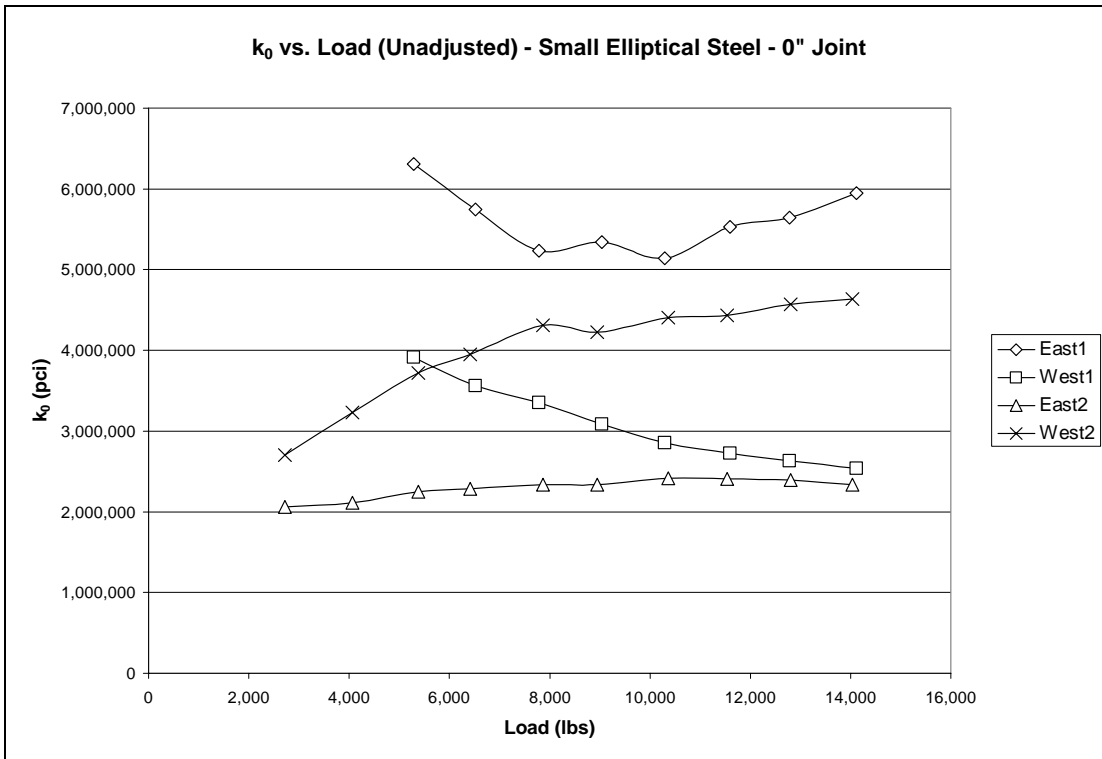


Figure A.13. k_0 plots, small elliptical steel, 0-inch joint, unadjusted loads

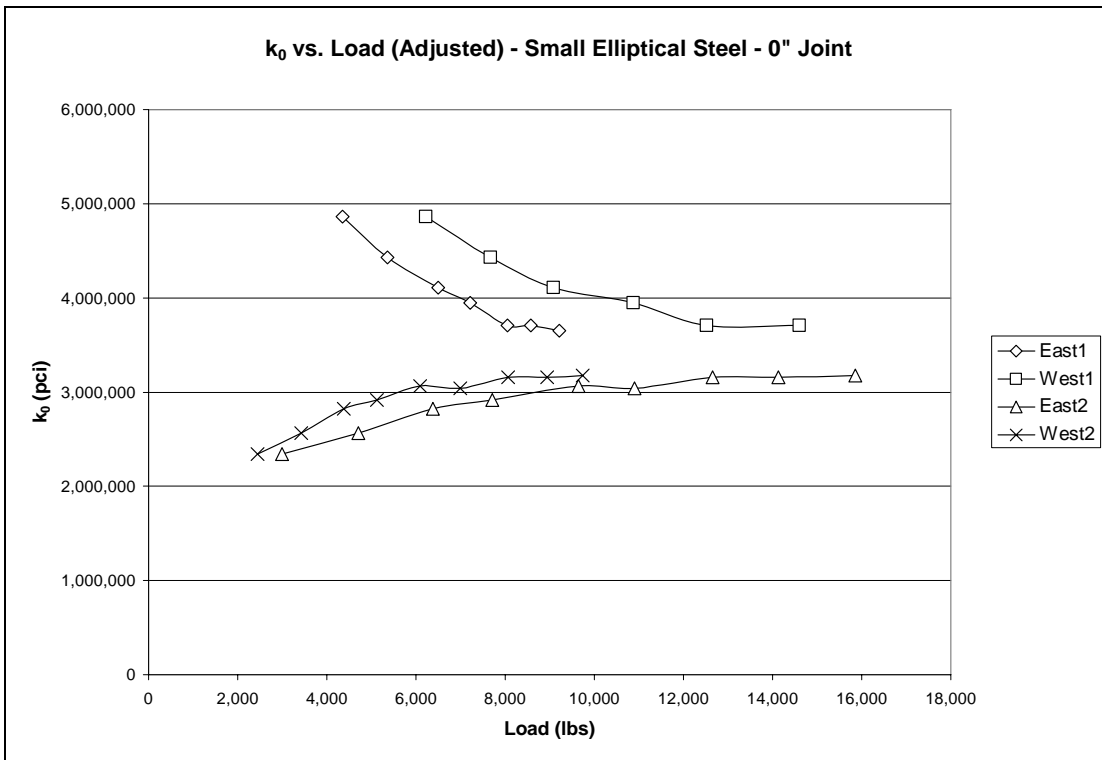


Figure A.14. k_0 plots, small elliptical steel, 0-inch joint, adjusted loads

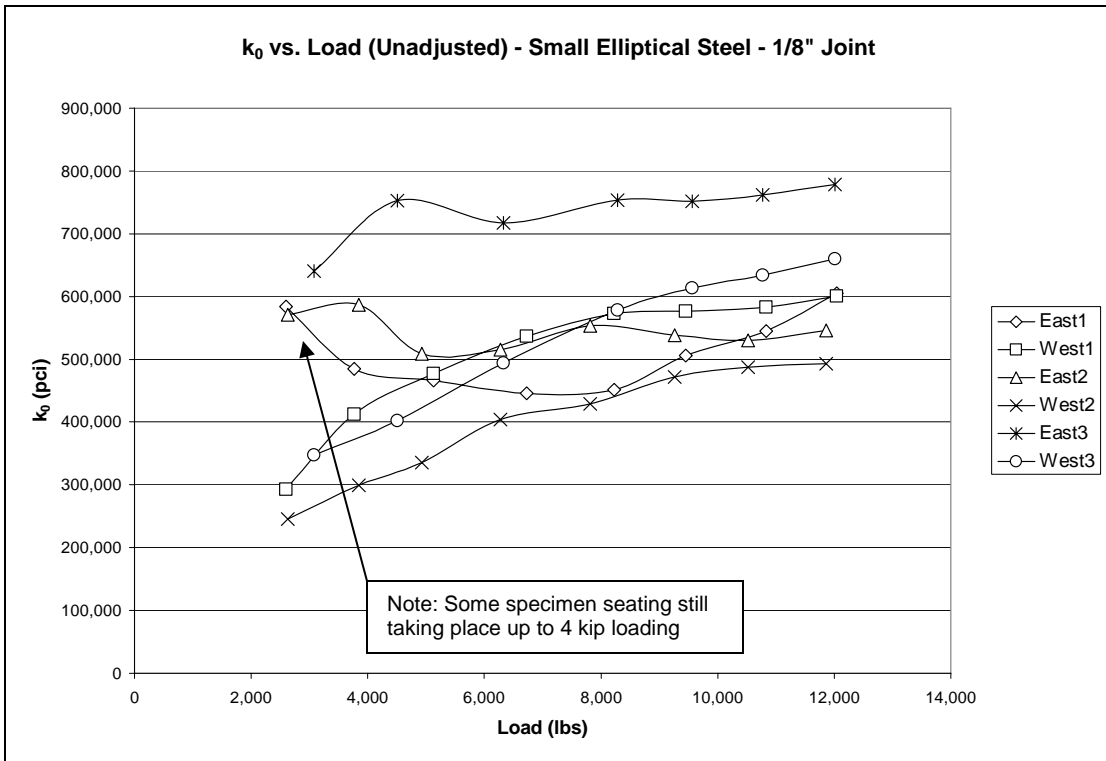


Figure A.15. k_0 plots, small elliptical steel, 1/8-inch joint, unadjusted loads

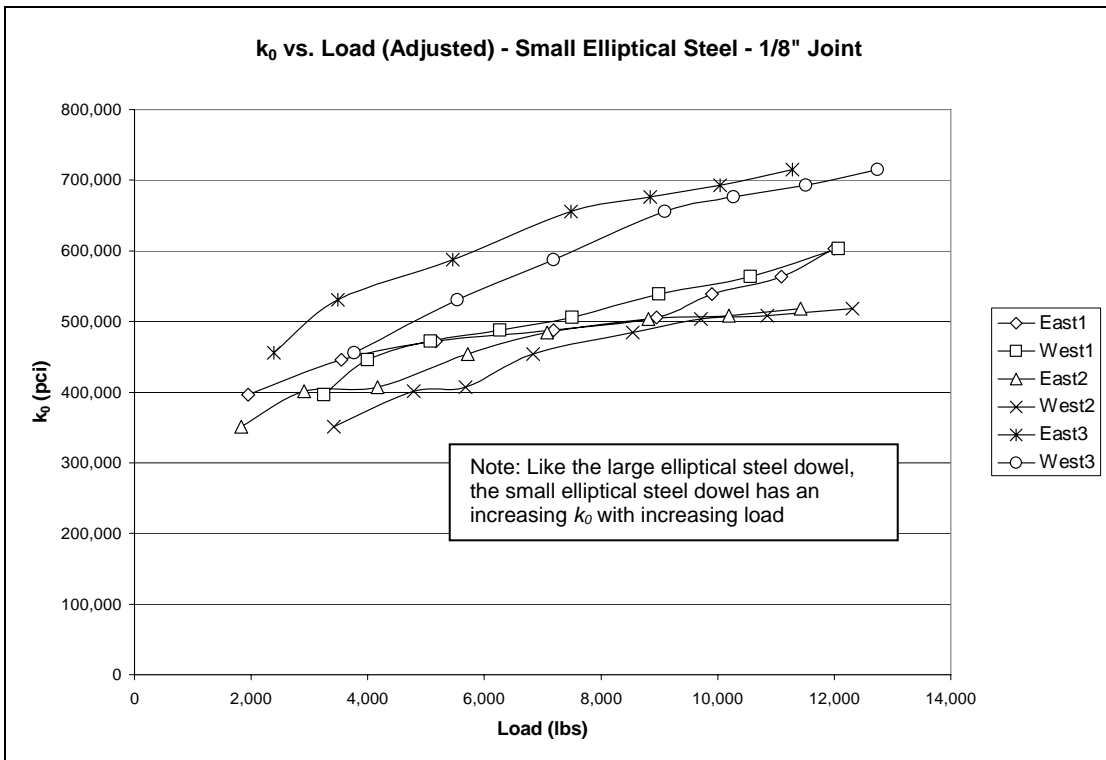


Figure A.16. k_0 plots, small elliptical steel, 1/8-inch joint, adjusted loads

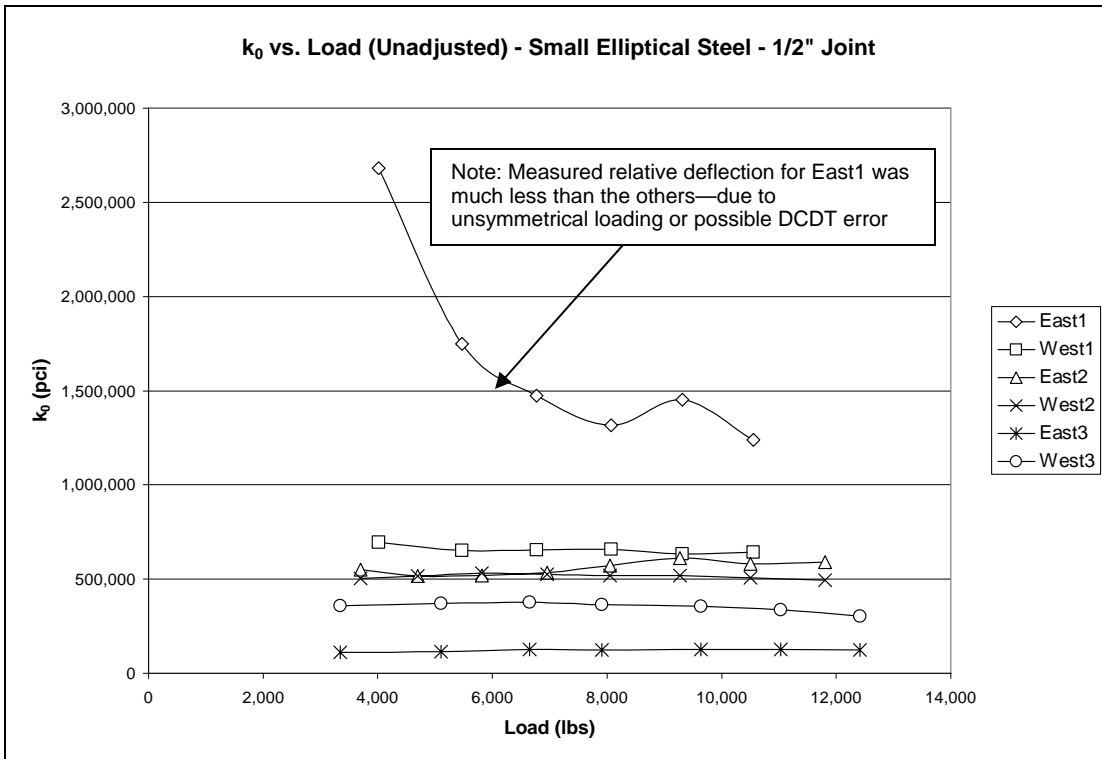


Figure A.17. k_0 plots, small elliptical steel, 1/2-inch joint, unadjusted loads

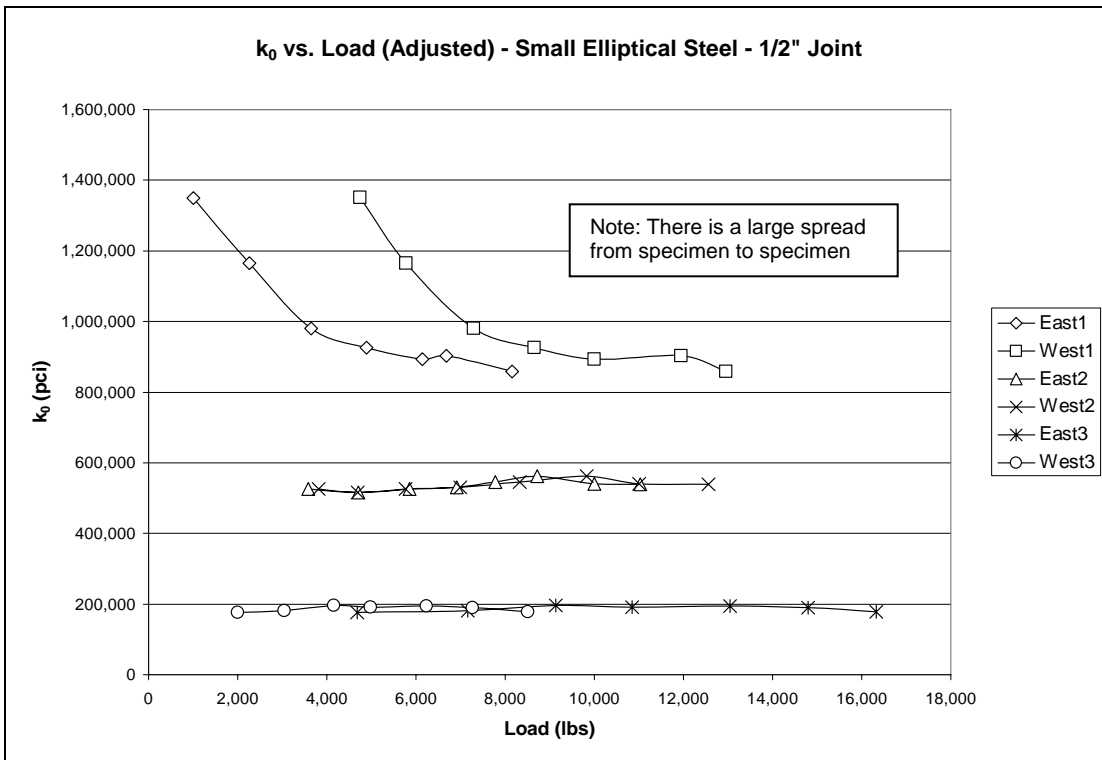


Figure A.18. k_0 plots, small elliptical steel, 1/2-inch joint, adjusted loads

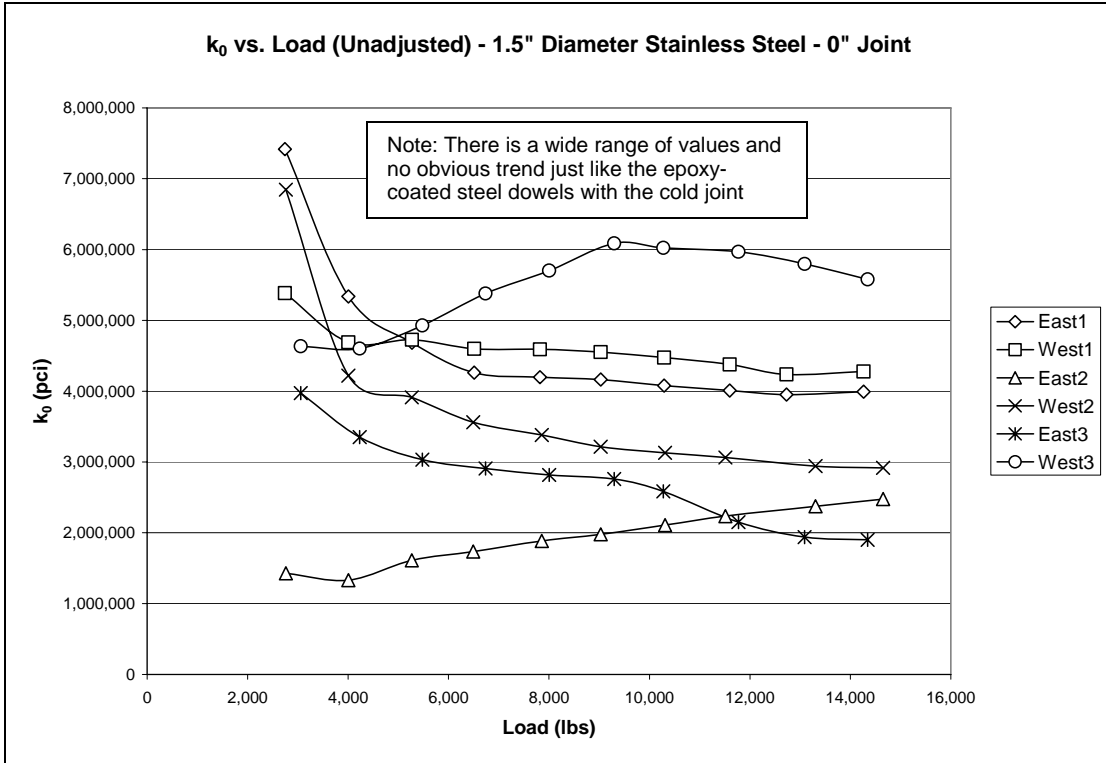


Figure A.19. k_0 plots, round stainless steel, 0-inch joint, unadjusted loads

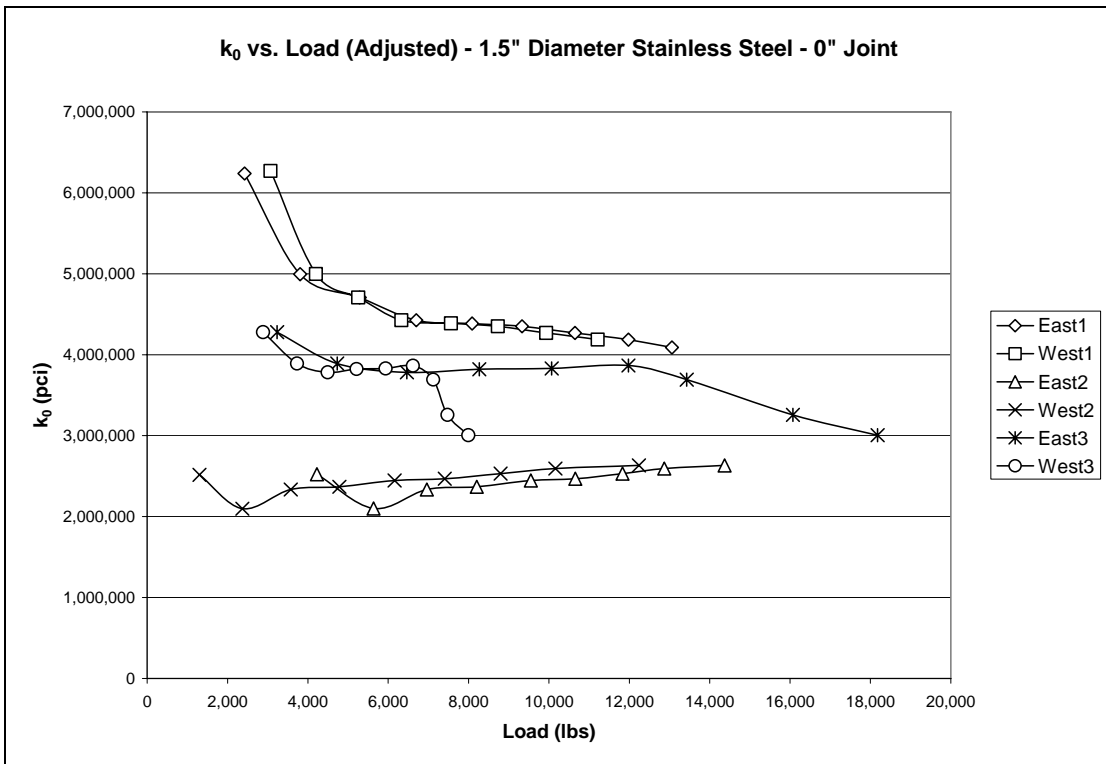


Figure A.20. k_0 plots, round stainless steel, 0-inch joint, adjusted loads

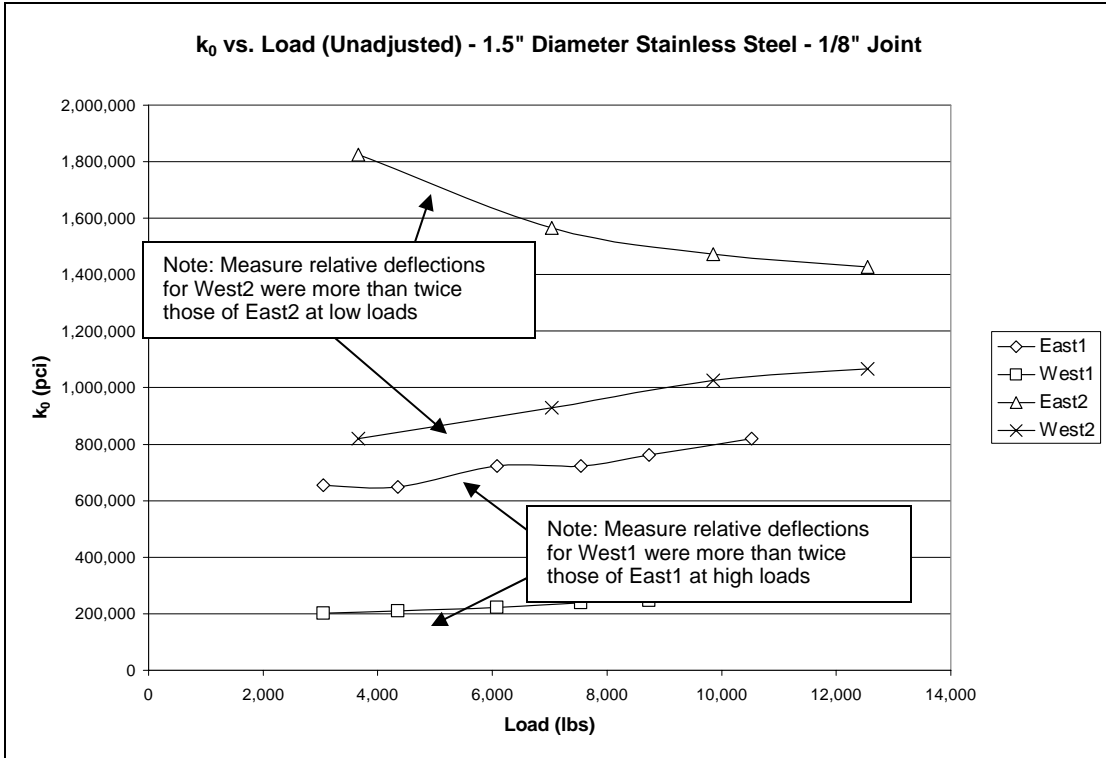


Figure A.21. k_0 plots, round stainless steel, 1/8-inch joint, unadjusted loads

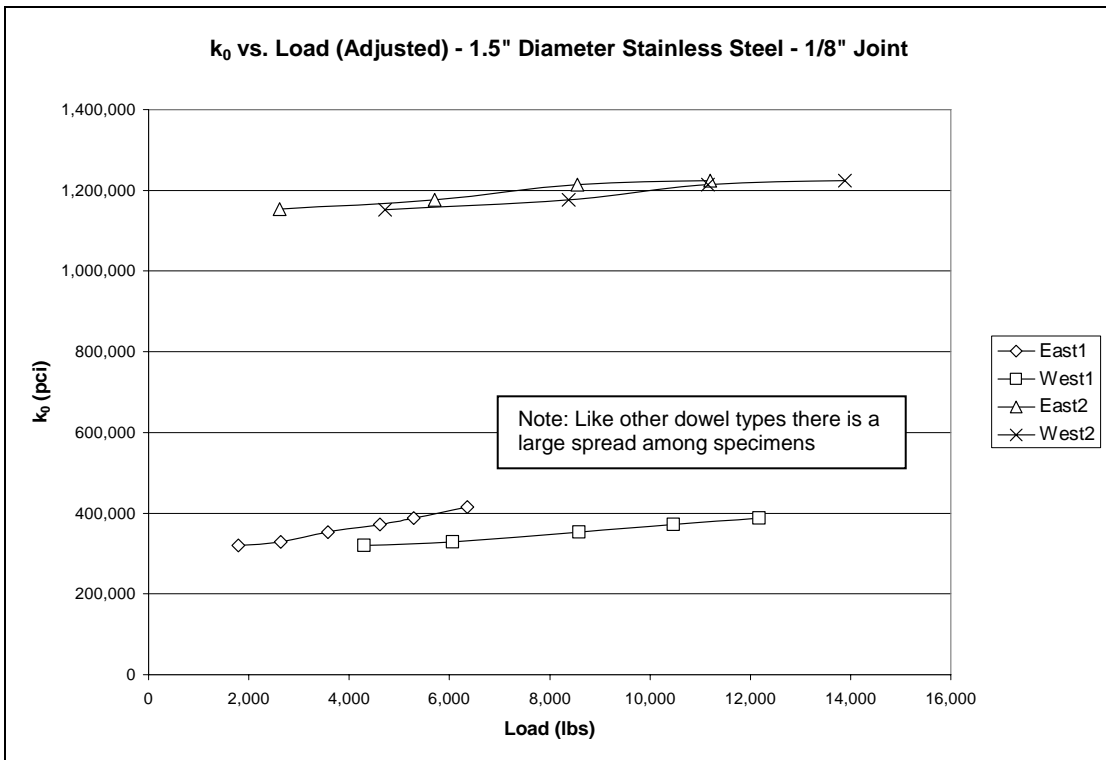


Figure A.22. k_0 plots, round stainless steel, 1/8-inch joint, adjusted loads

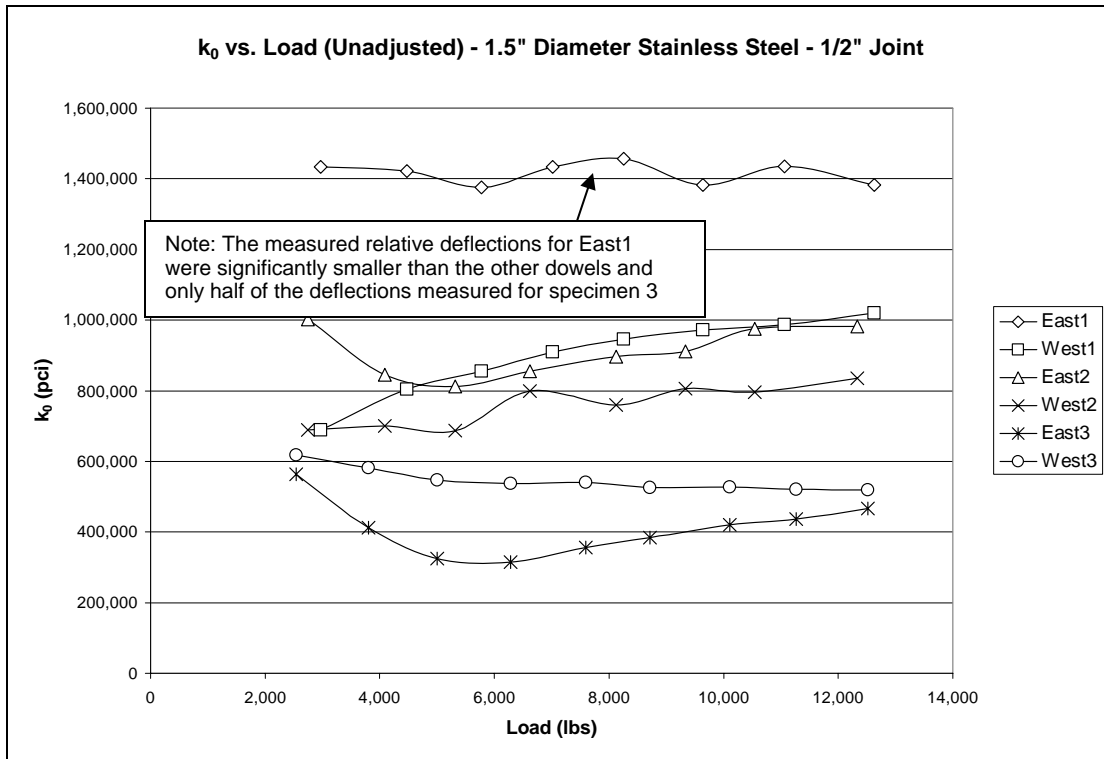


Figure A.23. k_0 plots, round stainless steel, 1/2-inch joint, unadjusted loads

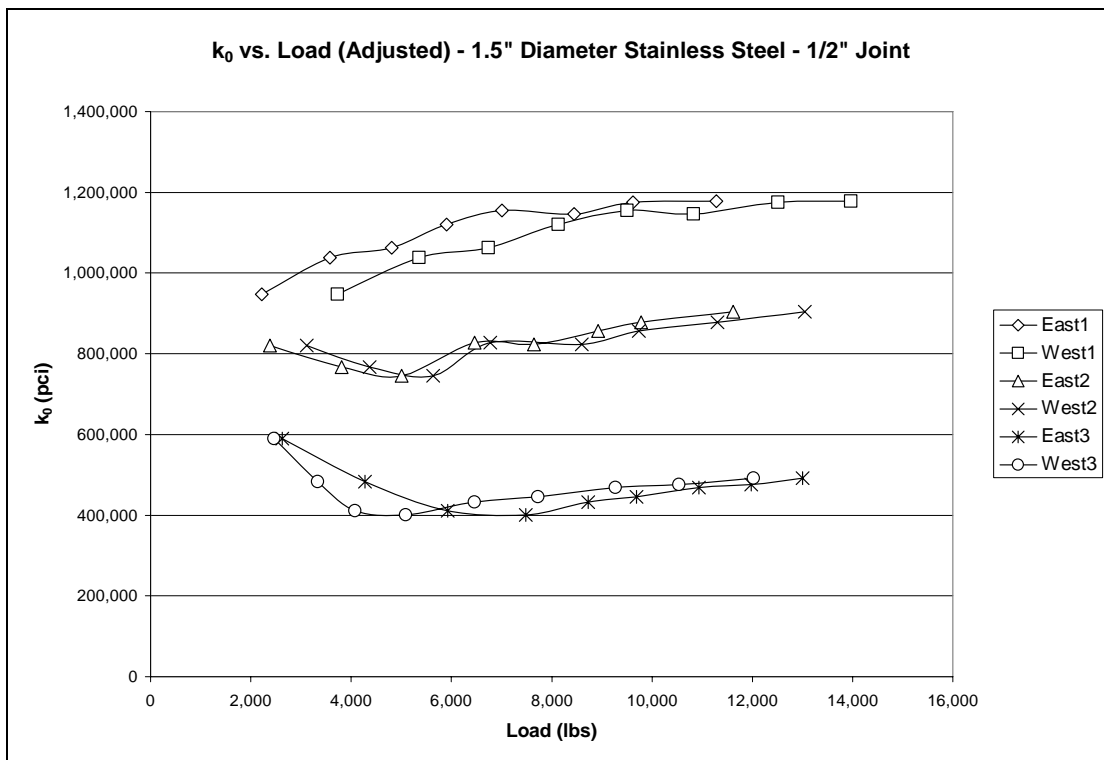


Figure A.24. k_0 plots, round stainless steel, 1/2-inch joint, adjusted loads

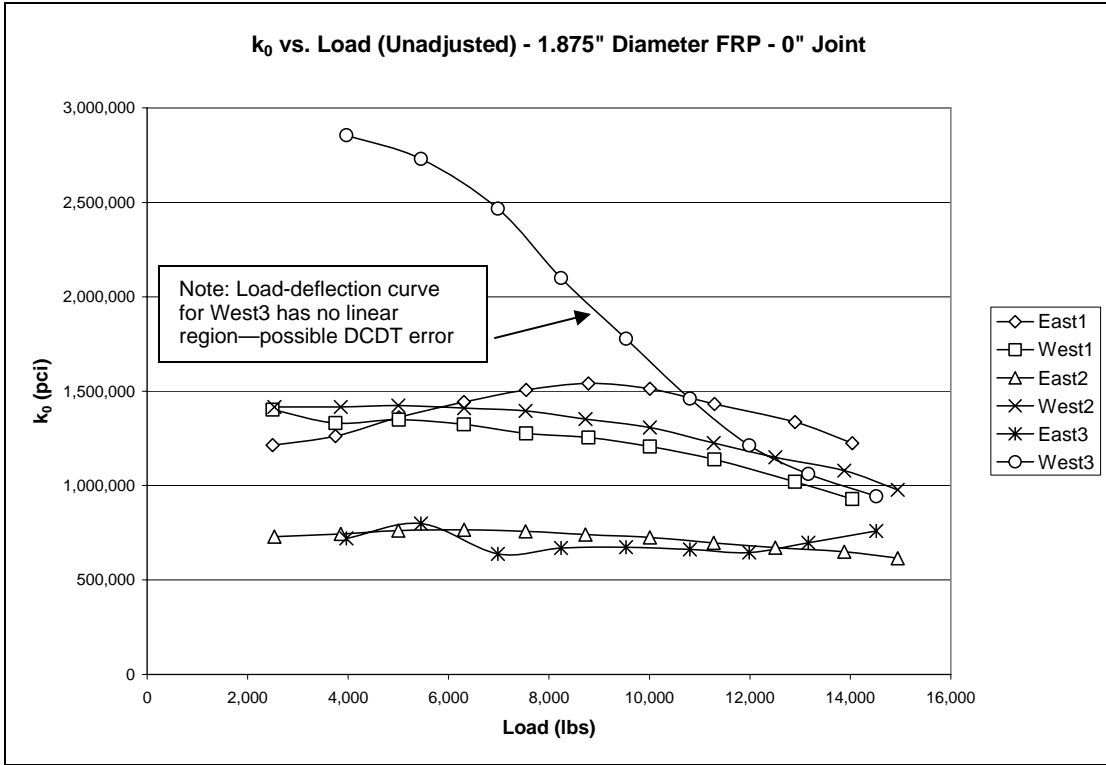


Figure A.25. k_0 plots, round GFRP, 0-inch joint, unadjusted loads

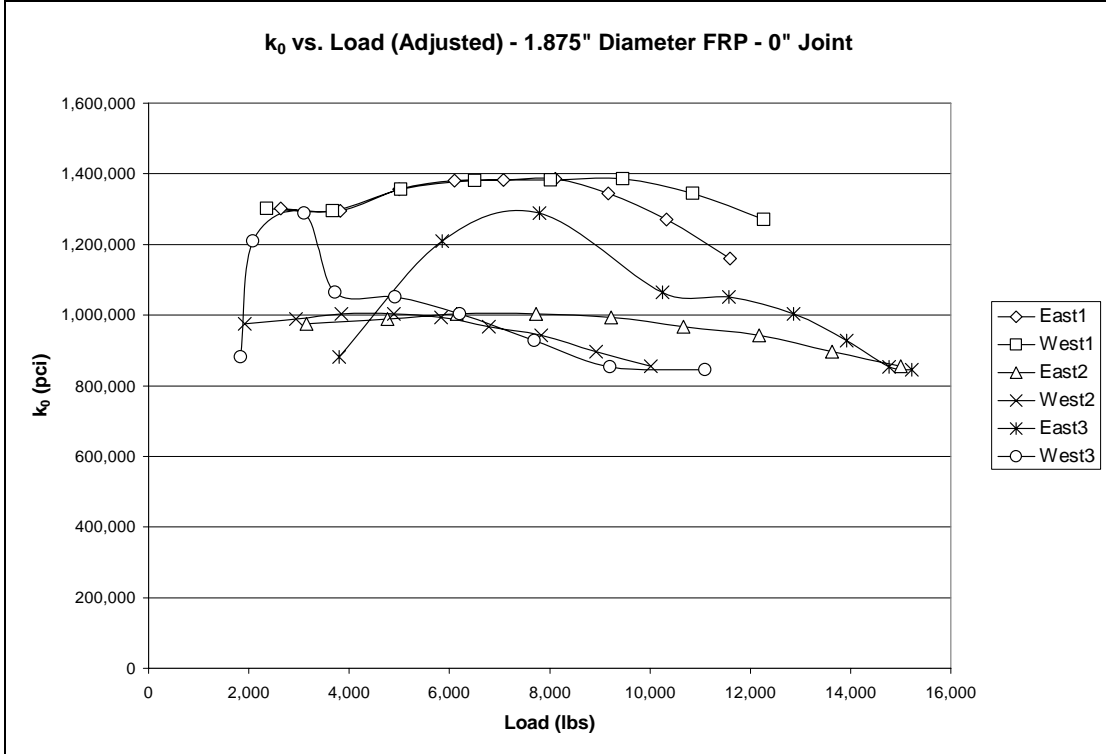


Figure A.26. k_0 plots, round GFRP, 0-inch joint, adjusted loads

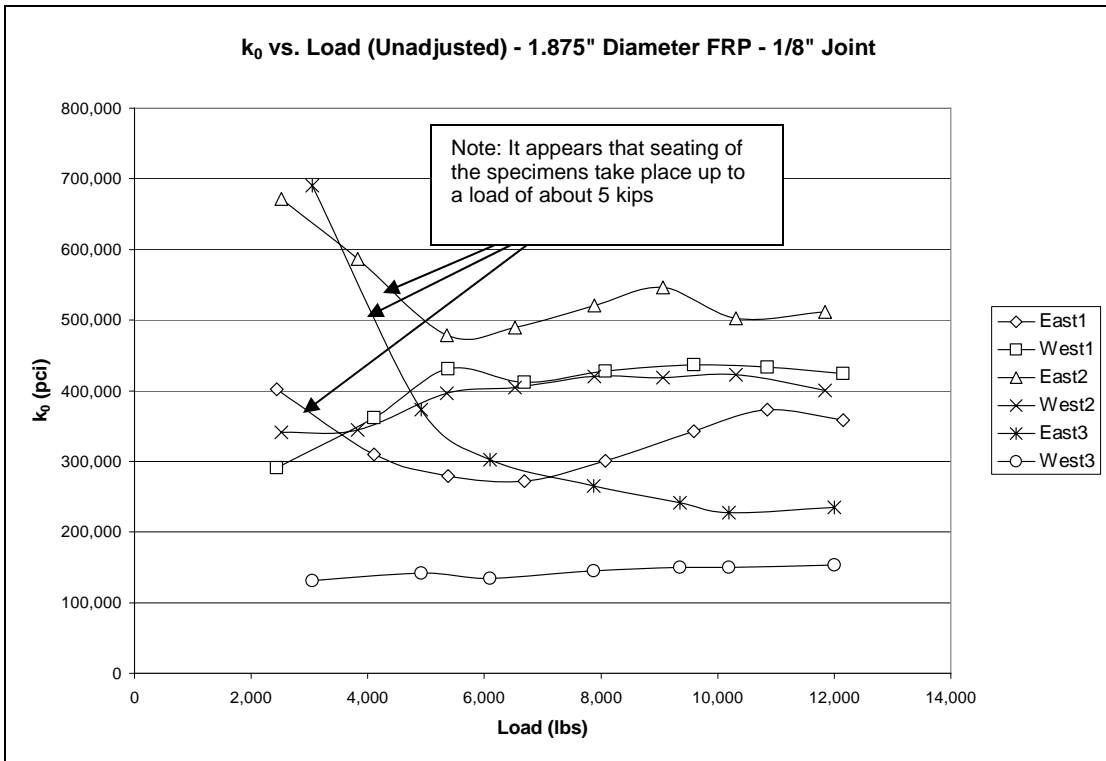


Figure A.27. k_0 plots, round GFRP, 1/8-inch joint, unadjusted loads

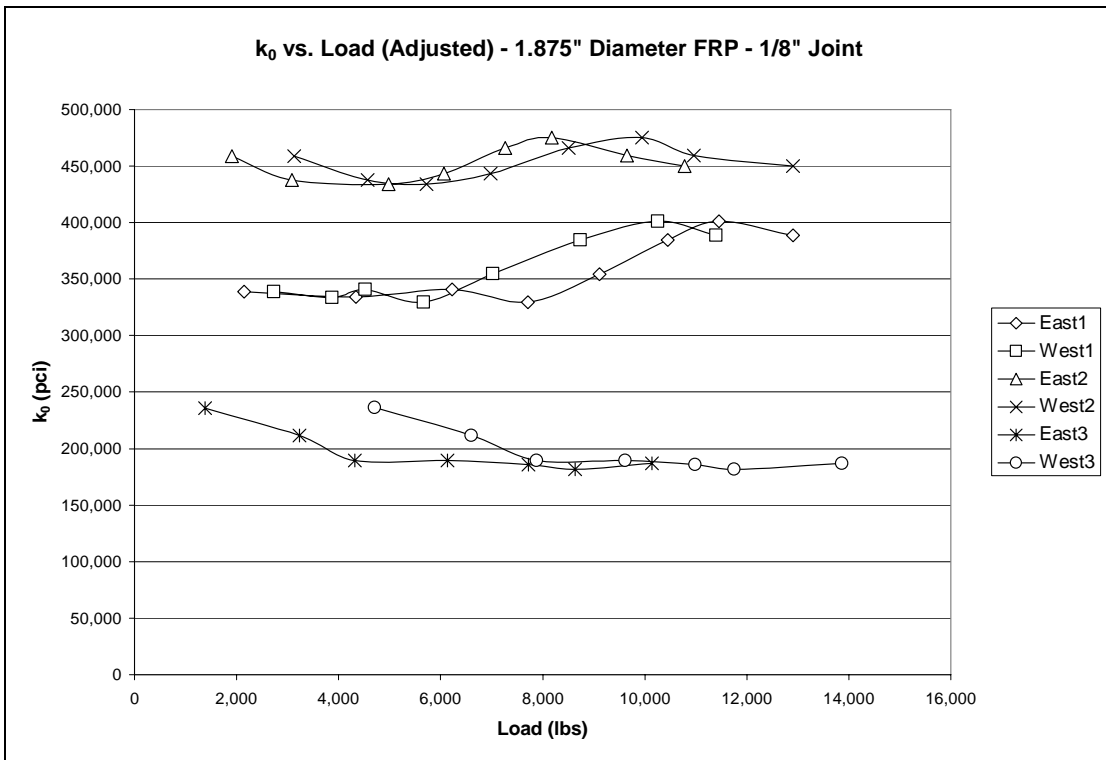


Figure A.28. k_0 plots, round GFRP, 1/8-inch joint, adjusted loads

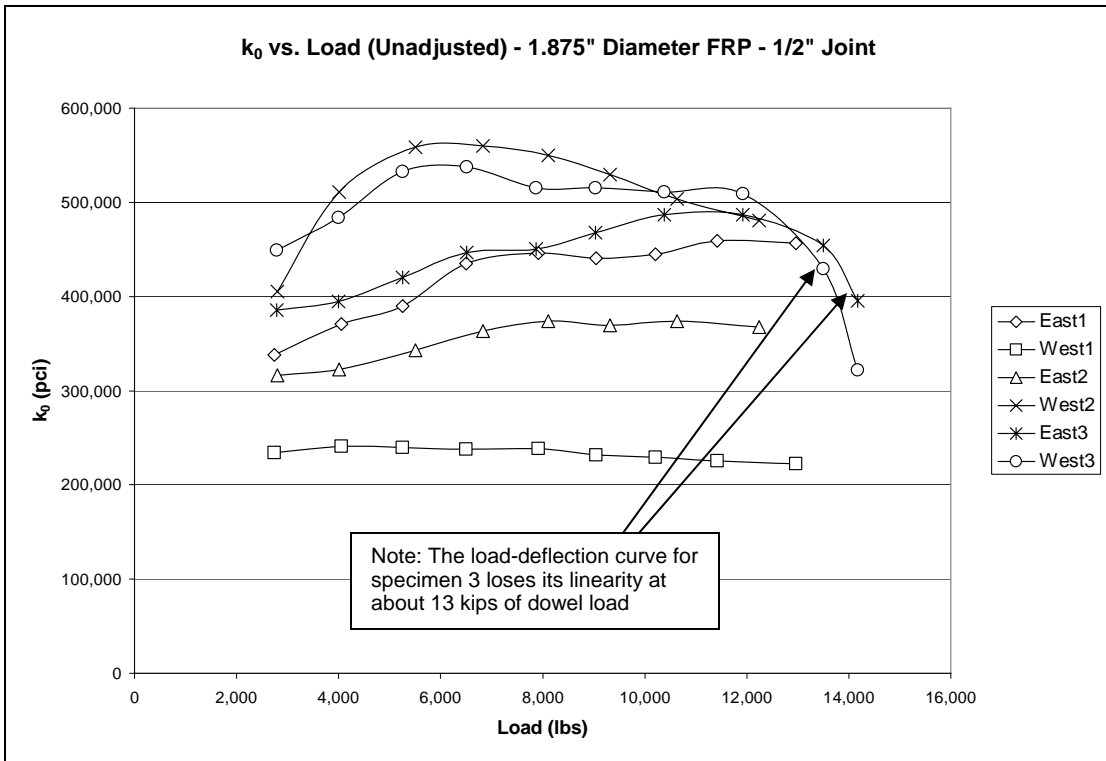


Figure A.29. k_0 plots, round GFRP, 1/2-inch joint, unadjusted loads

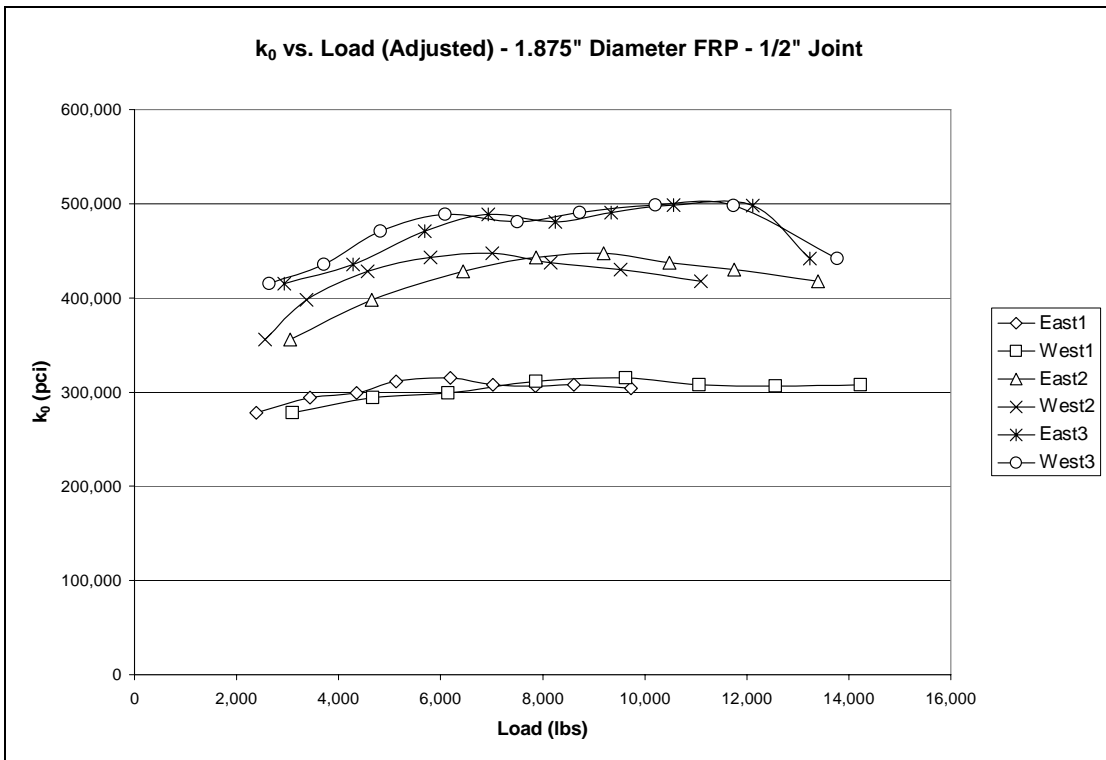


Figure A.30. k_0 plots, round GFRP, 1/2-inch joint, adjusted loads

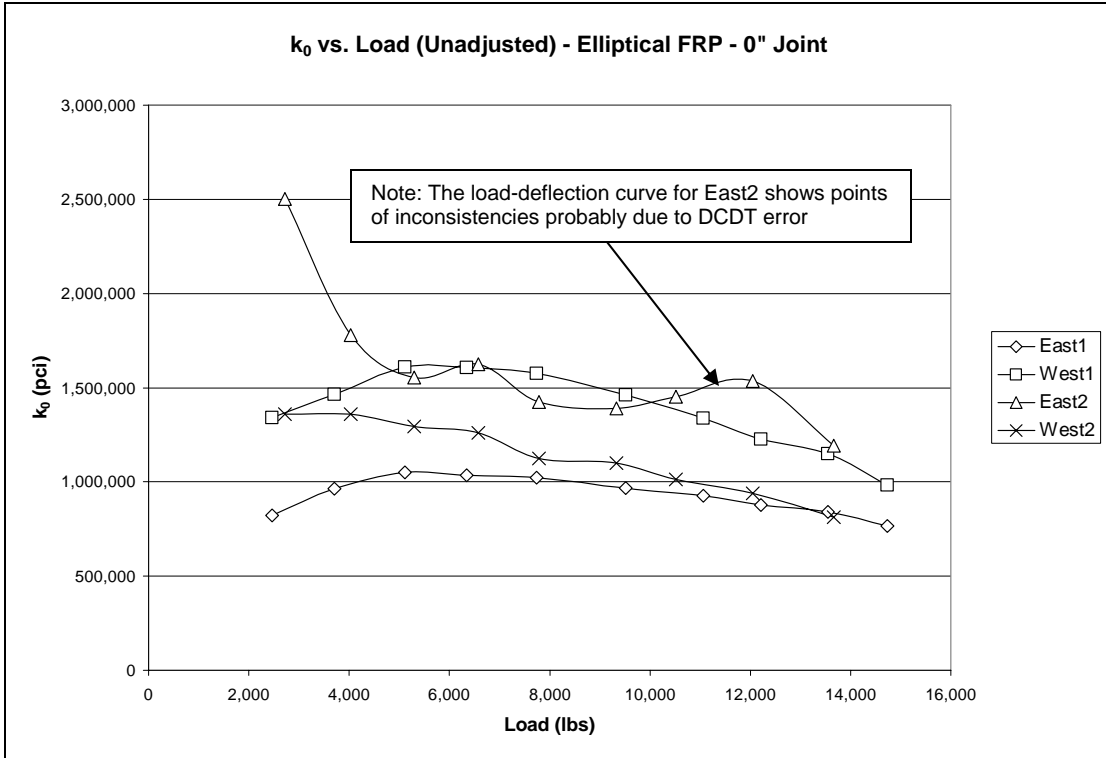


Figure A.31. k_0 plots, elliptical GFRP, 0-inch joint, unadjusted loads

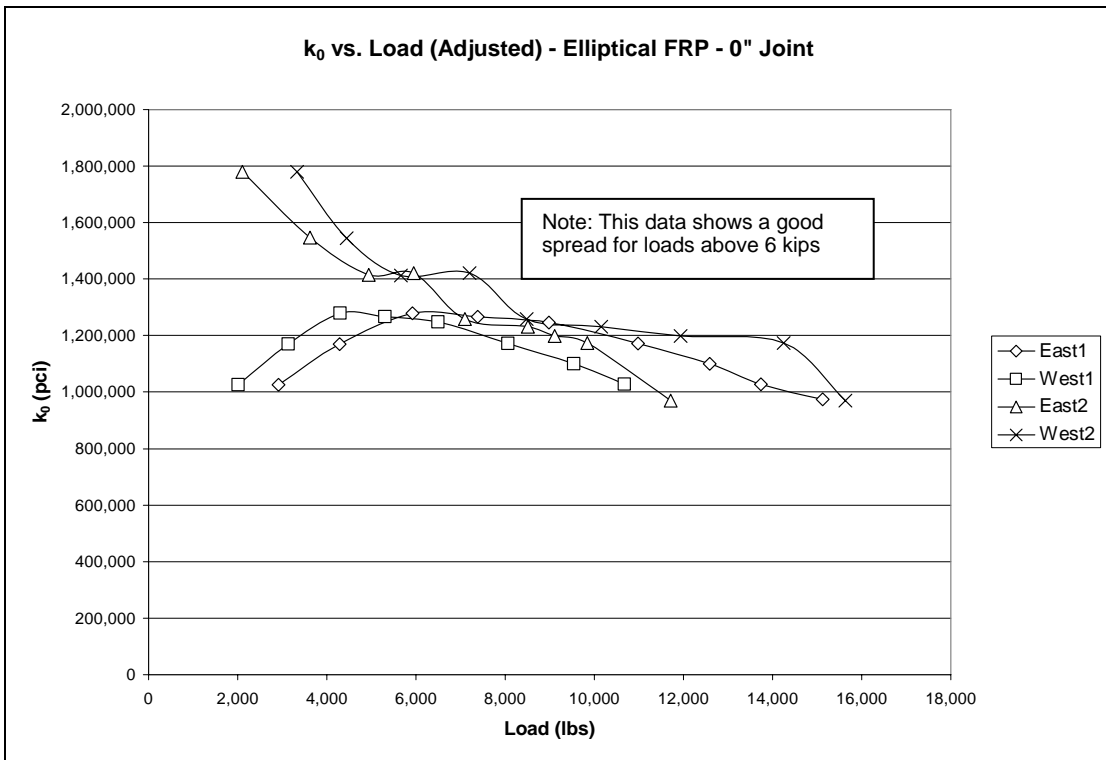


Figure A.32. k_0 plots, elliptical GFRP, 0-inch joint, adjusted loads

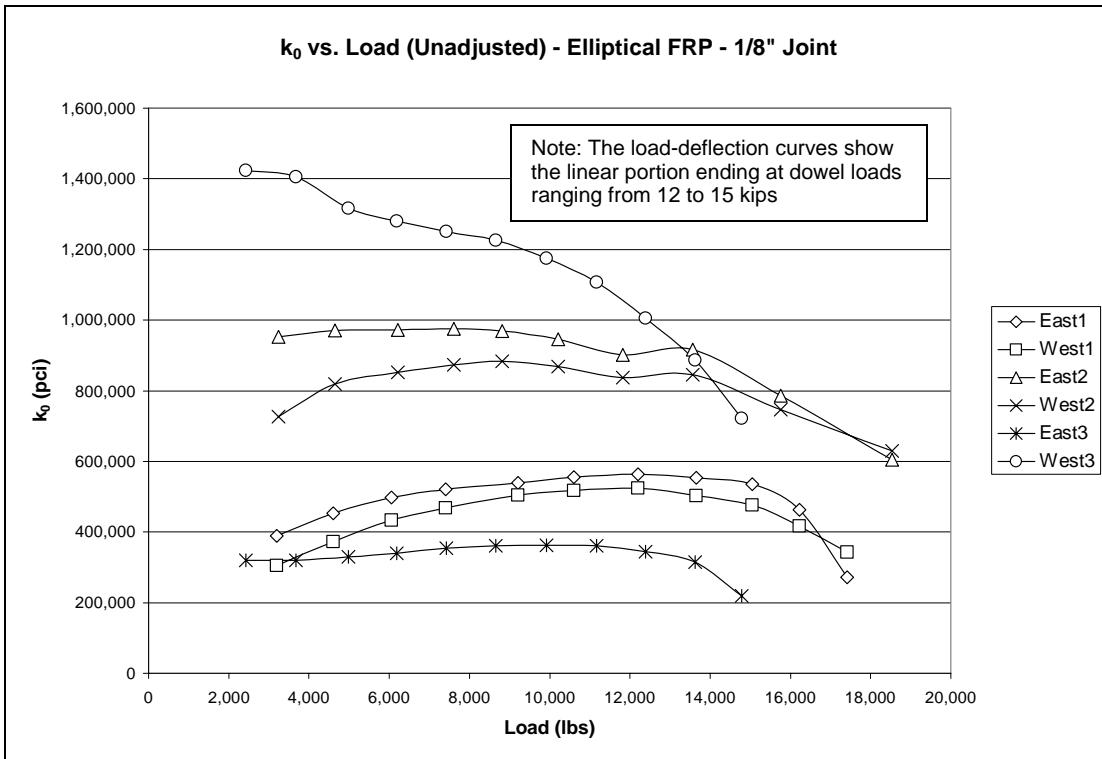


Figure A.33. k_0 plots, elliptical GFRP, 1/8-inch joint, unadjusted loads

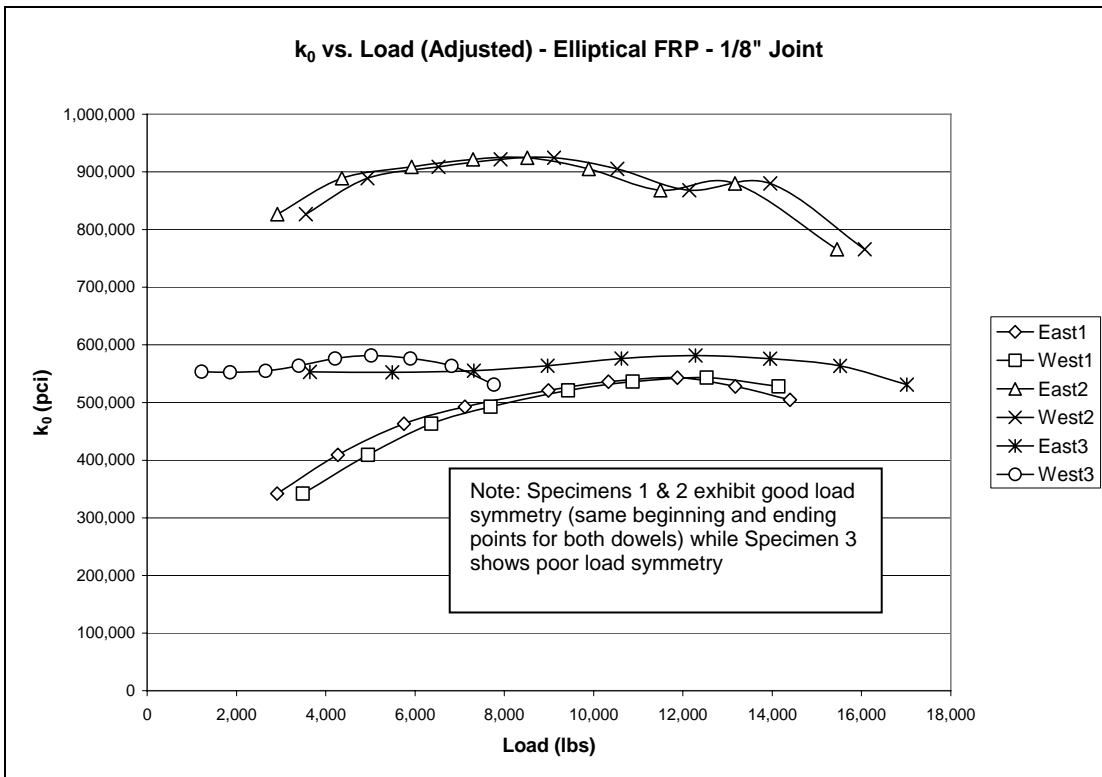


Figure A.34. k_0 plots, elliptical GFRP, 1/8-inch joint, adjusted loads

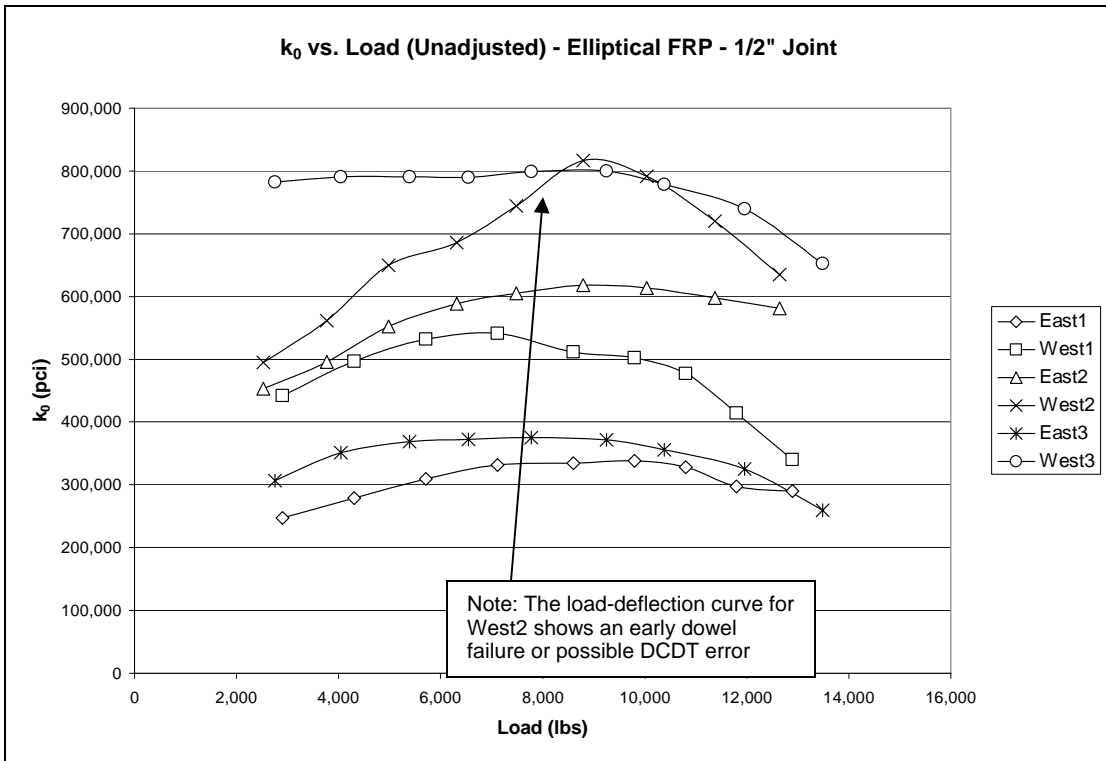


Figure A.35. k_0 plots, elliptical GFRP, 1/2-inch joint, unadjusted loads

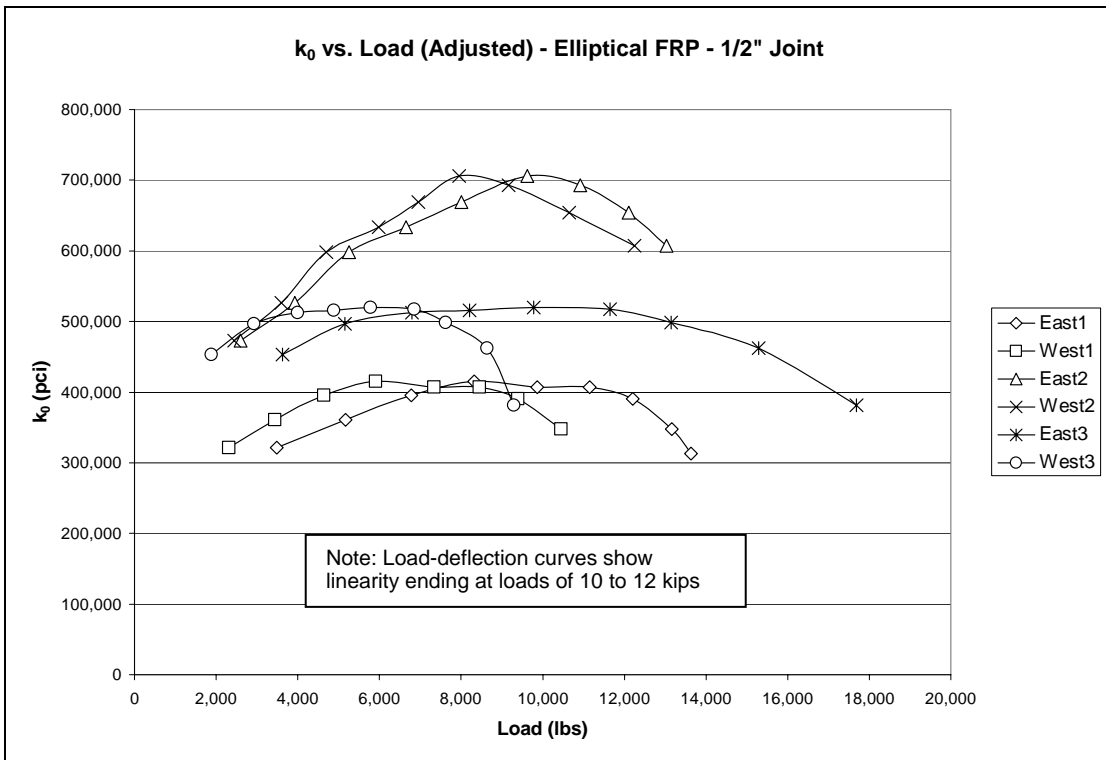


Figure A.36. k_0 plots, elliptical GFRP, 1/2-inch joint, adjusted loads

**APPENDIX B. DOWEL MOMENT DIAGRAMS: THEORETICAL AND STRAIN-
GAGE MEASURED**

Figures B.1 through B.16 show moments along the length of the dowel. Each figure contains two moment graphs: the measured moment and the theoretical moment. The measured moment is the moment calculated from the strain gages (see Section 3.4) where the magnitude of the strains at the top and bottom of the dowel at a point are averaged and the average strain is used to compute the moment. The theoretical moment is the moment from Timoshenko's theory (19) shown in Equation 3.10. All the moment curves' signs (positive or negative moment) have been adjusted to show uniformity among the figures.

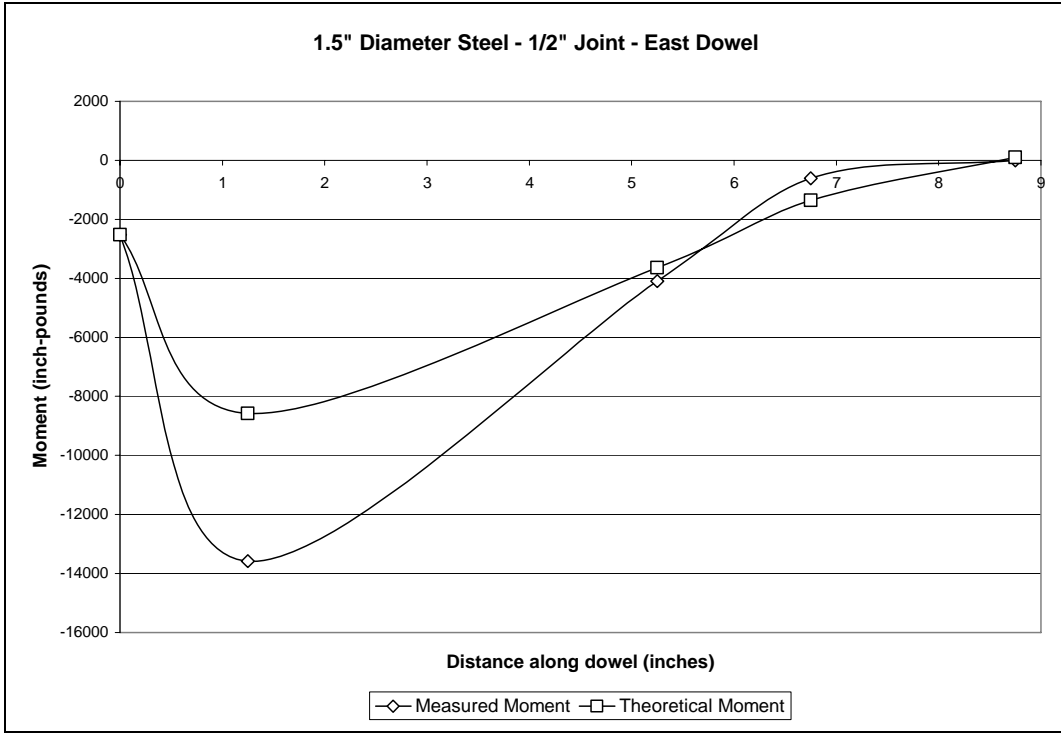


Figure B.1. Theoretical and measured moments, round steel specimen, east dowel, 1/2-inch joint

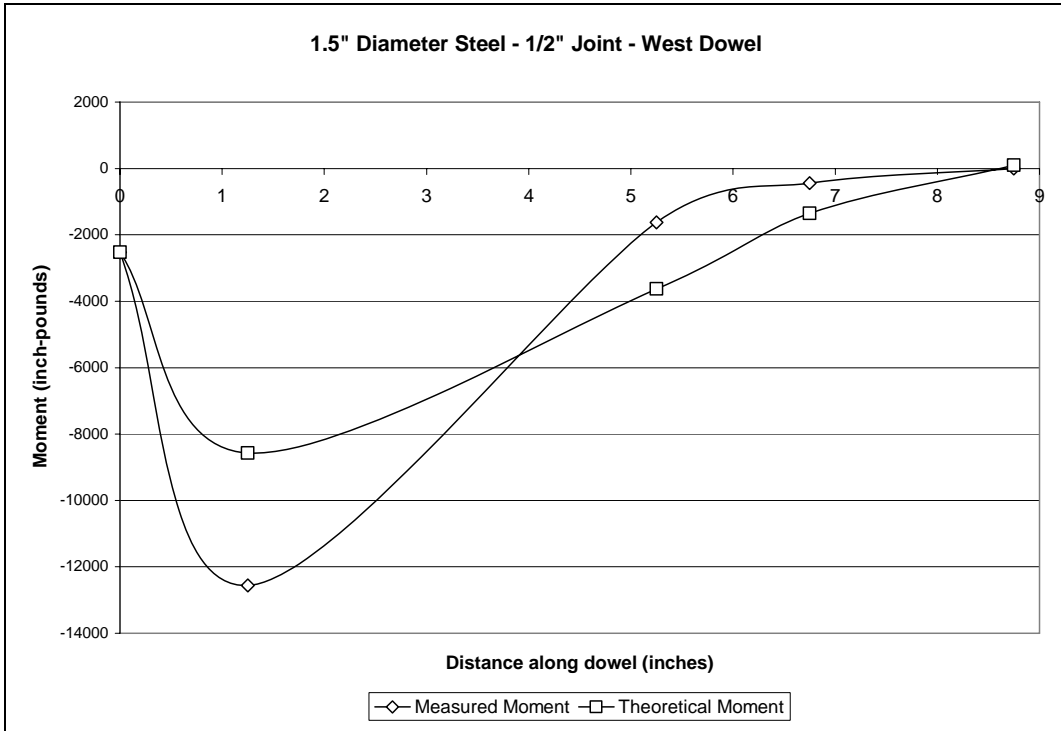


Figure B.2. Theoretical and measured moments, round steel specimen, west dowel, 1/2-inch joint

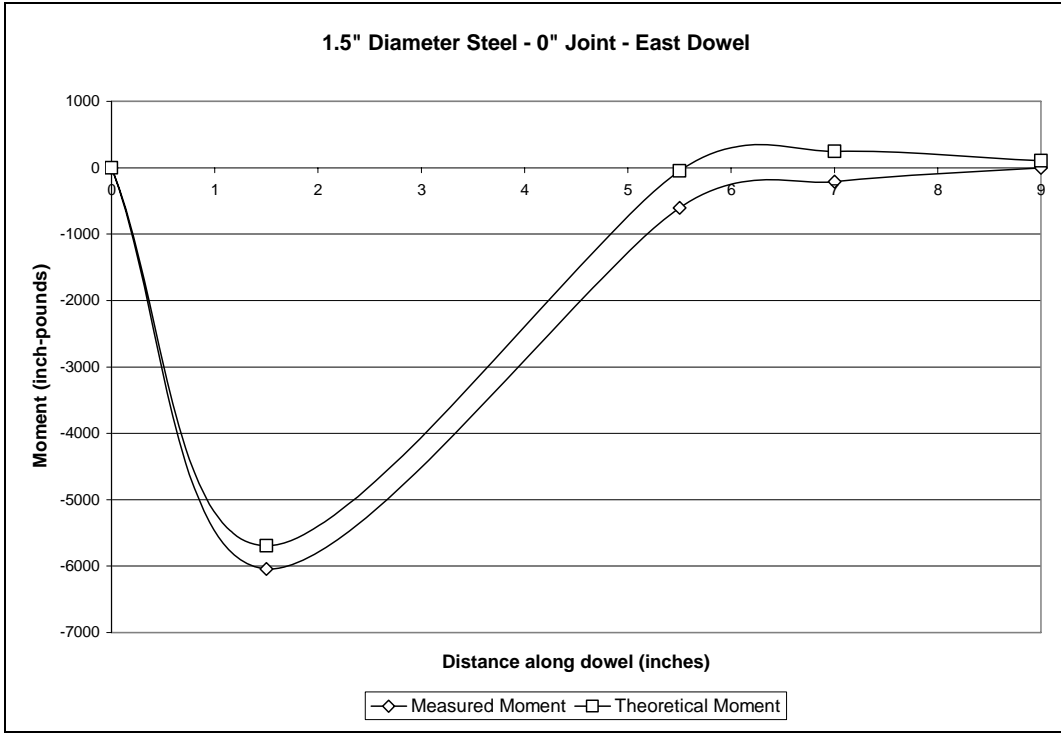


Figure B.3. Theoretical and measured moments, round steel specimen, east dowel, 0-inch joint

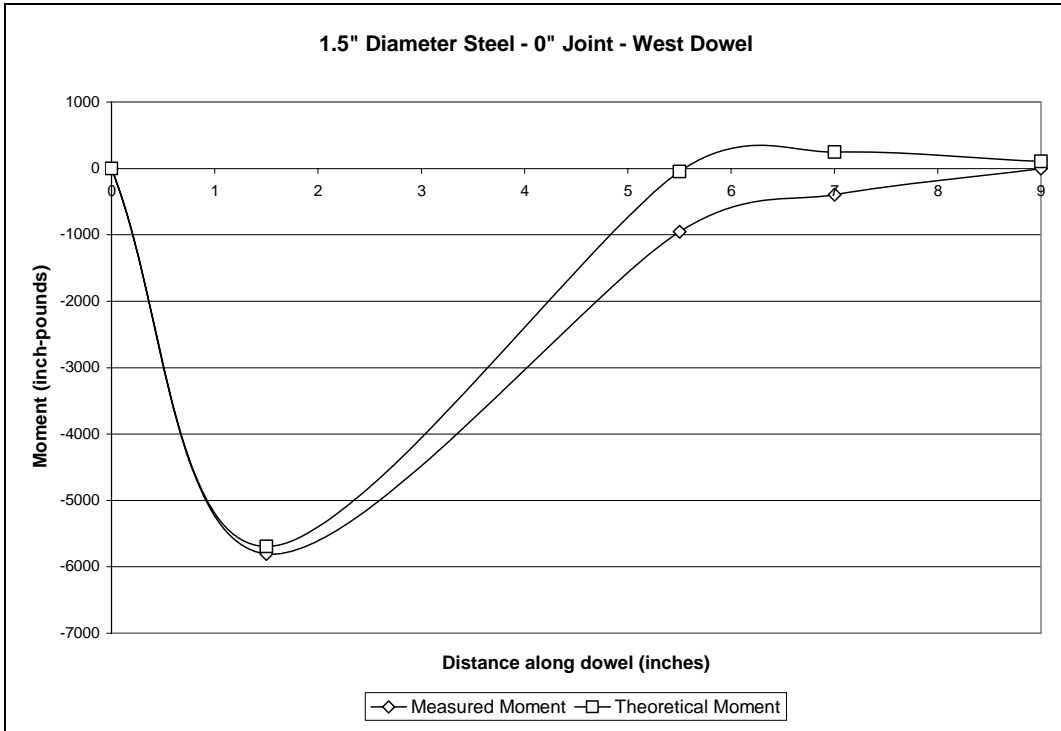


Figure B.4. Theoretical and measured moments, round steel specimen, west dowel, 0-inch joint

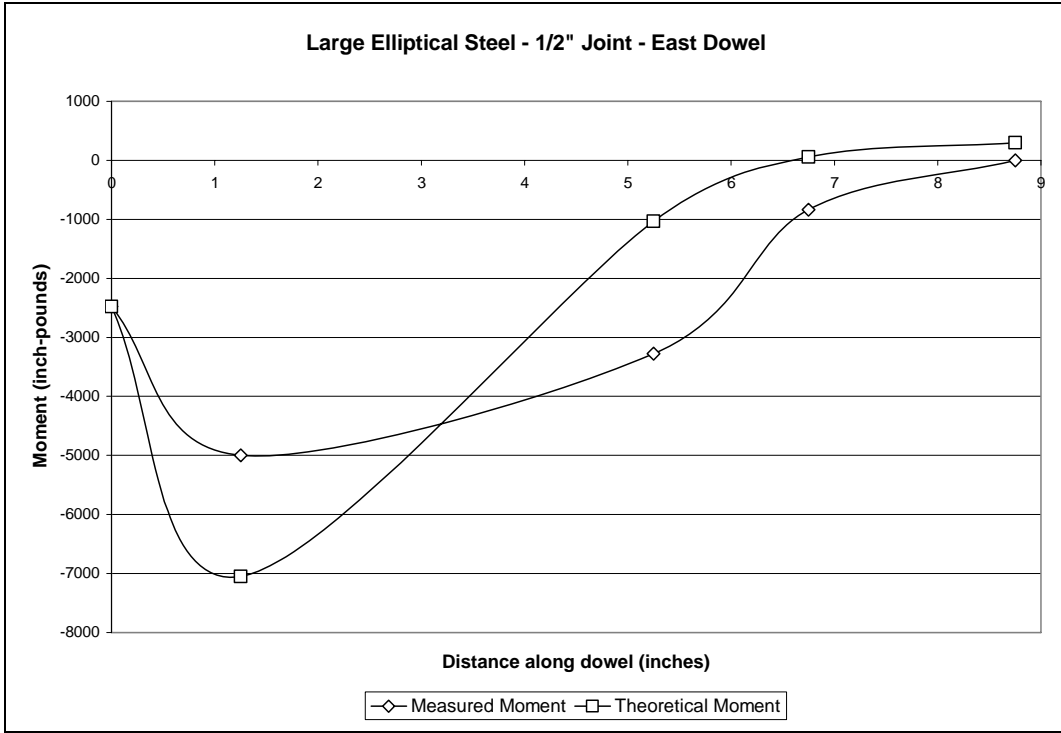


Figure B.5. Theoretical and measured moments, large elliptical steel specimen, east dowel, 1/2-inch joint

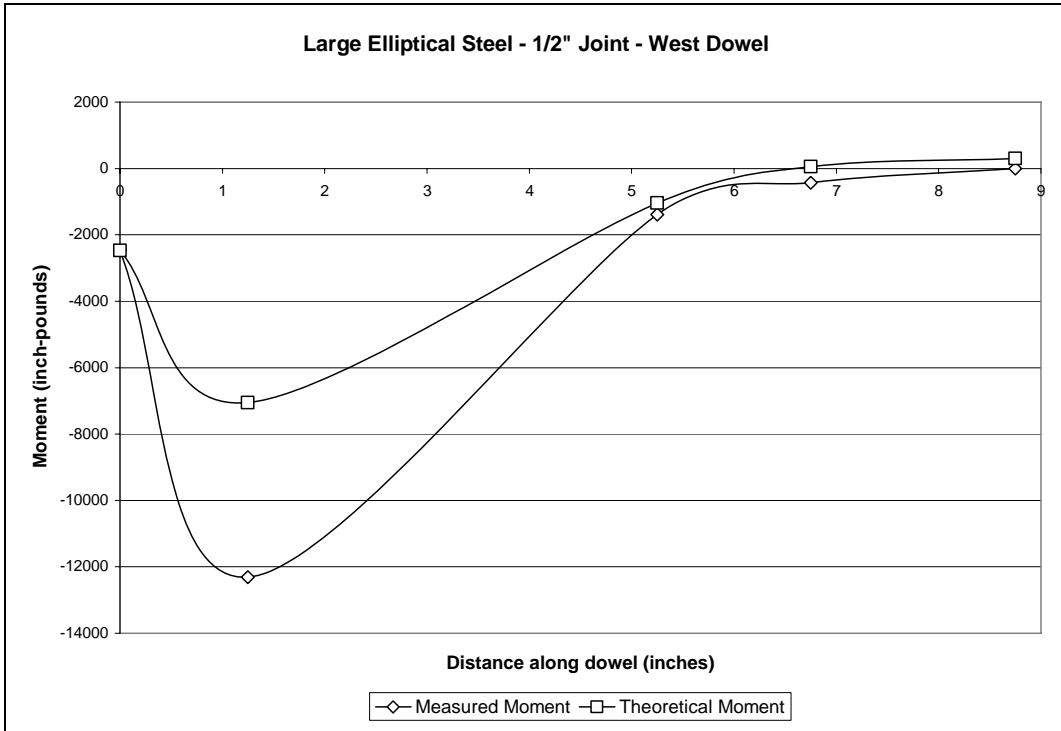


Figure B.6. Theoretical and measured moments, large elliptical steel specimen, west dowel, 1/2-inch joint

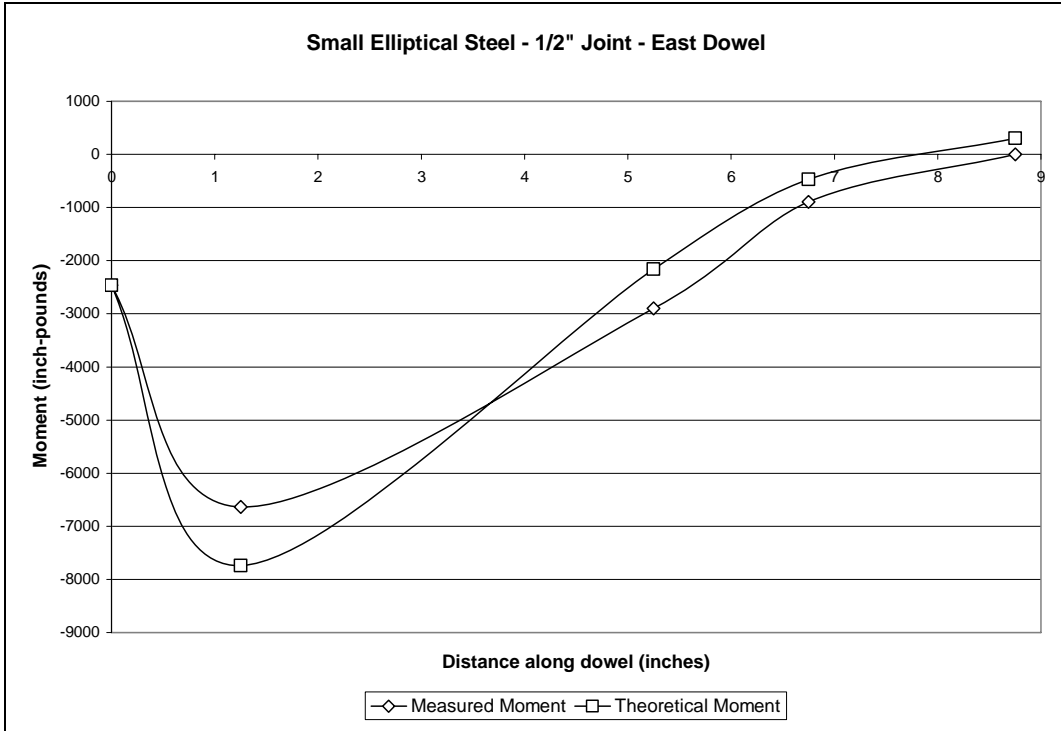


Figure B.7. Theoretical and measured moments, small elliptical steel specimen, east dowel, 1/2-inch joint

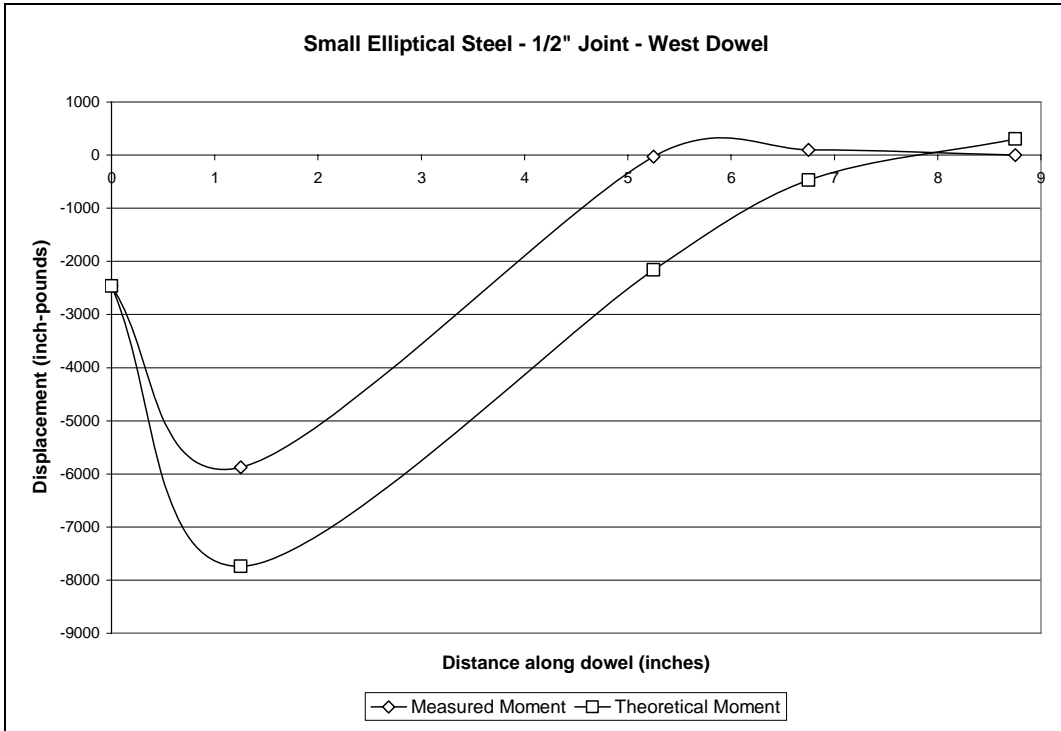


Figure B.8. Theoretical and measured moments, small elliptical steel specimen, west dowel, 1/2-inch joint

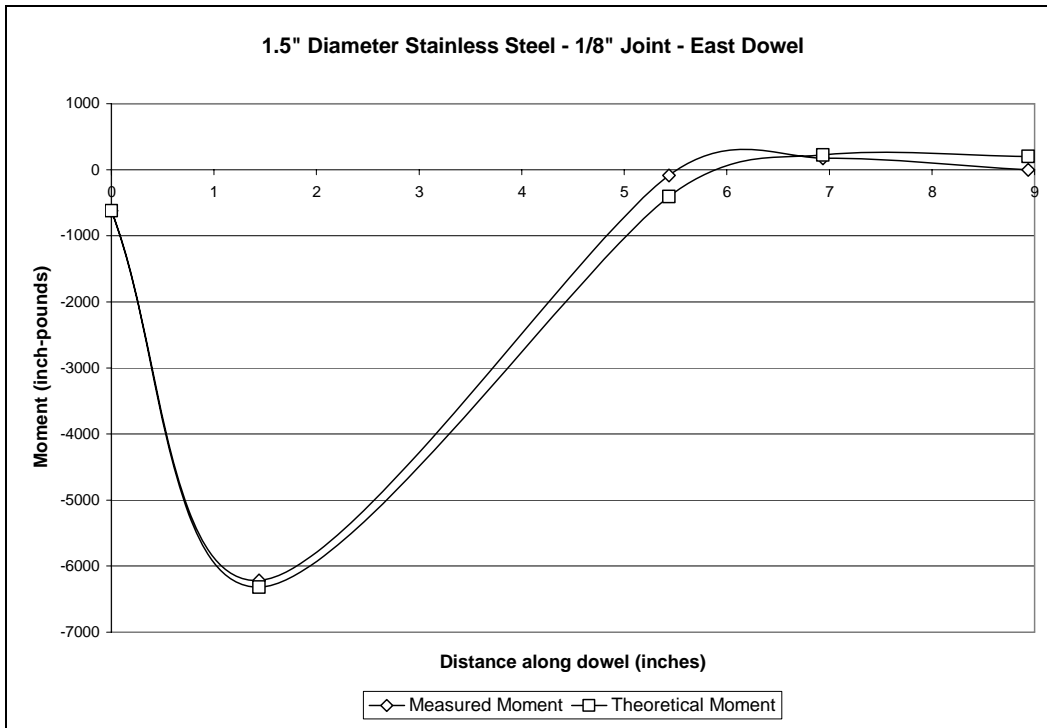


Figure B.9. Theoretical and measured moments, round stainless steel specimen, east dowel, 1/8-inch joint

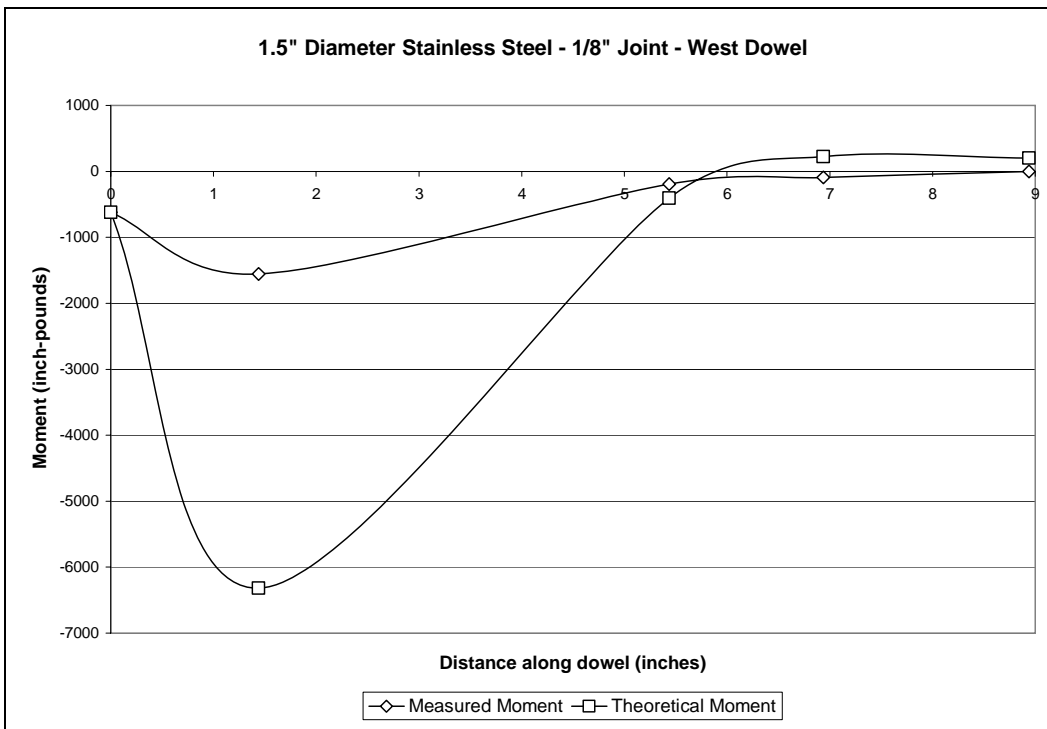


Figure B.10. Theoretical and measured moments, round stainless steel specimen, west dowel, 1/8-inch joint

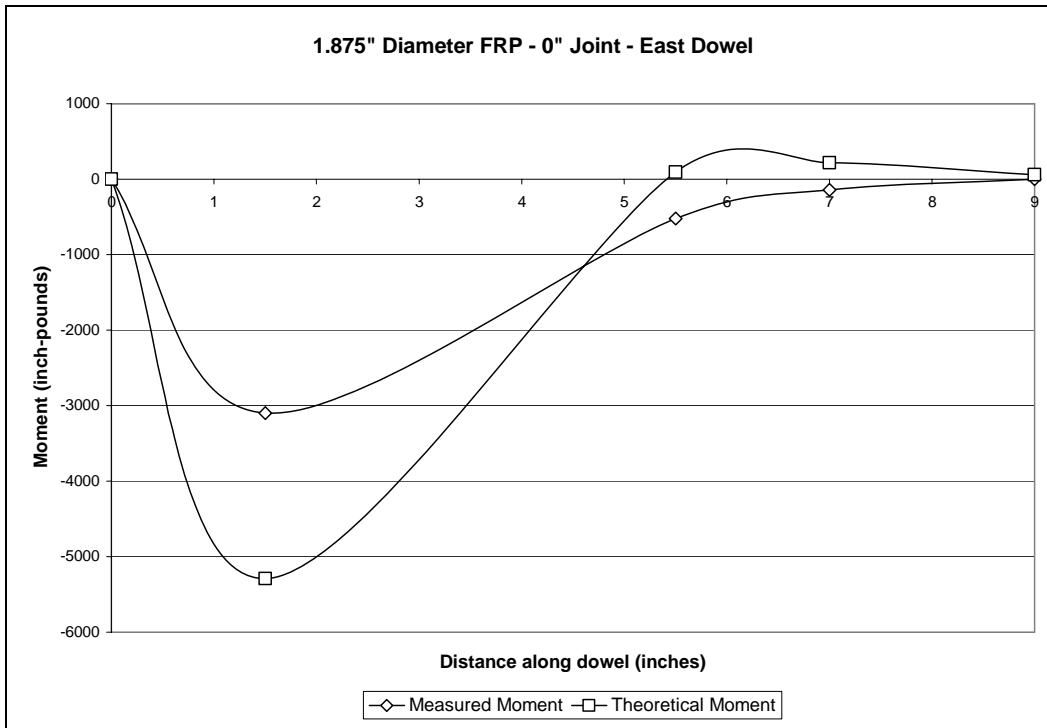


Figure B.11. Theoretical and measured moments, round GFRP specimen, east dowel, 0-inch joint

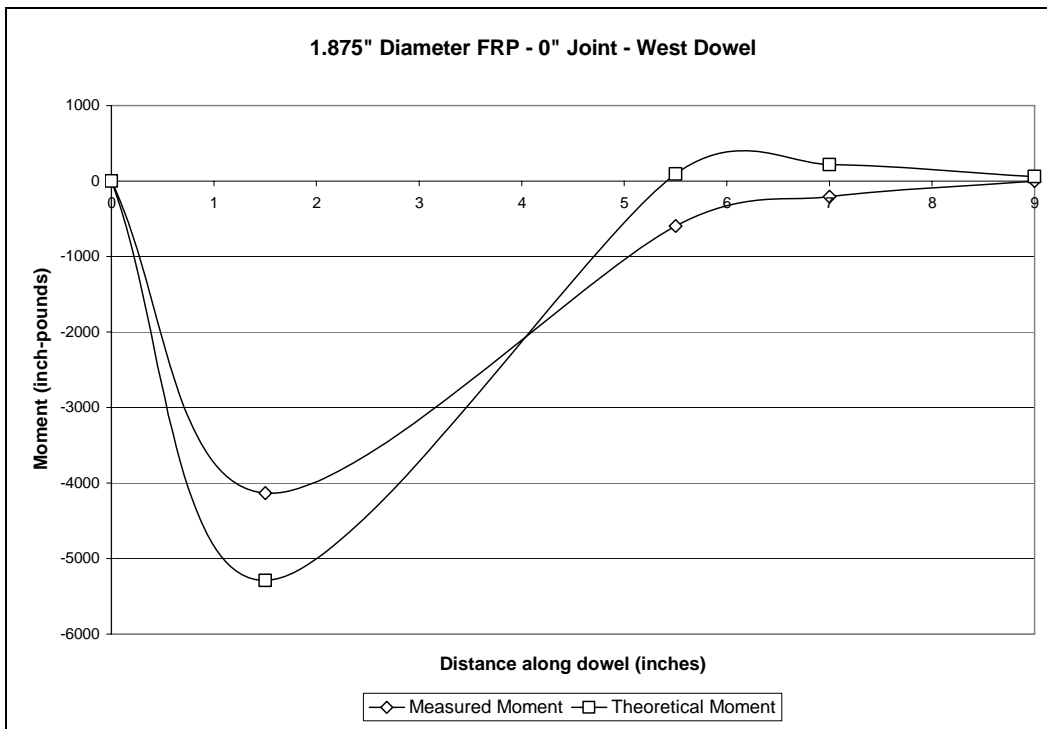


Figure B.12. Theoretical and measured moments, round GFRP specimen, west dowel, 0-inch joint

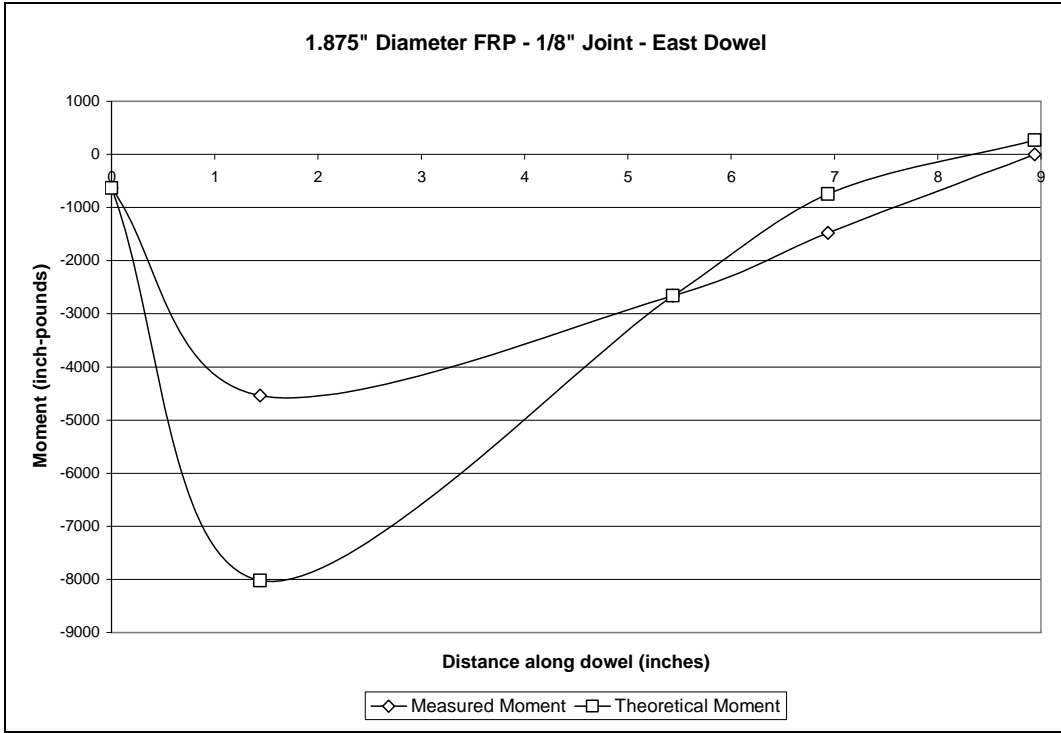


Figure B.13. Theoretical and measured moments, round GFRP specimen, east dowel, 1/8-inch joint

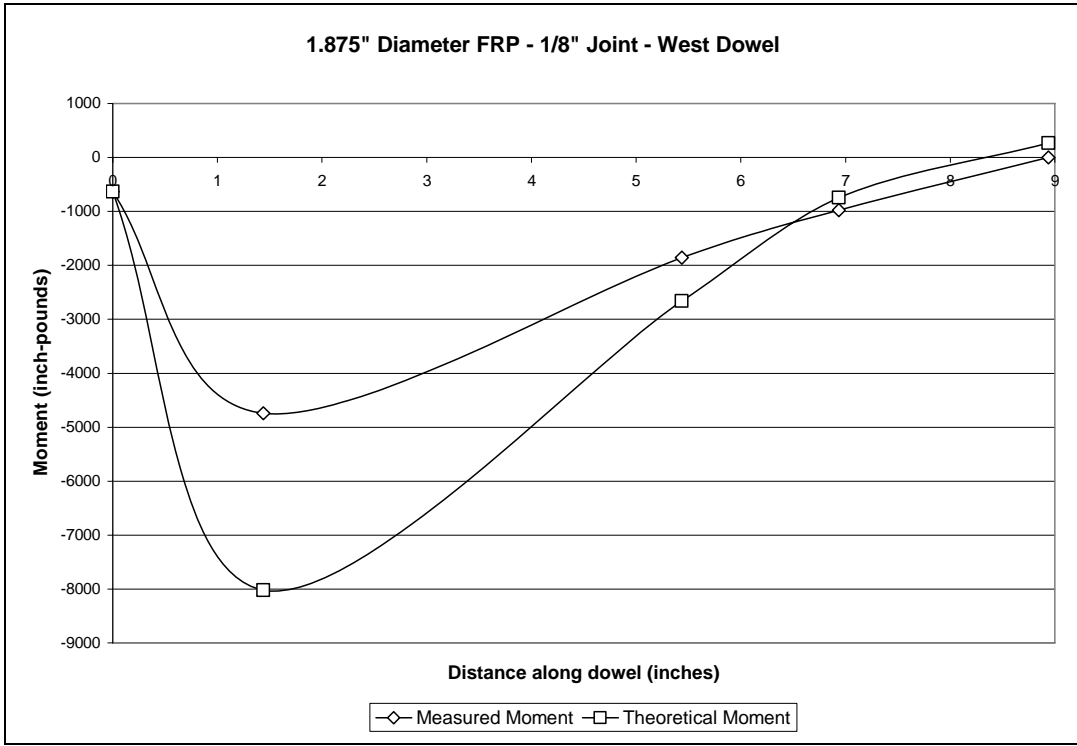


Figure B.14. Theoretical and measured moments, round GFRP specimen, west dowel, 1/8-inch joint

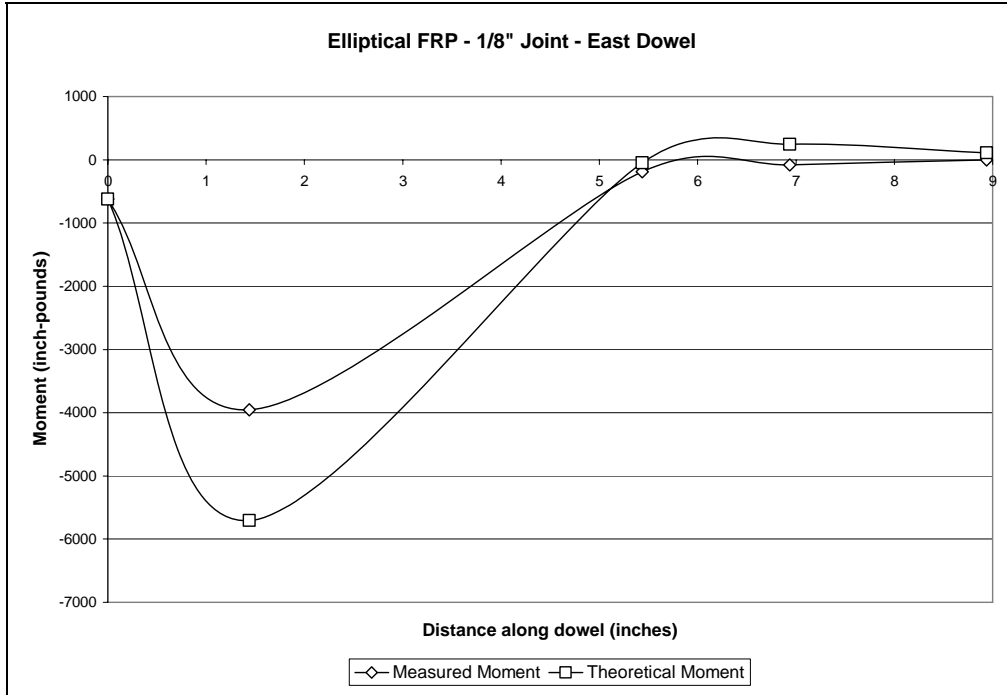


Figure B.15. Theoretical and measured moments, elliptical GFRP specimen, east dowel, 1/8-inch joint

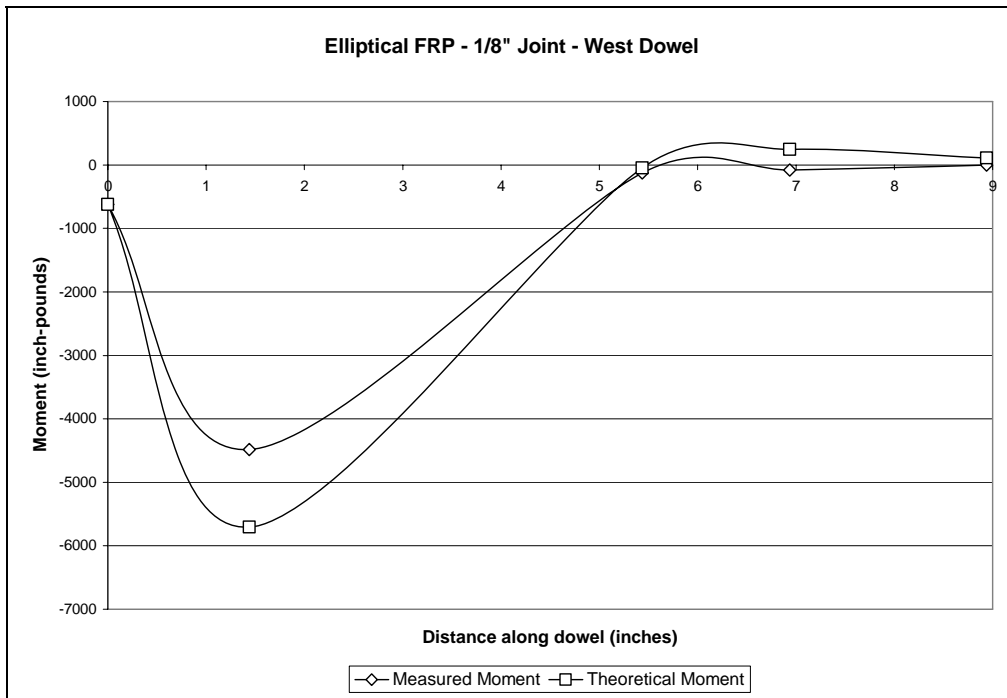


Figure B.16. Theoretical and measured moments, elliptical GFRP specimen, west dowel, 1/8-inch joint

**APPENDIX C. DOWEL DISPLACEMENT DIAGRAMS: THEORETICAL AND
OBSERVED**

Figures C.1 through C.8 show the theoretical displacement of the dowel along the length of the dowel and the observed displacement at the face of the joint, y_0 . The theoretical displacement is from Timoshenko's theory (20), as shown in Equation 3.9. The observed y_0 is the y_0 calculated for the same load used to plot the theoretical displacement curve.



Figure C.1. Theoretical displacement of round steel dowel, 0-inch joint

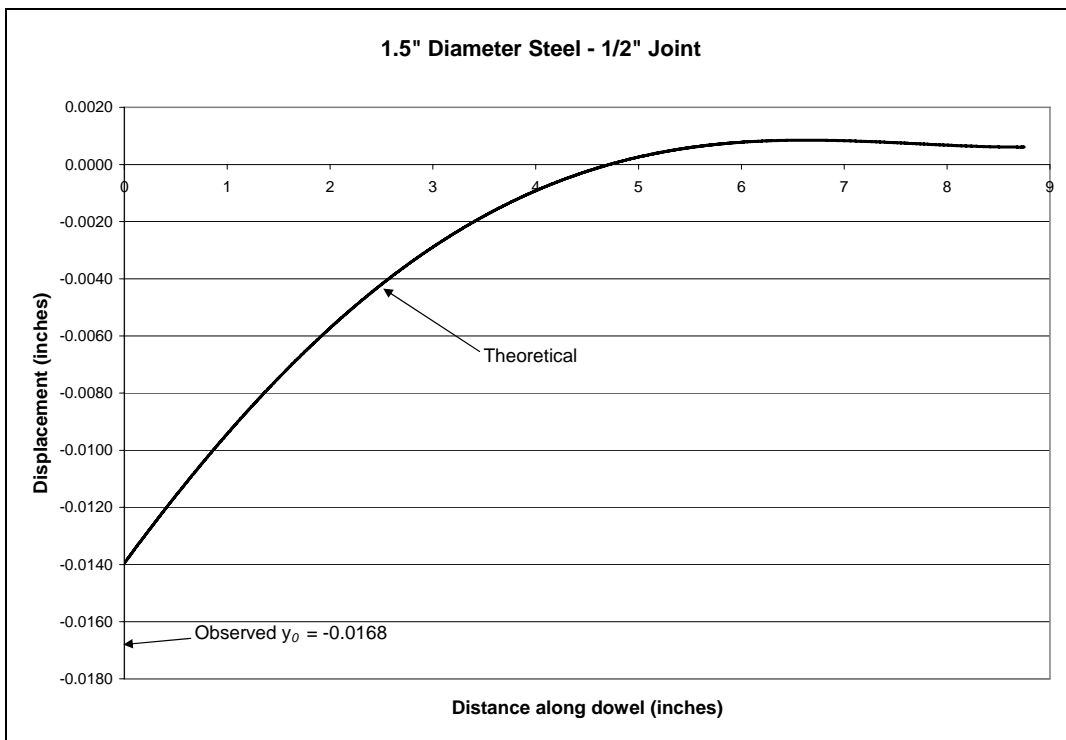


Figure C.2. Theoretical displacement of round steel dowel, 1/2-inch joint

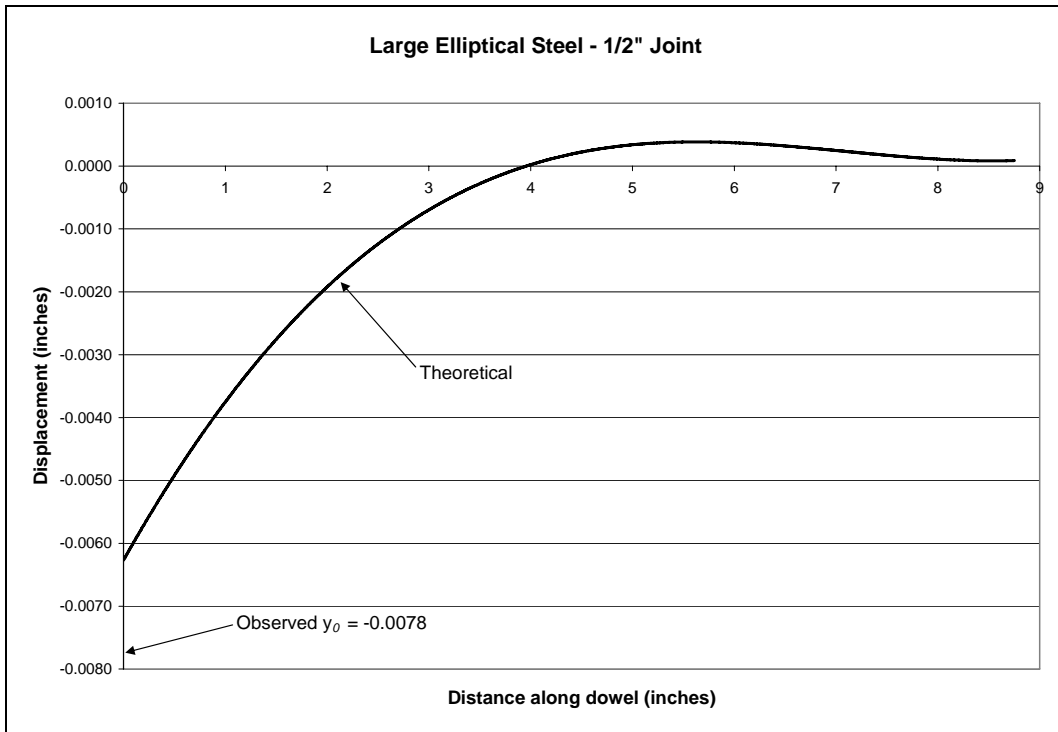


Figure C.3. Theoretical displacement of large elliptical steel dowel, 1/2-inch joint

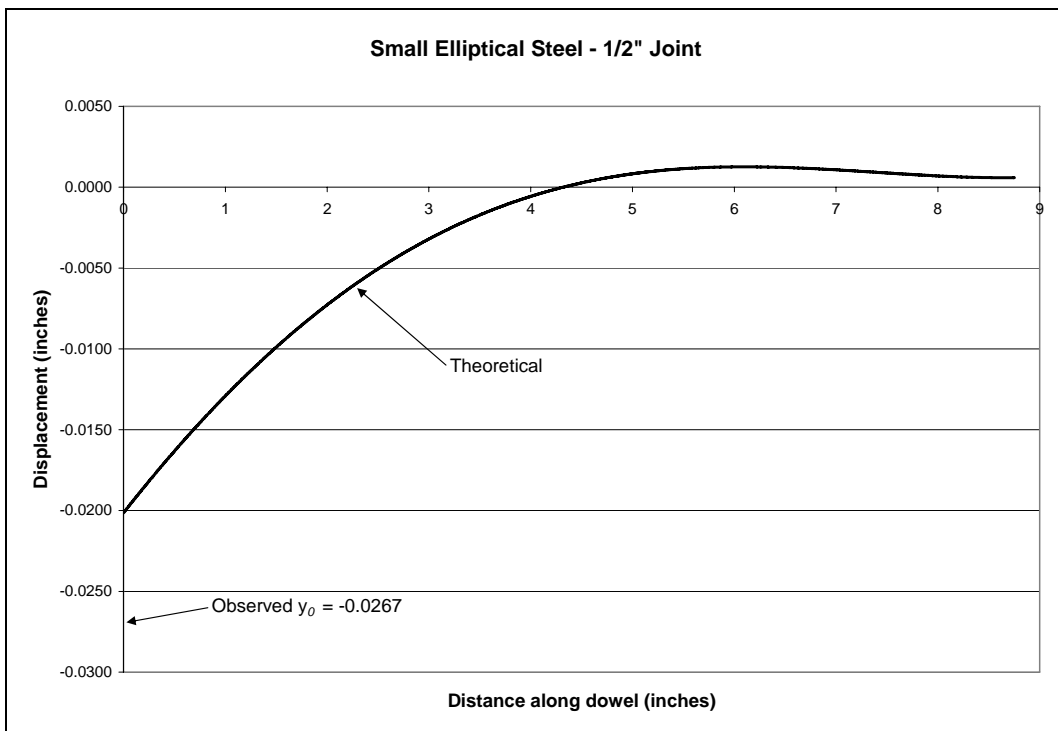


Figure C.4. Theoretical displacement of small elliptical steel dowel, 1/2-inch joint

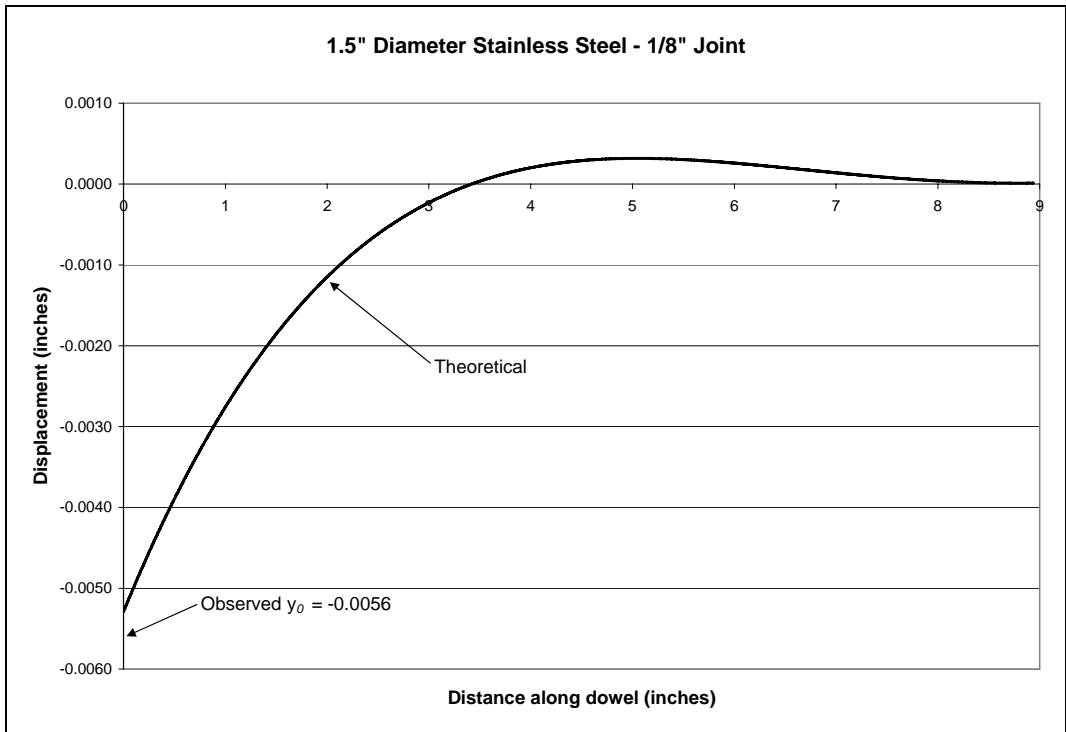


Figure C.5. Theoretical displacement of round stainless steel dowel, 1/8-inch joint

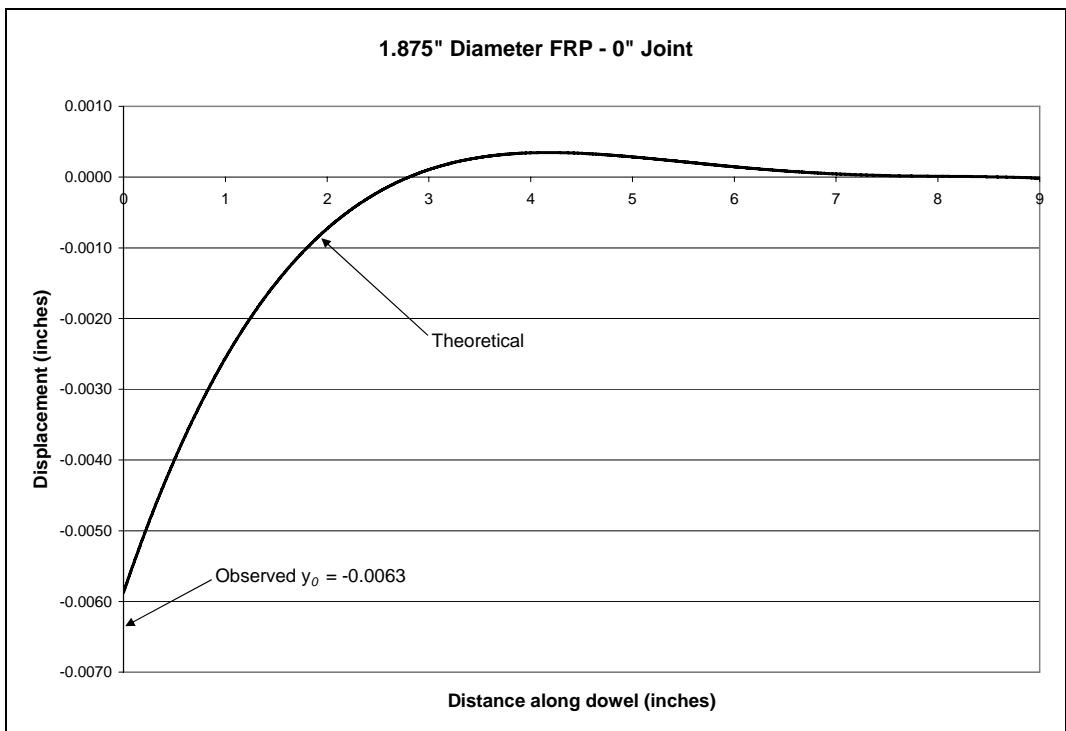


Figure C.6. Theoretical displacement of round GFRP dowel, 0-inch joint

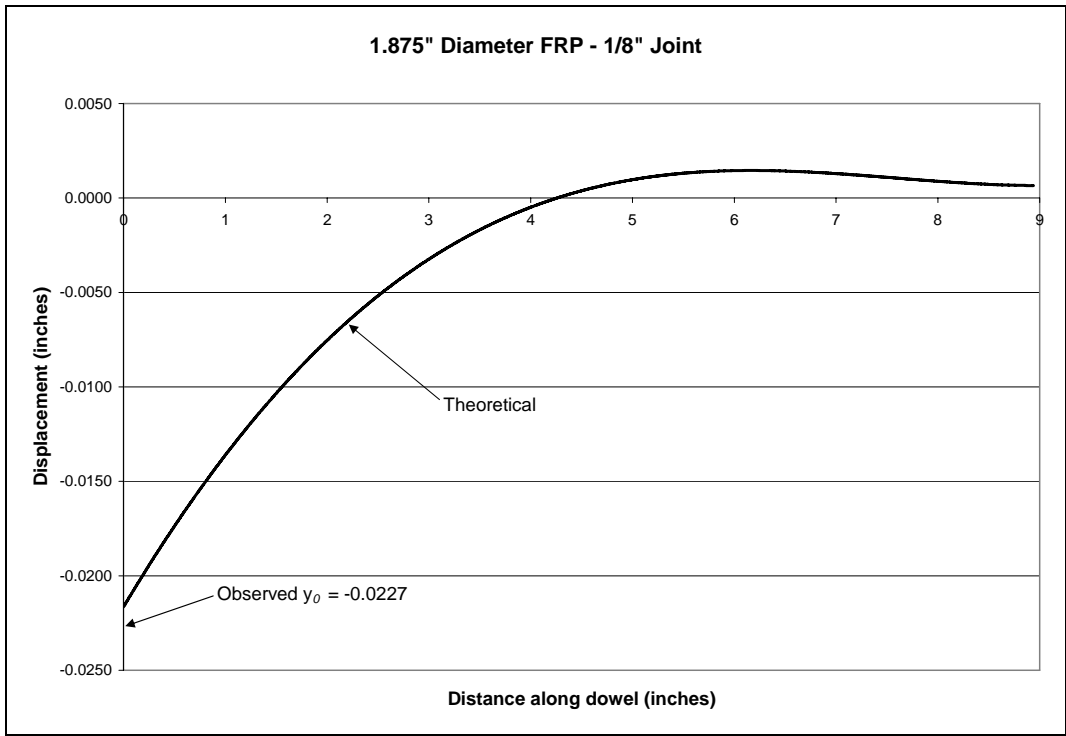


Figure C.7. Theoretical displacement of round GFRP dowel, 1/8-inch joint

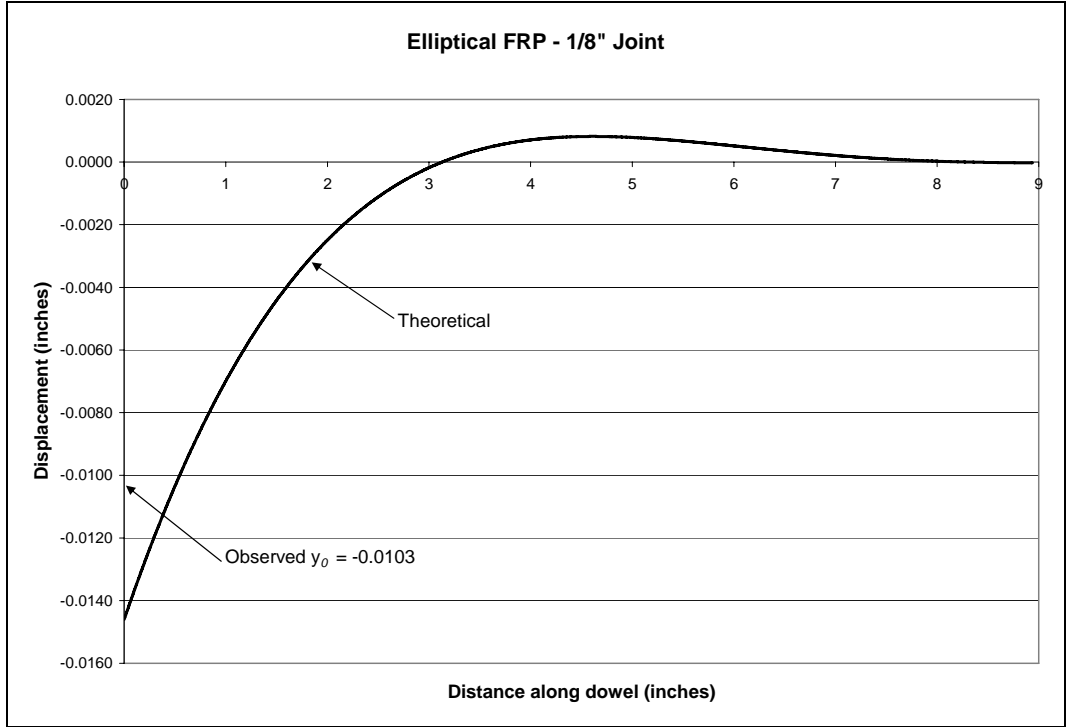


Figure C.8. Theoretical displacement of elliptical GFRP dowel, 1/8-inch joint

**APPENDIX D. CANTILEVER TEST MODULUS OF DOWEL SUPPORT VS. LOAD
DIAGRAMS**

Figures D.1 through D.6 show load vs. k_0 plots for all 18 cantilever specimens. Each figure shows all three specimens tested per dowel bar type.

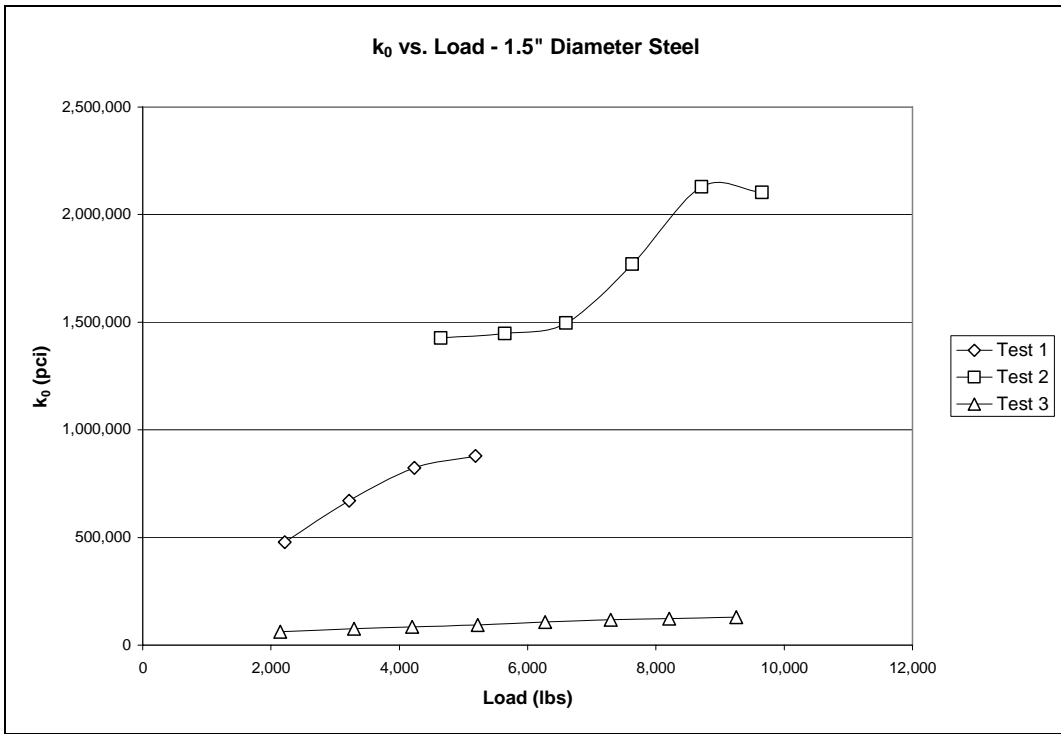


Figure D.1. k_0 vs. load plots for round steel cantilever specimens

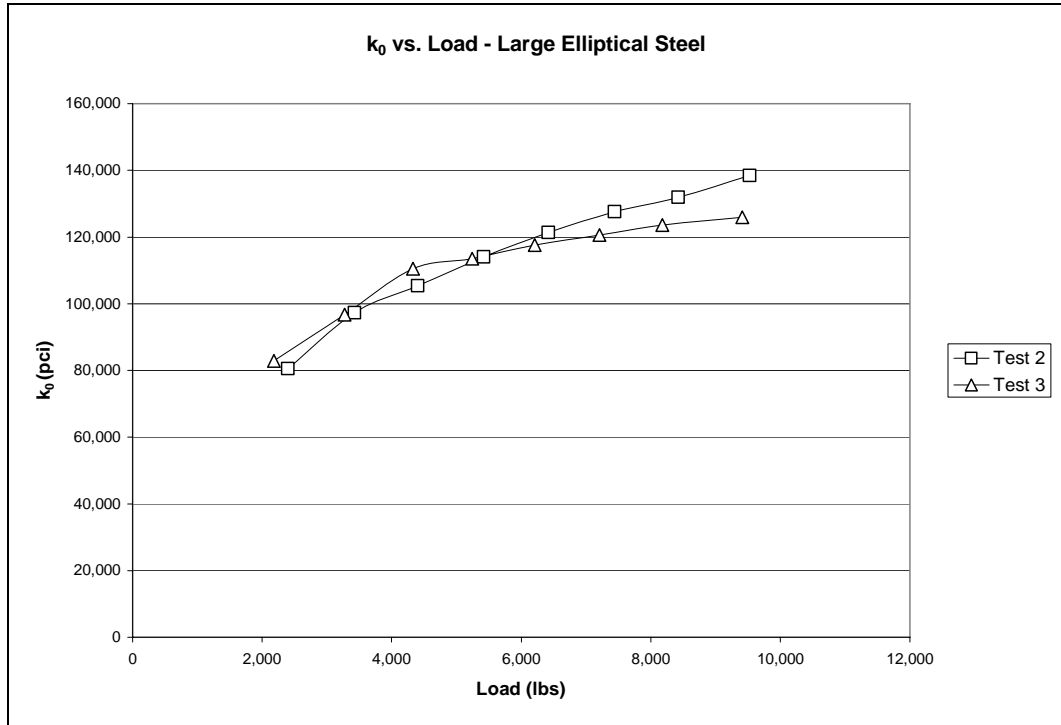


Figure D.2. k_0 vs. load plots for large elliptical steel cantilever specimens

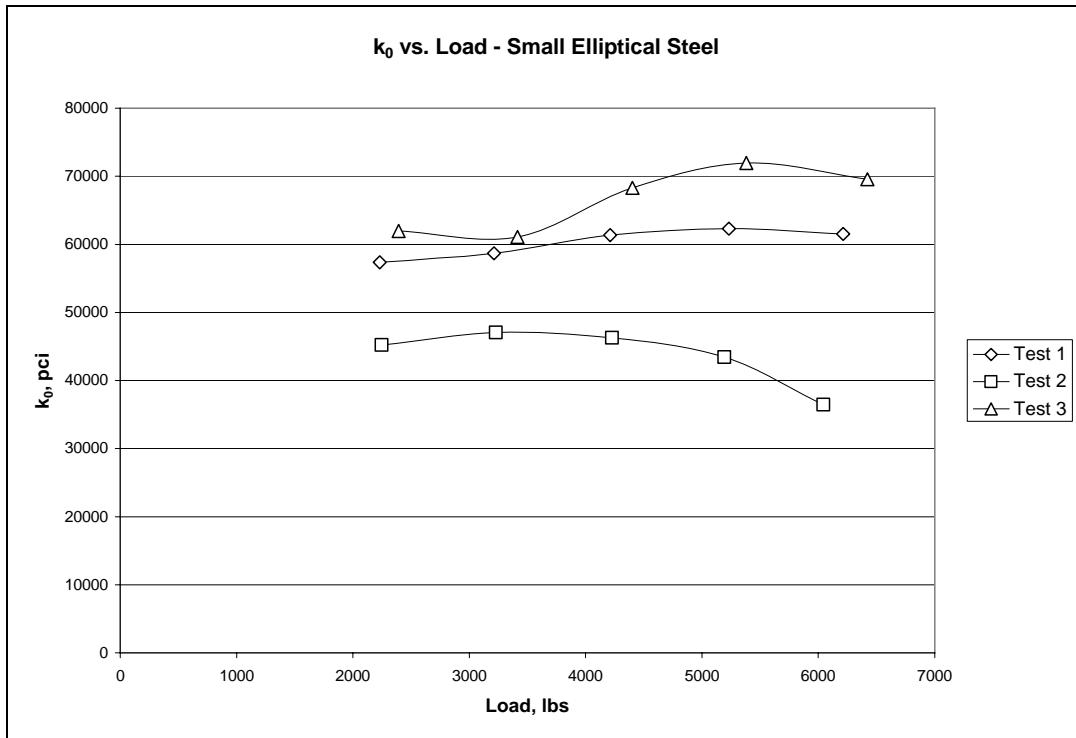


Figure D.3. k_0 vs. load plots for small elliptical steel cantilever specimens

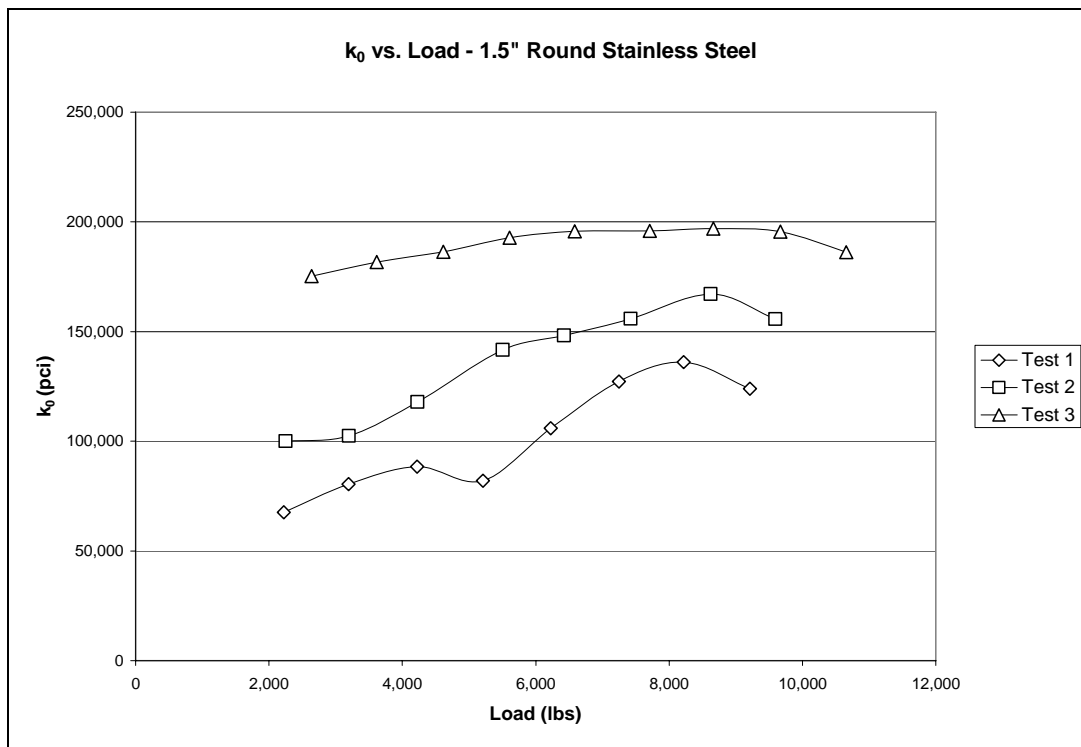


Figure D.4. k_0 vs. load plots for round stainless steel cantilever specimens

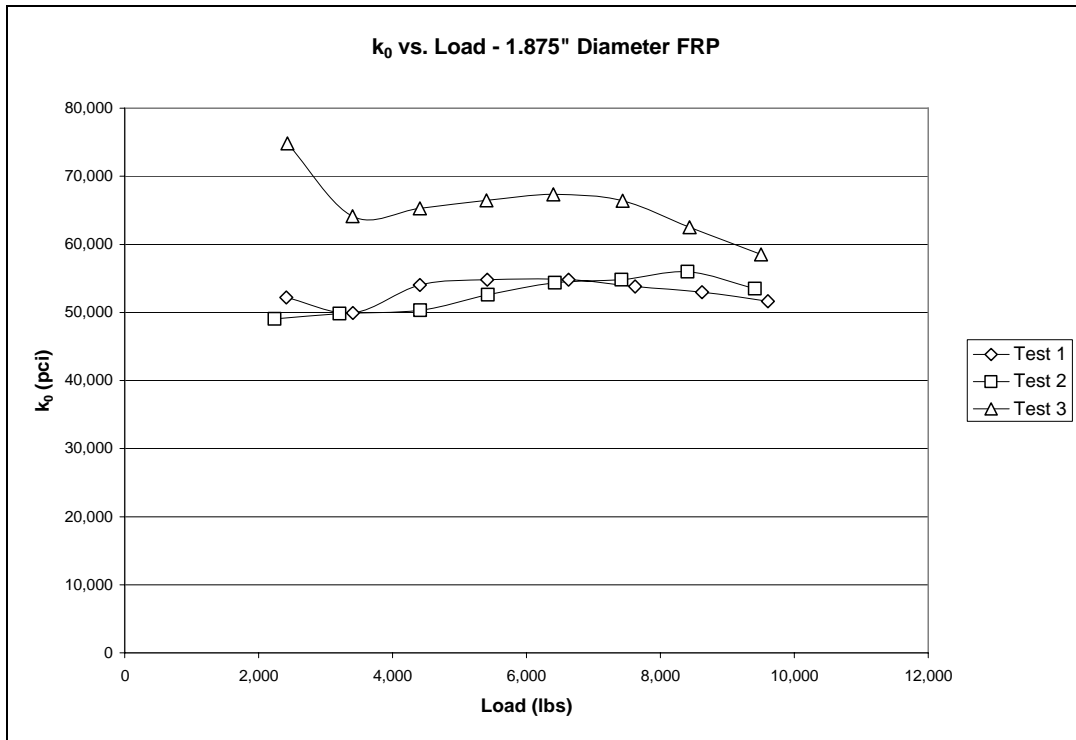


Figure D.5. k_0 vs. load plots for round GFRP cantilever specimens

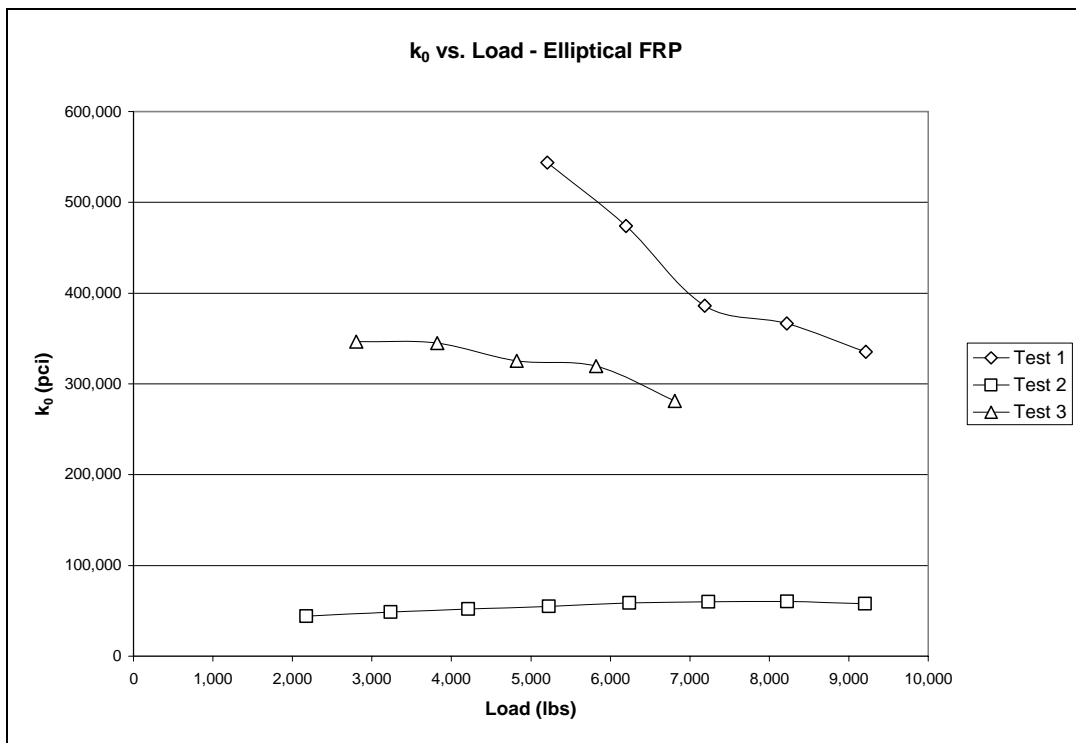


Figure D.6. k_0 vs. load plots for elliptical GFRP cantilever specimens